Synthetic Lethal Interactions of EPHB6 in Breast Cancer Cells

A Thesis Submitted to the College of
Graduate Studies and Research
in Partial Fulfillment of the Requirements
for the Degree of Master of Science
in the Department of Biochemistry
University of Saskatchewan
Saskatoon

By

James M. Paul

PERMISSION TO USE

By presenting this thesis in partial fulfillment of the requirements for a Postgraduate degree from the University of Saskatchewan, I agree that the libraries of this University may make it freely available for inspection. I further agree that permission for copying of this thesis in any manner, in whole or in part, for scholarly purposes, may be granted by the professors who supervised my thesis work or, in their absence, by the Head of the Department or the Dean of the College in which my thesis work was done. It is understood that any copying or publication or use of this thesis or parts thereof for financial gain shall not be allowed without my written consent. It is also understood that due recognition shall be given to me and to the University of Saskatchewan in any scholarly use which may be made of any material in my thesis.

Requests for permission to copy or to make other uses of the materials in this thesis in whole or in part should be addressed to:

Head of the Department of Biochemistry
107 Wiggins Road
University of Saskatchewan
Saskatoon, Saskatchewan, S7N 5E5, Canada

OR

Dean
College of Graduate Studies and Research
University of Saskatchewan
107 Administration Place
Saskatoon, Saskatchewan, S7N 5A2, Canada

ABSTRACT

Sequencing of tumor genomes has shown that many loss-of-function alterations exist in cancer cells. Some of these alterations are a product of the cancerous progression of such cells, while others play a causative role. Unlike gain-of-function or overexpression alterations, these loss-of-function alterations are difficult to target directly, meaning that alternative approaches are necessary. In this case, such alterations can be specifically targeted through utilizing synthetic lethal interactions, whereby simultaneous inhibition of a particular interacting partner gene causes lethality in the context of a previously inactivated gene. Such a loss-of-function alteration occurs in the case of the EPHB6 receptor tyrosine kinase, which is downregulated in multiple cancer types. This downregulation of EPHB6, along with its inherent anti-malignant properties, make it a logical target for the synthetic lethal approach. In my thesis, I describe the use of a large-scale genome-wide screen of EPHB6 in triple-negative beast caner cells to determine corresponding synthetic lethal genes, which may be therapeutically targeted. The screen revealed the SRC kinase as a synthetic lethal partner of EPHB6, whereby targeting of SRC in EPHB6-deficient cells results in lethality. In addition, small molecule SRC inhibitors, such as KX2-391, were used to improve elimination of EPHB6-deficient triple-negative breast cancer cells in both monolayer culture, as well as in xenograft tumor models. This work reveals EPHB6 to be a biomarker for the use of SRC inhibitors in triple negative breast cancer, and it contributes to larger synthetic lethal interaction maps of cancer as a whole.

ACKNOWLEDGEMENTS

I would like to thank all those who have helped to provide me with this experience. I would like to thank my supervisors, Dr. Franco Vizeacoumar and Dr. Andrew Freywald, for providing me with such an opportunity to carry out research under their guidance. Their character and leadership, as well as their love of science, have continually driven me forward in the pursuit of my education. They have invested many hours into teaching, correcting, and encouraging me in the area of cancer research, as well as providing continual direction for my project. Thanks as well to my committee members, Dr. Jeremy Lee and Dr. Erique Lukong, for providing me with direction and guidance, as well as to the Department of Biochemistry.

I would like to thank every other member of the Vizeacoumar and Freywald labs for all of the help, support, and insight that they have provided. This work would not have been possible without such dedicated colleagues. I would also like to thank Mark Boyd for being an excellent lab manager and for always being ready to help in times of need. Thanks as well to all of the other support staff in the Cancer Cluster, as well as the staff in the Laboratory Animal Services Unit.

I would also like to thank my parents, Tom and Laurie, as well as my siblings, in-laws, nieces, and nephews, for all of their support throughout this time of research and study.

Finally, I would like to thank my wife, Caitlin, for all of her care and support. She has provided me with tremendous encouragement and has always lifted my spirits when the work was challenging.

TABLE OF CONTENTS

LIST OF TABLES

LIST OF FIGURES

LIST OF ABBREVIATIONS

7-AAD	7-Aminoactinomycin D
90K	90,000
BFP	Blue fluorescent protein
BSA	Bovine serum albumin
CSLD	Compartments Subcellular Localization Database
DCC	Difference of cumulative change
DMSO	Dimethyl sulfoxide
E-MAP	Epistatic mini array profile
ER	Estrogen receptor
GFP	Green fluorescent protein
H&E	Haematoxylin and eosin
IQR	Interquartile range
MOI	Multiplicity of infection
MMP	Matrix metalloproteinase
NGI	Negative genetic interaction
PGI	Positive genetic interaction
PI	Propidium iodide
PR	Progesterone receptor
RFP	Red fluorescent protein
SCADEMS	Saskatchewan Cancer Agency differential essentiality mapping system
sgRNA	Single guide RNA
*sh*RNA	Short hairpin RNA
SL	Synthetic lethal(ity)
TCGA	The Cancer Genome Atlas
TNBC	Triple negative breast cancer

1.0 Introduction

1.1 Breast Cancer Subtypes

According to data collected by the International Agency for Research on Cancer, breast cancer is the most common cancer among women (Ferlay *et al*., 2015). In data from 2012, there were an estimated 1.67 million new diagnosed cases of breast cancer, with an estimated 522,000 deaths worldwide. While in Canada, about 25,000 new cases of breast cancer are being diagnosed per year, according to the Canadian Cancer Society (http://www.cancer.ca/en/cancer-information/cancer-type/breast/statistics). In addition, it is the most common cause of cancer-related death among women in developing countries, while in developed countries it ranks as the second most common, after lung cancer. As such, extensive research has been directed toward its treatment in the past decades. Breast cancer is divided into different subtypes, each of which has its own unique, biological differences (Table 1.1). These subtypes were determined largely based on the expression of particular genes, such as the estrogen receptor (ER), progesterone receptor (PR), and HER2 receptor. In a study by Perou *et al*. (2000), the variation of gene expression was elucidated from 65 different breast tumor samples. This study used complimentary DNA microarrays in order to assess the expression of 8,102 different human genes. This data was then organized by cluster analysis, whereby it revealed several clear divisions in gene expression based on tumor type. Those tumors determined to be ER positive were also found displaying a high expression level of many genes associated with breast luminal tissue, which was confirmed by immunohistochemistry. However, tumors of breast basal tissue origin lacked expression of both ER and genes that are normally co-expressed with ER.

Table 1.1 Breast cancer subtypes

Breast cancer subtype	Luminal A	Luminal B	HER2	Triple negative
Receptor expression	ER+, PR+, and HER2-	ER+, PR+, and HER2+	ER-, PR-, and HER2+	ER-, PR-, and HER2-
Incidence of subtype	50-60%	15-20%	15-20%	10-20%

The most common breast cancer subtype is luminal breast cancer, which is, in turn, divided into luminal A and luminal B types. These tumors, accounting for ~75% of all breast cancer, express ER and PR, as well as many other genes consistent with breast luminal tissue

(Perou *et al*., 2000; Vallejos *et al*., 2010; Yersal and Barutca, 2014). In addition to ER and PR, luminal B breast cancer is also known to express the HER2 receptor. Luminal breast cancer tumors are typically associated with a good prognosis, with luminal A being significantly more favorable than luminal B (Sørlie *et al*., 2001). Typically, luminal tumors are more responsive to hormone therapy than they are to chemotherapy (Brenton *et al*., 2005). The HER2 subtype, accounting for 15-20% of breast cancer cases, carries a less favorable prognosis, and is characterized by high expression of the HER2 receptor, but no expression of ER or PR (Yersal and Barutca, 2014; Dai *et al*., 2015). The less favorable prognosis of HER2 breast cancer is largely due to the higher chance of relapse in patients that have not experienced a full elimination of tumors (Brenton *et al*., 2005). However, due to the expression of HER2 in this subtype, treatment is possible with trastuzumab, which is an anti-HER2 monoclonal antibody. Lastly, the triple negative breast cancer (TNBC) subtype is characterized by the lack of ER and PR expression and does not overexpress the HER2 receptor (Dai *et al*., 2015). TNBC accounts for 10-20% of breast cancer cases and is associated with a very high rate of patient mortality due to the complete absence of targeted therapies (Boyle, 2012; Mayer *et al*., 2014). Therefore, there is an active search for efficient therapeutic targets that would allow treatment personalization in TNBC tumors. In particular, some members of the Eph family of receptor tyrosine kinases have been viewed as promising targets for breast cancer therapy.

1.2 Eph Receptors

The Eph family of receptor tyrosine kinases is represented by sixteen members, divided into two groups based on the ligands to which they bind (Truitt and Freywald, 2011). Their ligands, ephrins, are divided into ephrin-A and ephrin-B groups based on their molecular structures. The ephrin-A members, consisting of ephrin-A1 to ephrin-A6, are cell membrane proteins with GPI anchors, while the ephrin-B members, consisting of ephrin-B1 to ephrin-B3, have transmembrane and cytoplasmic domains (Figure 1.1). Therefore, the Eph receptors are classified as either EphAs, consisting of EPHA1 to EPHA10, which mostly bind ephrin-A ligands, or as EphBs, consisting of EPHB1 to EPHB6, which mostly bind ephrin-B ligands (Pasquale, 2008).

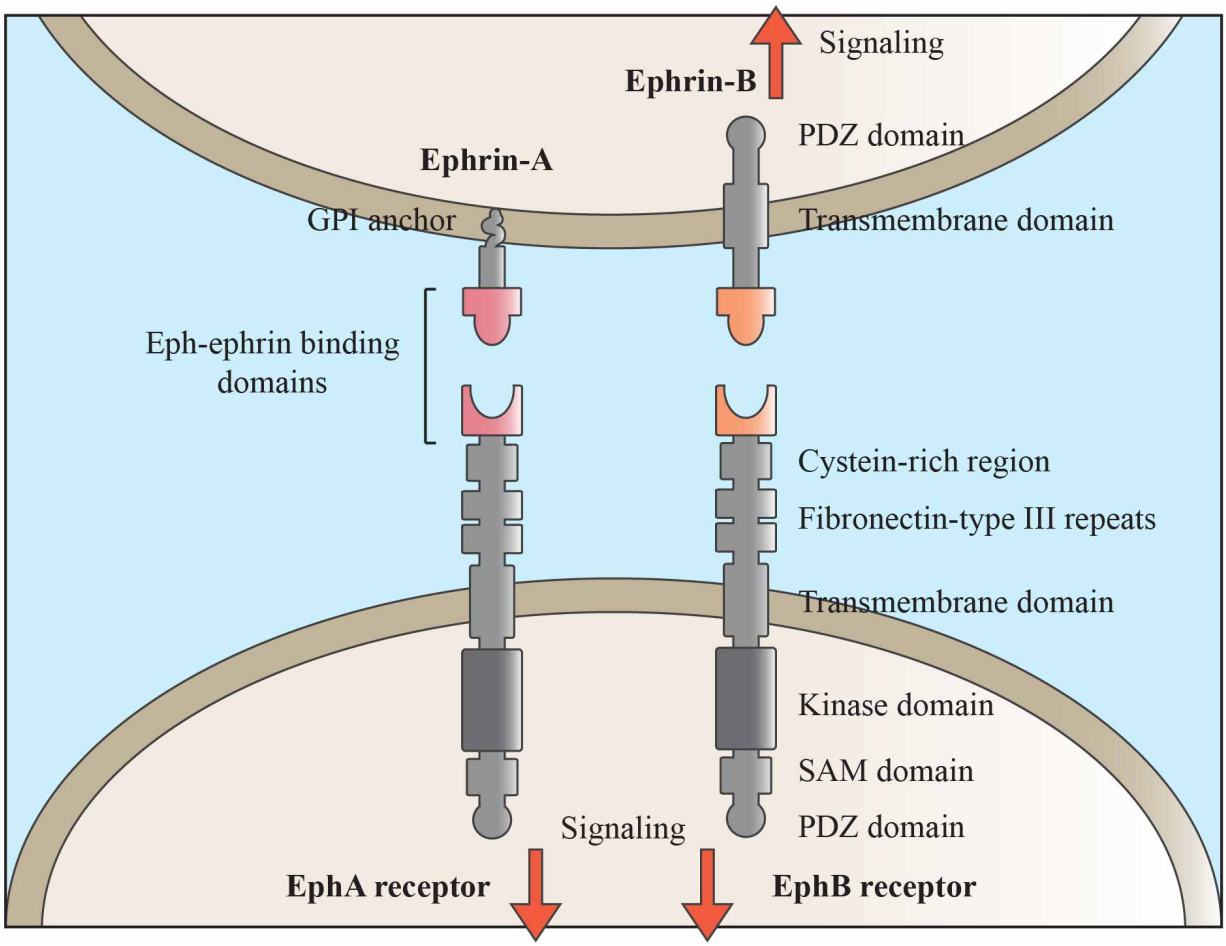

Figure 1.1 Eph receptors and ephrin ligands

This figure shows EphA and EphB receptors, with their typical ligands, ephrin-A and ephrin-B, respectively. Upon interaction with the ephrin ligands, the Eph receptor's kinase domain is converted to its active form. The Eph receptor can then phosphorylate tyrosine residues, thereby generating, or even suppressing signaling cascades in the cell. Further interactions with surrounding proteins may also be mediated by the SAM and PDZ domains. However, most Eph receptor signaling is mediated by phosphotyrosines (Pasquale, 2005). Additionally, ephrins are also capable of generating a signaling event following interaction, referred to as reverse signaling.

While EphA receptors mostly interact with ephrin-A ligands and EphB receptors mostly interact with ephrin-B ligands, within each group ligand-receptor interactions are quite broad, with most EphA receptors binding to any ephrin-A ligand and most EphB receptors binding to any ephrin-B ligand. Some Eph receptors however, are stricter in their binding, such as EPHB6, which has been reported to only bind ephrin-B1 and ephrin-B2, and not ephrin-B3

(Munthe *et al*., 2000; Freywald *et al*., 2002). Eph receptors are involved in a number of different processes through their basal or ligand-induced signaling, including embryo development (Poliakov *et al*., 2004) and the maintenance of homeostasis in multiple systems of adult organisms (Holmberg *et al*., 2006). This is in keeping with the Eph receptor ability to regulate multiple responses in different types of stem cells, including both adult and cancer stem cell populations (Holmberg *et al*., 2006; Chumley *et al*., 2007; Stokowski *et al*., 2007).

Like other receptor tyrosine kinases, Eph receptors are activated by interactions with their ligands, leading to receptor dimerization or oligomerization, and phosphorylation of tyrosine residues (Himanen *et al*., 2007). This phosphorylation enhances Eph receptor activity and increases interactions with cytoplasmic signaling molecules, thereby initiating signaling pathways in the cytoplasm (Murai and Pasquale, 2003). Interestingly though, both EphA and EphB receptor groups possess members which are kinase-deficient, EPHA10 and EPHB6, indicating that these receptors may be important for ephrin-induced responses (Truitt and Freywald, 2011). However, it has also been shown that these kinase-dead receptors are able to form complexes with other surface proteins, thereby allowing signaling to occur through an alternate route. This can be observed in the case of EPHB6, which is able to interact with other Eph receptors, such as EPHB1 and EPHB4, as well as with other proteins, such as c-CBL and the SRC family kinase FYN (Freywald *et al*., 2002; Matsuoka *et al*., 2005; Truitt *et al*., 2010).

1.3 Eph Receptors and Cancer

Increasing evidence has suggested that EphB receptors and their ligands play an important role in cancer activity (Truitt *et al*., 2010). EphB receptors have been associated with malignancies in a number of examples of their overexpression and even causal involvement in oncogenesis (Lugli *et al*., 2005). EPHB2 in particular, is often overexpressed in metastatic breast carcinomas (Fox and Kandpal, 2004), while EPHB4 enhances the growth of breast tumors (Kumar *et al*., 2006). In fact, EPHB4 has been shown to be involved in cancer invasion and metastasis in a number of ways. High expression of EPHB4 is considered to be an early event in the progression of prostate cancer. Additionally, it has been shown that EPHB4 is able to contribute to increased motility in prostate cancer cells through its regulation of integrin ß8, whereby high levels of EPHB4 expression also correlated with high integrin ß8 levels (Mertens-Walker *et al*., 2015).

While there is strong evidence for Eph receptors such as EPHB4 acting to promote cancer, other Eph receptors such as EPHB6 tend to show a different effect. In fact, a strong negative correlation has been determined between breast cancer aggressiveness and the receptor, with reduced EPHB6 activity being noted in cases of aggressive breast cancer (Fox and Kandpal, 2004). For example, through interaction with c-CBL, EPHB6 mediates the activation of the cytoskeleton regulator, ABL (Truitt *et al*., 2010). Although in this work a direct CBL-ABL complex could not be detected, this study showed that silencing of c-CBL resulted in the inability of EPHB6 to successfully initiate ABL phosphorylation, resulting in a further failure to inhibit morphological changes leading to invasion. This is understandable, as in addition to its function as an E3-ubiquitilase, c-CBL has been shown to act as an adaptor, linking cell surface receptors to signaling proteins in the cytoplasm, thus regulating cytoskeletal arrangement (Swaminathan and Tsygankov, 2006). In this way, EPHB6 signaling is able to promote cell adhesion, thereby reducing invasiveness of cancer cells (Figure 1.2). To this end, studies such as those involving neuroblastomas have shown that a high expression level of EPHB6 is indicative of a lower tumor stage, while more advanced malignancies have been shown to express lower levels of EPHB6 (Truitt and Freywald, 2011). In addition, through the use of reverse transcriptase-PCR, it has been shown that EPHB6 expression is able to reduce production of matrix metalloproteinase(MMP)7 and MMP19, in breast cancer cells (Fox and Kandpal, 2009). While the mechanism of this EPHB6 action is currently unclear, the observation is important due to the ability of MMPs to promote cell invasive capabilities through degradation of the extracellular matrix. Furthermore, other studies have revealed that EPHB6 promotes anoikis in breast cancer cells, while loss of EPHB6 expression promotes a resistance to anoikis (Akada *et al*., 2014). Therefore, it can be seen that EPHB6 not only suppresses invasive phenotypes, but also acts to eliminate cells that become detached.

Because EPHB6 acts in different ways to suppress cancerous activities, it makes sense that its expression would be low, or even lost in cancer cells. In fact, EPHB6 is consistently downregulated in various malignancies, including metastatic lung cancer (Muller-Tidow *et al*., 2005), melanoma (Hafner *et al*., 2003), prostate cancer (Mohamed *et al*., 2015)**,** ovarian carcinoma (Gu *et al*., 2016), gastric cancer (Liersch-Lohn *et al*., 2016)**,** aggressive neuroblastoma (Tang *et al*., 1999; Tang *et al*., 2000), and invasive breast cancer cell lines (Fox

and Kandpal, 2004; Fox and Kandpal, 2006). All of these findings suggest that there is an important role for the EPHB6 receptor in malignancy.

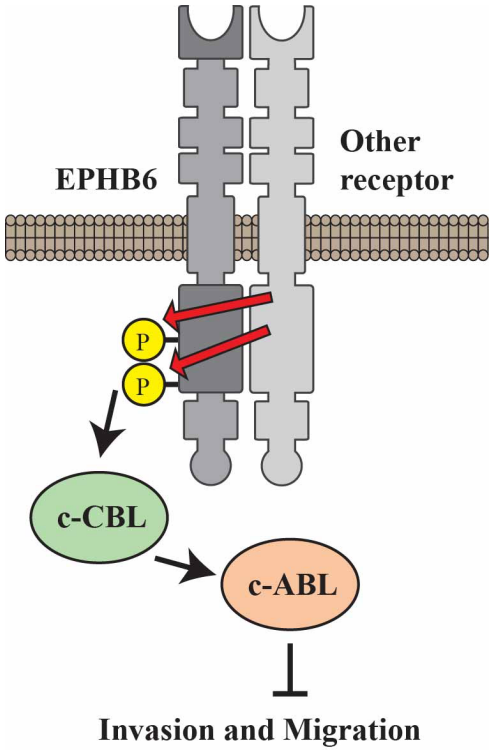

Figure 1.2 EPHB6 signals through c-CBL to suppress cancer invasion and migration

EPHB6 is kinase dead, and it often relies on interactions with other proteins in order to signal. In one such situation, EPHB6 interacts with c-CBL, which results in c-ABL phosphorylation, leading to suppression of invasion and migration. A direct CBL-ABL complex was not detected, but silencing of either CBL or ABL alone decreased EPHB6's ability to inhibit invasion and migration, thereby indicating an important role for the EPHB6-CBL-ABL signaling pathway in suppressing cancer invasiveness.

Despite the fact that overexpression of many EphB receptors often supports cancer aggressiveness, EPHB6 acts in an opposite fashion by consistently suppressing malignant activities. This agrees with EPHB6's unusual properties, as it is a catalytically inactive Eph receptor due to alterations in its kinase domain. Importantly, these alterations include replacement of lysine with a glutamine residue in the VAIK motif of kinase subdomain II, as well as replacement of aspartic acid with a serine residue in the HRD sequence of the

phosphotransfer site of subdomain VI (Gurniak and Berg, 1996; Matsuoka *et al*., 1997). Because of this, EPHB6 must initiate signaling by interacting with other EphB receptors to assure its phosphorylation (Truitt and Freywald, 2011). In fact, though many other Eph receptors are capable of promoting migration and invasion, regulation by EPHB6 has been found to reverse these effects. It has been shown that EPHB4 has a role in the phosphorylation of EPHB6, to the degree that inhibition of EPHB4 results in a blockage of EPHB6 phosphorylation (Truitt *et al*., 2010). This means that EphB6 resides in a system where, to a degree, it utilizes activated EPHB4 in order to function properly. This means that EPHB6 has an important role in regard to its interactions with EPHB4 (Pasquale, 2010). EPHB6 activation often leads to a decrease of invasiveness through its signaling, which means that it essentially reverses the overexpression activity of EPHB4 and other invasion-promoting receptors. It has been shown that in the absence of EPHB6, EPHB4 will continue to promote invasion (Truitt *et al*., 2010) (Figure 1.3). This reveals a balance that exists between the two receptors, as both have their own important role. But it should be noted that in this balance, the level of EPHB6 expression is very important, as it has the ability to turn EPHB4 from its otherwise invasion-promoting activities.

1.4 Synthetic Lethality

The correlation of decreasing EPHB6 activity with increasing cancer aggressiveness suggests that mutation or suppression of the *ephB6* gene could play an important role in malignant activity, meaning that the loss of EPHB6 could potentially be targeted for therapeutic strategies. However, because EPHB6 expression is lost, it becomes difficult to target directly, since there is no functional product that therapy can be directed toward. This means that an alternative approach must be taken. In recent years, efforts toward development of new anticancer drugs have lead to exploitation of the interactions between gene pairs, which can reveal their phenotypic relationships (Dixon *et al*., 2009). In broad terms, these genetic interactions can be classified either as negative genetic interactions (NGIs) that cause fitness defects, or as positive genetic interactions (PGI) that lead to growth and survival. Most phenotypic traits of cancer are caused by genetic alterations, including both gain-of-function mutations and loss-of-function mutations. Gain-of-function mutations can involve amplification or overactivation of proto-oncogenes, whereas loss-of-function mutations, such as

the loss of EPHB6, can be due to deletion or even epigenetic silencing of tumor suppressors. In the case of such alterations, NGIs that lead to fitness defects can be exploited for targeted therapy through an approach known as synthetic lethality (SL) (Paul *et al*., 2014). Two genes are determined to cause SL when an inactivating mutation in either gene alone leaves the cell viable, but when inactivated together, they cause cell death (Dixon *et al*., 2009) (Figure 1.4). It is generally understood that gene interactions are often functional and maybe even work in parallel cellular pathways. However, there is plasticity in the biological networks of cancer cells, meaning that genetic dependency may arise from previously unexpected pathways. Therefore, new possibilities of NGIs may arise in a situation referred to as 'induced essentiality' (Tischler *et al*., 2008).

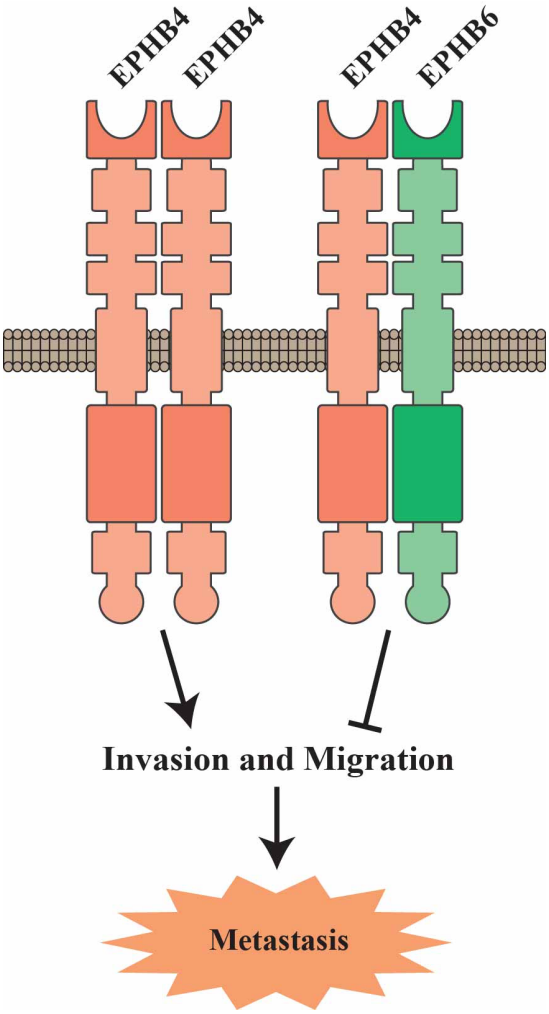

Figure 1.3 Interaction of EPHB6 and EPHB4 affects cancer metastasis

Though EPHB4 has been found acting to promote invasion and migration in many cancer cells, interaction with EPHB6 inhibits invasion and migration, thereby inhibiting metastasis.

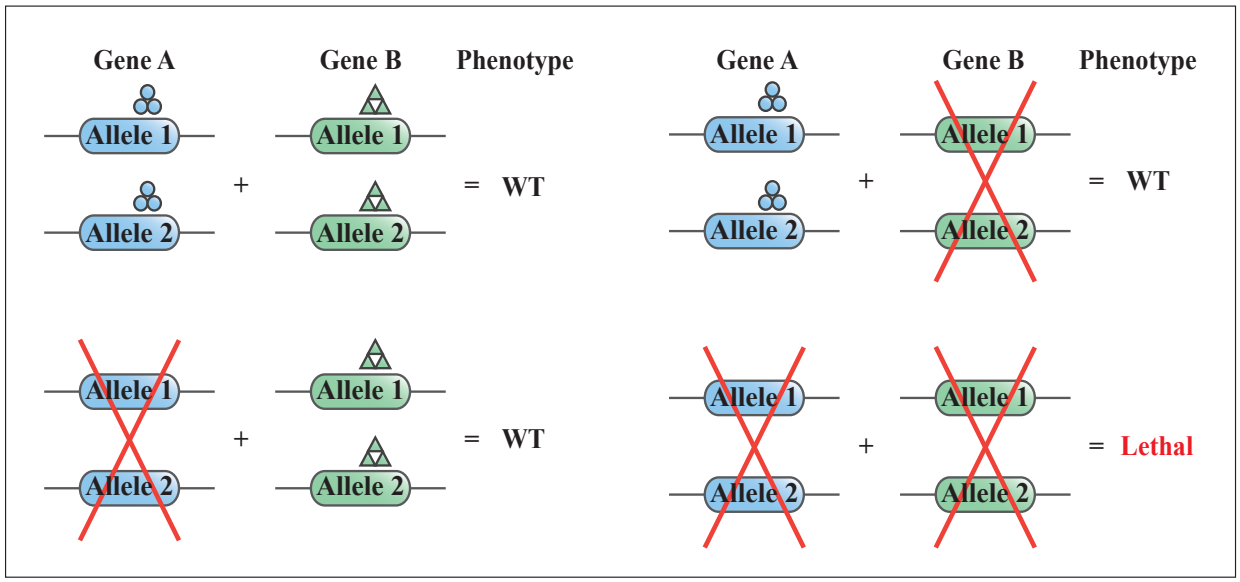

Figure 1.4 Synthetic lethality between two genes

Synthetic lethality occurs between two genes when suppression of one gene causes cell or organismal death only when the other gene is also inactivated.

Because EPHB6 expression is lost in many malignancies, it is likely that other genes may be found that exhibit a SL relationship with EPHB6. These could be genes that act in parallel pathways, or even interact directly with EPHB6 itself, whereby targeting of such gene partners could result in a NGI and subsequent loss of fitness in such cancer cells. This means that the next step toward taking advantage of EPHB6 loss is to determine a list of SL gene partners. In this regard, there are several approaches that have been used. A classical approach involves the use of model organisms to make inferences about NGI in humans. For example, information collected from the yeast *Saccharomyces cerevisiae* can be used to identify gene interactions in humans, provided that the genes and their functions are conserved (Hartwell *et al*., 1997) (Figure 1.5). Such use of model organisms has successfully predicted conserved SL interactions, such as the relationship observed between RAD54B and SOD1, wherein inhibition of SOD1 lead to apoptosis in RAD54B-deficient colorectal cancer cells (Sajesh *et al*., 2013). However, this method alone is not sufficient to comprehensively define human SL interactions, as only a portion of human genes can be mapped from organisms such as *Saccharomyces*

cerevisiae. Additional NGIs may be determined through years of experimental knowledge that have been accumulated. For example, work by Gurley and Kemp has successfully used mice to demonstrate SL interactions between ATM and DNA-PK, which are both genes known to be frequently mutated in cancer (Gurley and Kemp, 2001). Such a knowledge base will only continue to grow, providing further examples of NGIs that can be exploited for therapeutic solutions to loss-of-function mutations. However, to gain a comprehensive understanding of the many possible SL interactions that might occur with EPHB6 loss, it is important to take a more thorough approach.

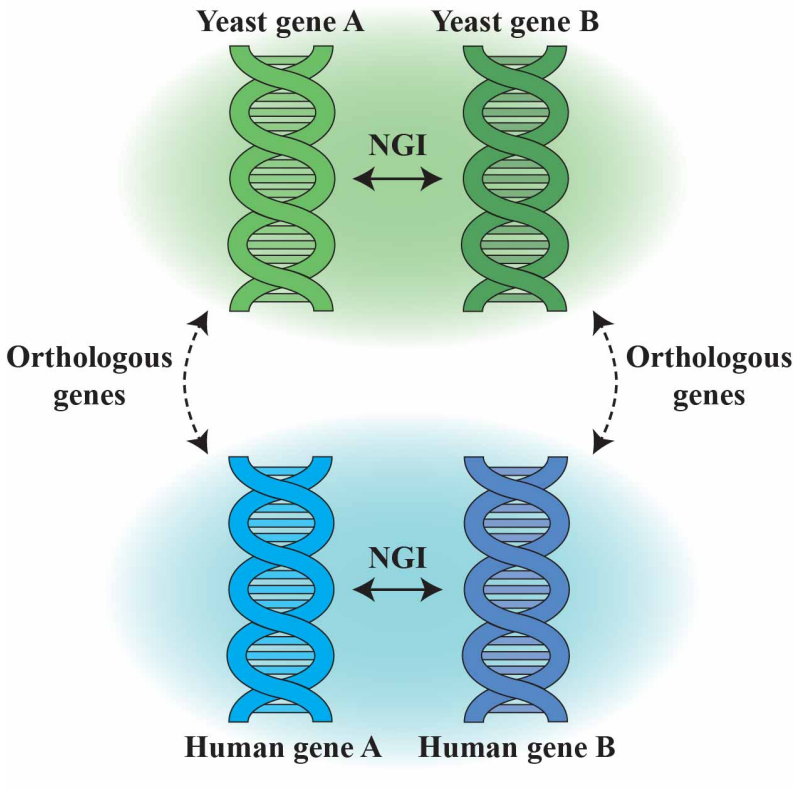

Figure 1.5 Predicting negative genetic interactions using model systems

If two genes are found to display a negative genetic interaction (NGI) in one species, such as yeast, then it may be possible that the corresponding orthologous human genes may display a similar NGI.

1.5 Pooled Screening for Synthetic Lethal Interactions

Pooled screening is a broad approach that is capable of providing NGI data for thousands of genes simultaneously. Originally, pooled screening emerged from strategies used to define genetic interactions in yeast collections, where growth defects were evaluated in a pool of yeast based on barcodes that had been incorporated into them (Pan *et al*., 2007). This process utilized transduction of cells with pooled lentiviral particles, which express unique sequences of short hairpin RNA (*sh*RNA) that can be integrated into the genome, and which could then be quantitated like a barcode (Vizeacoumar *et al.,* 2013). Because there is often genetic drift in human cancer cells, the use of isogenic cell lines is an ideal way to assess specific interactions associated with the alteration of a single molecule. The isogenic cell lines are transduced with *sh*RNAs, which are then incorporated, and the cells are cultured to allow for SL effects to occur. The SL interaction can then be quantified by amplifying the barcode sequences from a single mixture of genomic DNA using universal primers. The abundance of each sequence can then be measured using barcode microarrays (Figure 1.6). The loss of specific sequences within a mutated cell population, when compared to the isogenic parental control, would identify which *sh*RNA targets are SL. Therefore, in the case of EPHB6, two isogenic cell lines could be generated, whereby one expresses EPHB6 and one does not. Following microarray deconvolution, SL effects could be compared between the two cell lines based on the abundance of *sh*RNAs retrieved from the genomic DNA.

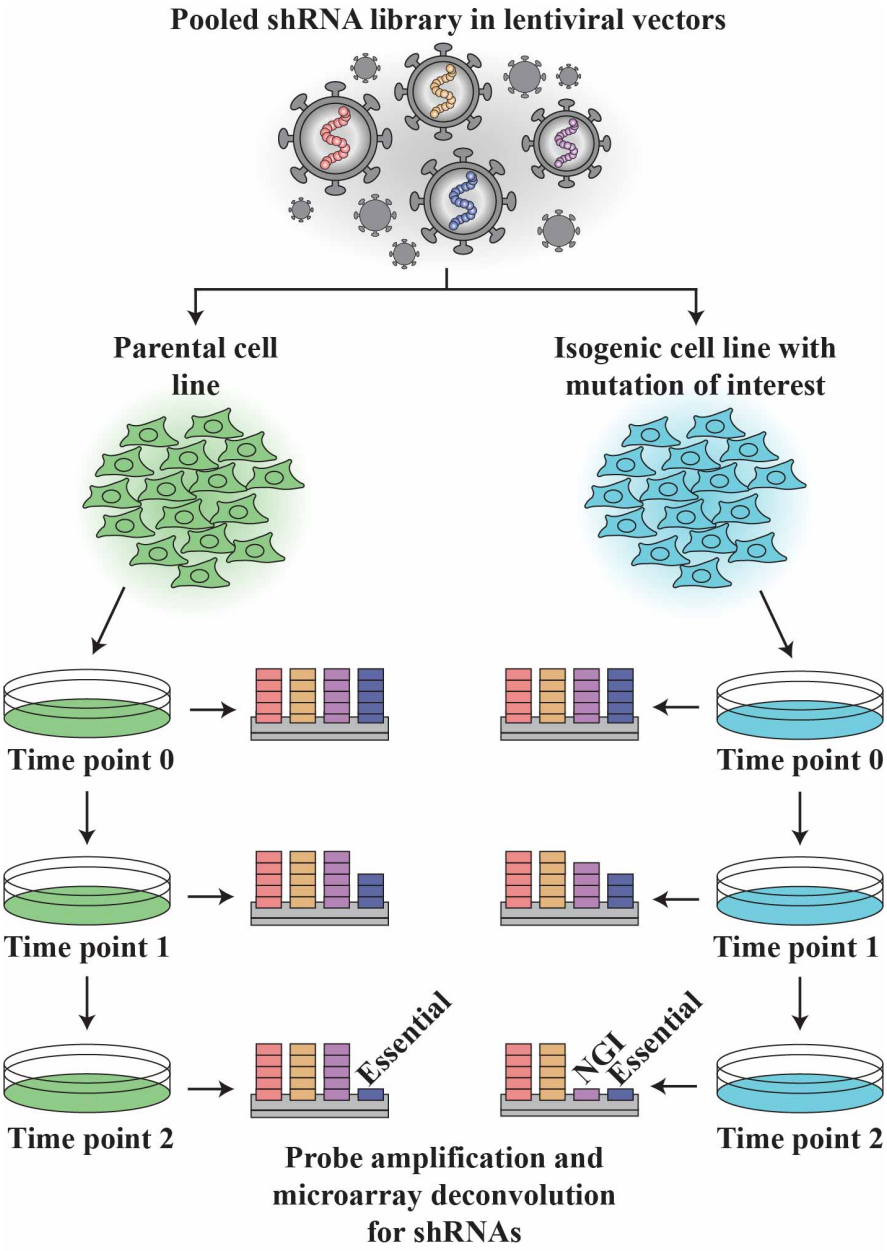

Figure 1.6 Pooled screening overview

Graphical representation showing the steps of the *sh*RNA pooled screening pipeline. A pooled *sh*RNA library, encoded in lentiviral vectors, is applied to isogenic cell lines that differ in a mutation of interest. The cells are passaged over multiple generations and genomic DNA from several time points is analyzed by microarray deconvolution. *sh*RNAs that drop out in both cell lines identify essential genes, while *sh*RNAs that drop out only in the mutated cell line identify genes that display a negative genetic interaction (NGI) with that mutation.

An extended application of the pooled screening format in cancer target identification is its application in chemical genetics. Predicting which combination of drugs will work successfully in therapy remains a major challenge. Such trials are expensive, time consuming, and often not rationally designed. To circumvent these limitations, pooled screens offer the unprecedented advantage to systematically search for targets that would act synergistically with a clinically approved drug (Bajrami *et al*., 2014). For example, a clinically approved EGFR inhibitor, cetuximab, efficiently treats patients with cancer who harbor activating mutations in EGFR. However, patients carrying activating mutations in both EGFR and KRAS will not respond to cetuximab treatment alone due to the EGFR-independent activation of KRAS effector pathways. Determination that the cell surface receptor CD83 exhibits NGI with both KRAS and cetuximab treatment offers a new therapeutic opportunity (Vizeacoumar *et al*., 2013). Such targets can be examined with a much higher degree of confidence for a positive response. Ideally, in the application of SL to the discovery of cancer drugs, the main goal would be to identify target genes which, when either mutated or inhibited, would kill cells containing a specific cancer-related alteration but would otherwise spare identical healthy cells lacking such an alteration. Therefore, in the context of low expression of EPHB6, the identification of a corresponding SL gene would be therapeutically advantageous.

1.6 Building Genetic Interaction Maps

Targeting strategies such as large-scale pooled screening do not depend on aspects such as tissue specificity, but instead are dependent on genetically determined differences between normal and cancerous tissue. However, these differences embodied by tumor genetics are not due to routine genetic redundancies. The situation in which cancer cells continue to undergo mutations as a part of their malignant evolution forces them to genetically depend on compensatory alternative pathways, resulting in a deviation from the standard redundancies. Therefore, it is essential to develop a blueprint of the cellular circuitry in order to understand the genetic dependencies of various cancer cells. Previously, researchers studying yeast adopted an epistatic mini array profile (E-MAP) approach, in which they focused on functionally related genes rather than taking a whole genome approach (Collins *et al*., 2007). Such an approach results in the construction of high-density maps for a given biological process revealing specific molecular interactions (Bassik *et al*., 2013; Roguev *et al*., 2013). Similarly,

recent methods to map interactions in human cells are just beginning (Liberali *et al*., 2014), and building a map of the cancer genome requires an E-MAP style concerted effort from the cancer genomics community. In fact, a large-scale data-driven study has recently demonstrated that SL networks can predict gene essentiality, clinical prognosis of patient survival, and even drug response (Choung *et al*., 2014). Tumor sequencing has shown that there is only a limited set of genes that are typically altered in the majority of tumors (Wood *et al*., 2007; Vogelstein *et al*., 2013). This means that creating a detailed classification of different malignancies based on their genetic causes, as well as generating a complete interactome of these genetic lesions could yield a much more accurate understanding and identification of therapeutic targets. Such a strategy depends on building an overall map of cancer cell interactions, which holds promise for personalized medicine. Therefore, large-scale pooled screens of individual gene expression, such as the EPHB6 screen carried out in this study, are necessary for a piecewise construction of such an interaction map.

2.0 Hypothesis and Objectives

2.1 Hypothesis

As EPHB6 is frequently downregulated in breast cancer malignancies, we hypothesize that the loss of EPHB6 will represent new, efficient therapeutic targets, based on its synthetic lethal interactions.

2.2 Objectives

1. Identification of synthetic lethal interactions associated with the absence of EPHB6 expression.
2. Validation of synthetic lethal interactions and rationalization of target selection.
3. Testing of selected target genes in cell lines and xenograft tumors.

3.0 Materials and Methods

3.1 Uncommon Reagents

Table 3.1 Uncommon reagents

Reagent	Supplier
7-Aminoactinomycin D (7-AAD)	BD Biosciences (Mississauga, ON, Canada)
Anti-C-SRC	Santa Cruz Biotechnology (Dallas, TX, USA)
Anti-phospho-SRC	Life Technologies (Burlington, ON, Canada)
Anti-β-tubulin	Santa Cruz Biotechnology (Dallas, TX, USA)
Bovine serum albumin (BSA)	BioShop Canada Inc. (Burlington, ON, Canada)
Dimethyl sulfoxide (DMSO)	Sigma-Aldrich (St. Louis, MO, USA)
FITC-conjugated anti-sheep secondary antibody	R&D Systems (Minneapolis, MN, USA)
Human anti-EPHB6 antibody	R&D Systems (Minneapolis, MN, USA)
KX2-391	Selleckchem (Houston, TX, USA)
Polybrene	Sigma-Aldrich (St. Louis, MO, USA)
Propidium iodide (PI)	ThermoFisher Scientific (Burlington, ON, Canada)
Puromycin	ThermoFisher Scientific (Burlington, ON, Canada)
Resazurin	R&D Systems (Minneapolis, MN, USA)
Sheep IgG control antibody	R&D Systems (Minneapolis, MN, USA)
SU6656	Santa Cruz Biotechnology (Dallas, TX, USA)

3.2 Expression Analysis and Methylation Box-and-Whisker Plots

3.2.1 Data Collection

Expression data from The Cancer Genome Atlas (TCGA) datasets for different cancer types was collected in regard to both EPHB6 and SRC. The distribution was plotted for both tumor patients and normal patients. TCGA methylome data was also collected for EPHB6 and the distribution was plotted for both tumor patients and normal patients.

3.2.2 Interpretation of Box-and-Whisker Plot Data

Data from TCGA, whether of expression or methylation, was organized into box-and-whisker plots (Figure 3.1). The plots were arranged such that, for each set of data, the values were organized into quartiles. In these plots, each box contains the first to third quartile of the data, with the median indicated by a horizontal line inside the box. Extending from the box, the

upper whisker is calculated as the third quartile plus 1.5 times interquartile range above the third quartile, and the lower whisker is calculated as the first quartile minus 1.5 times interquartile range below the first quartile, where the interquartile range is the difference between the third and first quartile. Data points outside this range are considered as outliers and were indicated by dots above the upper whisker and below the lower whisker.

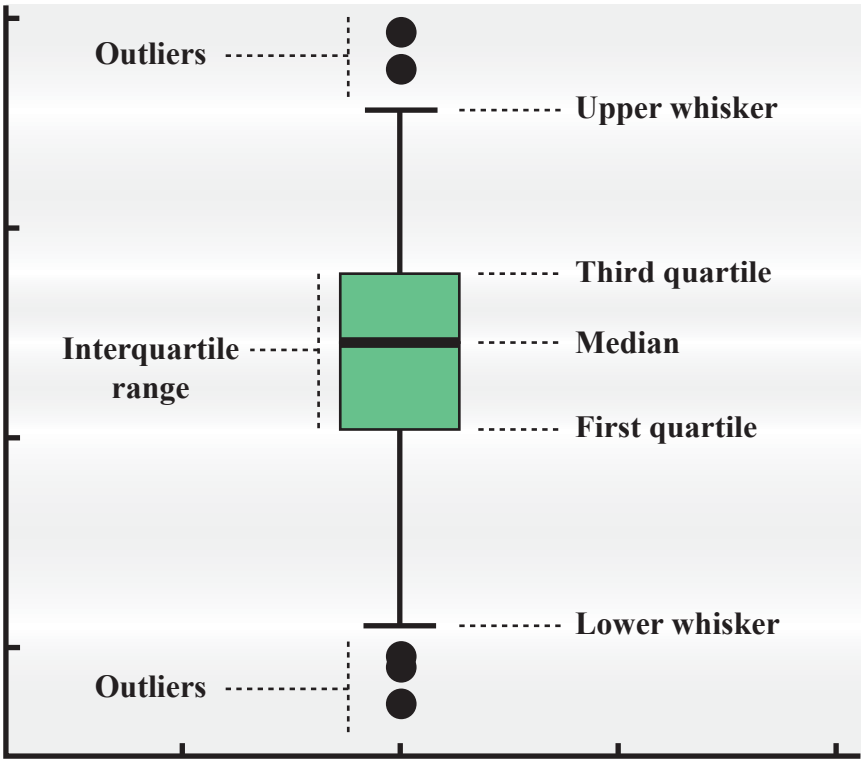

Figure 3.1 How to interpret a box-and-whisker plot

Box-and-whisker plots are arranged so that data is organized into quartiles. Each box is enclosed by the upper and lower quartiles, with a horizontal line indicating the median of the data. The interquartile range (IQR) spans from the first to the third quartile. The upper whisker is the third quartile plus 1.5 times IQR above the third quartile, and the lower whisker is the first quartile minus 1.5 times IQR below the first quartile. Additionally, the data above the upper whisker and below the lower whisker are outliers, represented as dots.

3.3 Cell Lines

3.3.1 Cell Lines and Culture Conditions

MDA-MB-231 and BT-20 cells were purchased from the American Type Culture Collection (Manassas, VA, USA). Cells were passaged for less than three months at a time

following resuscitations and therefore, no additional authentication was performed. Both MDA-MB-231 and BT-20 monolayer cultures were maintained in the DMEM medium containing 10 % FBS (Gibco, Life Technologies), 1 % penicillin/streptomycin (Gibco, Life Technologies) and 1 mM sodium pyruvate (HyClone, GE Life Sciences,).

3.3.2 Generation of Stable Cell Lines

Stable MDA-MB-231 cell lines with restored EPHB6 expression were generated by transfecting MDA-MB-231 cells with the pcDNA3 expression vector encoding wild-type EPHB6 (MDA-B6) or Myc-tagged EPHB6 (MDA-B6-M). Transfection with the empty vector was used as a control (MDA-pc3). Stable EPHB6 knockdowns were generated using EPHB6-targeting *sh*RNA encoded in lentiviral particles (Santa Cruz Biotechnology, Dallas, TX, USA). Cells were transduced in the presence of 10 μg/mL polybrene (Sigma-Aldrich), followed by 5 days of selection in the presence of 10 μg/mL puromycin (Sigma-Aldrich). Transduction with SRC-targeting *sh*RNA constructs and with green fluorescent protein (GFP)- or red fluorescent protein (RFP)-encoding cDNAs, required preparation of lentiviral particles.

3.4 Generation of Lentiviral Particles

Lentiviral particles were generated by transfection of HEK-293T cells, grown in 10 cm plates to ~70% confluence with psPAX2, pMD2.G, and with the lentiviral vector encoding the genes of interest. Transfection took place in 10 mL of tissue culture medium with 1,400 μL Opti-Mem (Gibco, Life Technologies) and 93.6 μL X-treamGENE 9 DNA Transfection Reagent (Roche, Mississauga, ON, Canada). Medium was changed after 18 hr and replaced with DMEM containing 2% w/v BSA and viral particles were collected 48 hr and 72 hr after transfection. MDA-B6 and MDA-pc3 cells were transduced with the lentiviral particles by incubation overnight in medium containing 8 μg/mL polybrene. The transduction medium was removed and transduced cells were incubated for 48 hr in cell culture medium containing 2 μg/mL puromycin.

3.5 Pooled Screening Pipeline

3.5.1 Determination of Multiplicity of Infection

3 x 10^6 MDA-B6, MDA-B6-M, and MDA-pc3 cells were infected in duplicate with 0, 0.031, 0.125, 0.5, 2, or 8 mL of the 90K lentiviral *sh*RNA library in 15 cm tissue culture dishes. Cells were transduced in the presence of 8 µg/mL polybrene. After 24 hr, media was removed and replaced with either medium containing 2 µg/mL puromycin or a control with medium alone for each viral volume. Cells were incubated in puromycin-containing media or control media for 48 hr before being collected and counted. The amount of living cells with each volume of virus was compared to the corresponding control in order to determine percentage of survival. The percentage of survival, therefore, indicated the percentage of cells that were successfully transduced and acquired puromycin resistance. The viral volume resulting in 30-40 % survival indicates a multiplicity of infection (MOI) of 0.3-0.4 (Figure 3.2).

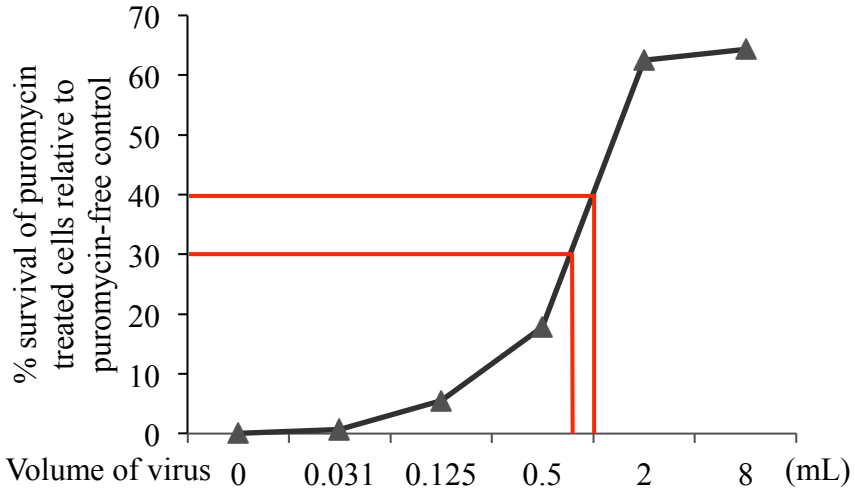

Figure 3.2 Determination of viral volume needed for 0.3-0.4 MOI

MDA-MB-231 cells were seeded in 15 cm plates with indicated volumes of lentiviral particles containing the 90K *sh*RNA library, as well as 8 µg/mL of polybrene. Cells were incubated in media containing 2 µg /mL puromycin and were counted after 48 hr and compared to puromycin-free controls. Red lines indicate the range of viral volume that corresponds to a 0.3-0.4 multiplicity of infection (MOI).

3.5.2 Transduction with 90K Library

9 x 10^7 MDA-B6, MDA-B6-M, and MDA-pc3 cells were transduced with 90K lentiviral *sh*RNAs from the RNAi Consortium lentiviral library (Sigma-Aldrich) in 15 cm tissue culture dishes at an MOI of 0.3-0.4. Cells were transduced in the presence of 8 μg/mL polybrene. After 24 hr, media was removed and replaced with DMEM containing 2 μg/mL puromycin to eliminate uninfected cells. Cells were incubated in the presence of puromycin for 48 hr before being collected and divided into 3 replicates of 1.8 x 10^7 cells per cell line. This was time point 0 (T0) of the screen, and in addition, 3 tubes of 2 x 10^7 cells from each cell line were pelleted and frozen for T0 genomic DNA.

3.5.3 Outgrowth Assay

After T0 of the screen, individual replicates of MDA-B6, MDA-B6-M, and MDA-pc3 were passaged separately. 1.8 x 10^7 cells of each replicate were passaged to fresh plates upon reaching ~80% confluency. As with T0, 3 tubes of 2 x 10^7 cells from each replicate were pelleted and frozen for genomic DNA extraction. Cells were kept in DMEM containing 2 μg/mL puromycin throughout the outgrowth assay. The assay was terminated 17 days after the initial puromycin selection (T17).

3.5.4 Genomic DNA Extraction and Processing

Frozen cell pellets from the pooled screen were thawed, resuspended in 4.5 mL PBS, and vortexed thoroughly. Genomic DNA was then extracted from the cell suspensions using the QIAamp DNA Blood Maxi Kit (Qiagen, Toronto, ON, Canada), according to the manufacturer's instructions. Following elution in buffer AE (Qiagen), the eluted DNA solution was made up to 500 μL with addition of water. 20 μL of 5 M NaCl (Sigma) was added to the DNA, followed by 1 mL of -20 °C 96 % ethanol. Tubes were mixed by inversion, and centrifuged for 15 min at 15,000 xg and 4 °C. The supernatant was aspirated and the DNA pellet was washed by the addition of 500 μL of -20 °C 70 % ethanol and subsequent inversion. Tubes were centrifuged for 10 min at 15,000 xg and 4 °C, followed by aspiration of the supernatant and air-drying for 5 min. DNA pellets were resuspended in 10 mM Tris-HCl pH 7.5 for a final concentration of 400 ng/μL and heated for 1 hr at 50 °C. Extracted genomic DNA was stored at -20 °C until the probe preparation.

3.5.5 Probe Preparation

Genomic DNA was amplified by large-scale PCR. A master mixture was prepared for each sample containing 28 µg of template DNA, 2x PCR buffer, 2x enhancer solution, 300 µM of each dNTP, 900 µM of each oligonucleotide primer (PCR_BF 5'- Biotin-AATGGACTATCATATGCTTACCGTAACTTGAA-3' and PCR_R 5'-TGTGGATGAATACTGCCATTTGTCTCGAGGTC-3') (Sigma), 50 mM $MgSO_4$, 18 µL of Platinum Pfx polymerase (Invitrogen), and water up to 1,200 µL. The master mix was divided into 50 µL aliquots for PCR. The amplification PCR reaction was carried out by denaturing once at 98 °C for 3 min, followed by (98 °C for 10 sec, 55 °C for 15 sec, 72 °C for 15 sec) x29, 72 °C for 5 min, then cooling to 4 °C. A test sample of PCR product (178 bp) was run on a 2% agarose gel to ensure that amplified *sh*RNAs did not form into cruciform structures (225 bp). The PCR products were then purified using the QIAquick PCR Purification Kit (Qiagen) according to the manufacturer's instructions. Purification was done immediately to avoid conversion of linear *sh*RNAs to cruciform structures. Amplification products were purified and digested with *Xho*I (New England Biolabs, Whitby, ON, Canada). 120 µL of PCR product was mixed with 10x NEB Buffer 2 (New England Biolabs) and 100x BSA. The digestion reaction was carried out at 37 °C for 2 hr, followed by 65 °C for 20 min, then cooling to 4 °C. The digested product was then gel purified using low-melting agarose and remaining salts were removed using a PCR Purification Kit (Qiagen). The final product was eluted in two 30 µL volumes of EB Buffer (Qiagen), with an average yield of 4 to 6 µg of purified sample.

3.5.6 Microarray Hybridization

Hybridization of the stable half-hairpins was carried out on UT-GMAP 1.0 microarrays (Affymetrix Inc, Santa Clara, CA, USA). After warming to room temperature, microarrays were preconditioned by filling with Pre-Hybridization Mix from the GeneChip Hybridization, Wash, and Stain kit (Affymetrix) and incubation in a hybridization oven at 40 °C for 30 min at 60 rpm. A hybridization mixture was prepared for each sample containing 66 µL of 2x hybridization buffer (Sigma), 1.32 µL of 50 mg/mL BSA, 1.32 µL of 10 mg/mL herring sperm DNA (Invitrogen), 1.3 µL of 5 nM B213 (Sigma), 1.38 µL of spike-in controls (Sigma), 25 µL of 20 µM blocking oligo mixture (Sigma), and 13.2 µL DMSO. To the hybridization mix was added 28.5 µL containing water and 2 µg of purified probe sample. The hybridization mix was

incubated at 99 °C for 10 min, followed by incubation at 40 °C for 5 min, and then centrifuged at 15,000 xg for 5 min. The hybridization mix was then added to the preconditioned microarray and the microarray was incubated in the hybridization oven at 40 °C for 24 hr at 60 rpm.

3.5.7 Microarray Washing

Mashing of the hybridized microarrays was carried out using Stain Cocktails 1 and 2 from the GeneChip Hybridization, Wash, and Stain kit (Affymetrix). Prior to washing, hybridization mix was removed from microarrays and stored at -20 °C, and microarrays were filled with wash buffer A. Microarray washing was carried out in a GeneChip Fluidics Station 450 (Affymetrix) according to the manufacturer's instructions using the FlexFS450_0001 protocol.

3.5.8 Microarray Scanning

Microarray scanning was carried out using a GeneChip Scanner 3000 (Affymetrix). The generated .CEL files were read using the Saskatchewan Cancer Agency differential essentiality mapping system (SCADEMS) in order to determine individual *sh*RNA probe intensities.

3.6 Computational Analysis of Screen Results

For each hairpin, the signal intensity was normalized and converted to log2 scale for each time point of both MDA-wild type, and MDA-pc3 samples. Note that the MDA-wild type samples were either MDA-B6 or MDA-B6-M. Hairpins whose signal was below the background (i.e. log2 scale of less than 8) at time point T0 were discarded. Likewise, hairpins with fold-change greater than or equal to 1.25 at a time point relative to the corresponding previous time point were also discarded. For each replicate, the difference of cumulative change (DCC) between the MDA-pc3 and MDA-wild type conditions were calculated for time points relative to the corresponding previous time point using the formula:

$$DCC = \sum_{t=1}^{T}(x_{t,k}^{pc3} - x_{t-1,k}^{pc3}) - \sum_{t=1}^{T}(x_{t,k}^{w} - x_{t-1,k}^{w})$$

where $x_{t,k}^{pc3}$ is the normalized signal intensity at time point $t \in (0,..,T)$ and for replicate $k \in (1,..,K)$ for MDA-pc3 samples. Likewise, $x_{t,k}^{w}$ represent the same for MDA-B6 or MDA-

B6-M samples. The DCC fitness score was then calculated for each gene by taking the two hairpin DCC values that were the most negative values for that gene.

$$DCC_g = arg\min_{h,h'}[\,DCC_{g,h} + DCC_{g,h'}\,]/2$$

Next, the permutation test was performed by randomly shuffling the DCC scores. This process was repeated and an empirical distribution of the DCC fitness scores over all of the genes was constructed. Finally, significant p-values for each observed fitness score were estimated as the frequency of randomized, shuffled DCC with more negative scores.

$$p = \frac{1}{NL}\sum_{r=1}^{NL} I(DCC_r < DCC_g)$$

where N is the number of genes, L is the number of repeats done to construct an empirical distribution, DCC_r is the randomized shuffle with more negative score, and $I(\,)$ is a binary indicator that gives 1 for a true statement, and 0 otherwise.

3.7 CRISPR/Cas9 Analysis and Validation

MDA-B6 and MDA-pc3 cells were seeded in 6-well plates and transduced with *src*-targeting sgRNA lentiviral constructs that also encoded BFP, from MilliporeSigma/welcome trust Sanger (Sigma-Aldrich), in the presence of 8 μg/mL of polybrene. Following 48 hr of selection with 2 μg/mL puromycin, selected cells were seeded in 96-well optical bottom plates (ThermoFisher Scientific), allowed to adhere for 24 hr, and transfected with CMV-Cas9-2A-GFP (Sigma) using the Lipofectamine LTX and Plus Reagent kit (ThermoFisher Scientific) according to the manufacturer's instructions. Cells were imaged every 24 hr for six days after transfection using the ImageXpress Micro XLS widefield automated fluorescence microscope (Molecular Devices, Sunnyvale, CA, USA) to capture BFP and GFP signals. Cells expressing BFP or co-expressing BFP and Cas9-GFP were quantified using MetaXpress version 6 (Molecular Devices). *src* knockout was confirmed using the GeneArt Genomic Cleavage Detection kit (ThermosFisher Scientific) according to the manufacturer's instructions.

3.8 Drug Sensitivity Assays

3.8.1 Drug Sensitivity for Individual Cell Lines

MDA-MB-231 and BT-20 cell monolayers were incubated in 96-well plates for 72 hr and 96 hr, respectively, in the presence of indicated concentrations of SU6656 or KX2-391, or

matching volumes of DMSO as a solvent control. Treated cells were stained using resazurin by following the manufacturer's instructions and fluorescence was measured using a SpectraMax M5 microplate reader.

3.8.2 Drug Sensitivity for Mixed Fluorescent Cell Lines

For color assays, MDA-B6 and MDA-pc3 cells were transduced with pLD-GFP-Puro and pLD-RFP-Puro (Previsouly described in Vizeacoumar *et al*., 2013) in lentiviral vectors, in medium containing 8 µg/mL polybrene. After 48 hr, transduced cells were selected in the presence of 2 µg/mL puromycin to produce stable cell lines. MDA-B6-GFP and MDA-pc3-RFP, or MDA-B6-RFP and MDA-pc3-GFP cells were co-seeded in equal numbers in 12-well plates at indicated cell densities. Seeded cells were incubated for 72 hr in the presence of 25 nM KX2-391 or a matching volume of DMSO. Treated cells were collected and quantitated by flow cytometry. Results were analyzed using the FlowJo software (FLOWJO LLC, Ashland, OR, USA).

3.9 Immunoprecipitation and Western Blotting

Cells were rinsed with ice-cold PBS and lysed using lysis buffer containing 0.1 M EDTA, 0.3 M Tris, 0.1 M NaCl, 6 mM PMSF, and 3 mM sodium ortho-vanadate. Cell debris was removed by centrifugation. For immunoprecipitation, 2-3 µg of required antibody, with 25 µL of protein G Sepharose beads (GE Healthcare Life Sciences, Baie d'Urfe, QB, Canada) were added. Samples were rotated at 4 °C overnight and beads were washed three times with lysis buffer. Cell lysates or immunoprecipitates were resolved using SDS-PAGE, followed by transfer to nitrocellulose membranes (Amersham, GE Healthcare Life Sciences). Membranes were blocked with 5 % non-fat dry milk in 0.1 % PBS/Tween-20, or with 5 % BSA in TBS/Tween-20 and incubated overnight with primary antibodies at 4 °C. At this stage, membranes were rinsed 3 times with PBS or TBS, incubated for 1 hr with fluorescently labeled secondary antibodies (LI-COR Biotechnology, Guelph, ON, Canada), and protein images were acquired using the LI-COR Odyssey imaging system (LI-COR Biotechnology). Figures were generated using the Odyssey, Carestream, and PowerPoint software. Cropping of Western blot images was done with PowerPoint. Brightness and contrast were adjusted in Western blot

images using Carestream and PowerPoint software to optimize image presentation. Western blotting with anti-tubulin was used as a loading control.

3.10 Cell Death Assays

3.10.1 Propidium Iodide Staining

For PI staining, MDA-MB-231 and BT-20 cells were incubated in glass-bottom plates (MatTek, Ashland, MA, USA) for 72 hr and 96 hr, respectively, in the presence of 25 nM and 35 nM KX2-391, respectively, and matching volumes of DMSO. Cells were then incubated in the presence of 2.7 μg/ml PI for 12 minutes and washed with phenol red-free medium. The amount of PI-stained cells was analyzed by microscopy using a Zeiss Observer Z1 at 200 x magnification. Brightness of presented confocal microscopy images was adjusted using the Zen 2012 Software (version 8.0) to optimize the visualization of PI staining. PI-stained cells were counted in at least 10 randomly captured frames, normalized on the total number of cells in matching frames, and compared between DMSO controls and treated cells.

3.10.2 7-AAD Staining

For 7-AAD staining, MDA-MB-231 and BT-20 cells were incubated in 6-well plates for 72 hr and 96 hr, respectively, in the presence of 25 nM KX2-391 and matching volumes of DMSO. Cells were collected and stained with 7-AAD according to the manufacturer's instructions, prior to flow cytometry analysis. Results were analyzed using the FlowJo software (FLOWJO LLC).

3.11 Tumor Xenograft Studies

3.11.1 Mouse Models

Breeder pairs of NOD SCID gamma mice were purchased from The Jackson Laboratory and a colony was established at the Laboratory Animal Services Unit, University of Saskatchewan. Mice were housed in sterile cages and maintained in pathogen-free aseptic rooms, while being fed autoclaved food pellets and water *ad libitum*. All animal protocols were reviewed and approved by the University of Saskatchewan Animal Research Ethics Board. Xenograft tumors were established by injection of $1x10^6$ MDA-B6 or MDA-pc3 in 100 μL PBS into the mammary fat pads of 4-6 week old female animals. Treatment with KX2-391 was

initiated when tumors became palpable. Mice were fed with either KX2-391 in DMSO (5 mg/kg) or a matching volume of DMSO diluted with ultra-pure water. Treatments were administered orally twice per day for at least 20 days. Digital caliper measurements were taken every 3 days and tumor volume was calculated by the formula $A/2*B^2$ (where A and B were the long and short diameters of the tumor respectively). At the end of the experiments animals were sacrificed and tumors were removed. Tumors were fixed in 10% buffered formalin for paraffin embedding.

3.11.2 Immunohistochemistry

For the immunohistochemical staining, tumors were dissected and fixed in 10% neutral-buffered formalin for 24-48 hr. The tumors were paraffin embedded, sectioned to 4 μm thickness, and affixed on a slide. Simultaneous dewaxing and antigen retrieval was performed on the Dako PT Link using Target Retrieval Solution-High pH (Dako Canada, Burlington, ON, Canada). Staining was performed on the Dako Autostainer Link using anti-CD34 (Abcam, Toronto, ON, Canada) antibody and the Dako FLEX DAB+Detection Kit. In each stained tumor section, 12, 3, 6 and 9 o'clock fields were imaged at 100 x magnification and the density of stained blood vessels per field was quantified using the Image-Pro Premier software.

4.0 Results

4.1 Expression Analysis

A systematic analysis of the gene expression data from The Cancer Genome Atlas (TCGA) dataset (https://tcga-data.nci.nih.gov/tcga/) was carried out in the Freywald lab by Frederick Vizeacoumar. The data provided by TCGA showed mRNA expression levels, which had been analyzed using RNA Seq V2 and was normalized using the RSEM normalization. This analysis confirmed that EPHB6 is indeed downregulated in many malignancies (Figure 4.1). Therefore, if targetable synthetic lethal partners could be determined for EPHB6, then the therapeutic results would be potentially applicable to a wide array of cancer types. Additionally, it has previously been suggested that transcriptional regulation of EPHB6 is controlled by promoter methylation in breast cancer cell lines (Fox and Kandpal, 2006). Therefore, cancer methylome data for multiple malignancies was obtained from TCGA and analyzed in the Freywald lab by Frederick Vizeacoumar. For each cancer type, one *ephB6* methylation site was selected that most negatively correlated with EPHB6 expression. This methylation site was then compared between normal and tumor tissues. In this analysis, it was found that EPHB6 is methylated in the promoter region in a number of different malignancies, including breast, colon, lung, and prostate tumors, relative to normal tissue (Figure 4.2).

Assessment of TCGA data for immunohistochemistry-based breast cancer subtype classification, carried out in the Freywald lab by Frederick Vizeacoumar, revealed that EPHB6 is also significantly downregulated in patient samples, representing very heterogeneous and aggressive tumors of the TNBC group (Figure 4.3). The data provided by TCGA showed mRNA expression, which had been analyzed using RNA Seq V2 and was normalized using the RSEM normalization. Computational analysis confirmed that 37% of TNBC samples showed a two-fold lower expression of EPHB6 when compared to expression in normal tissue samples.

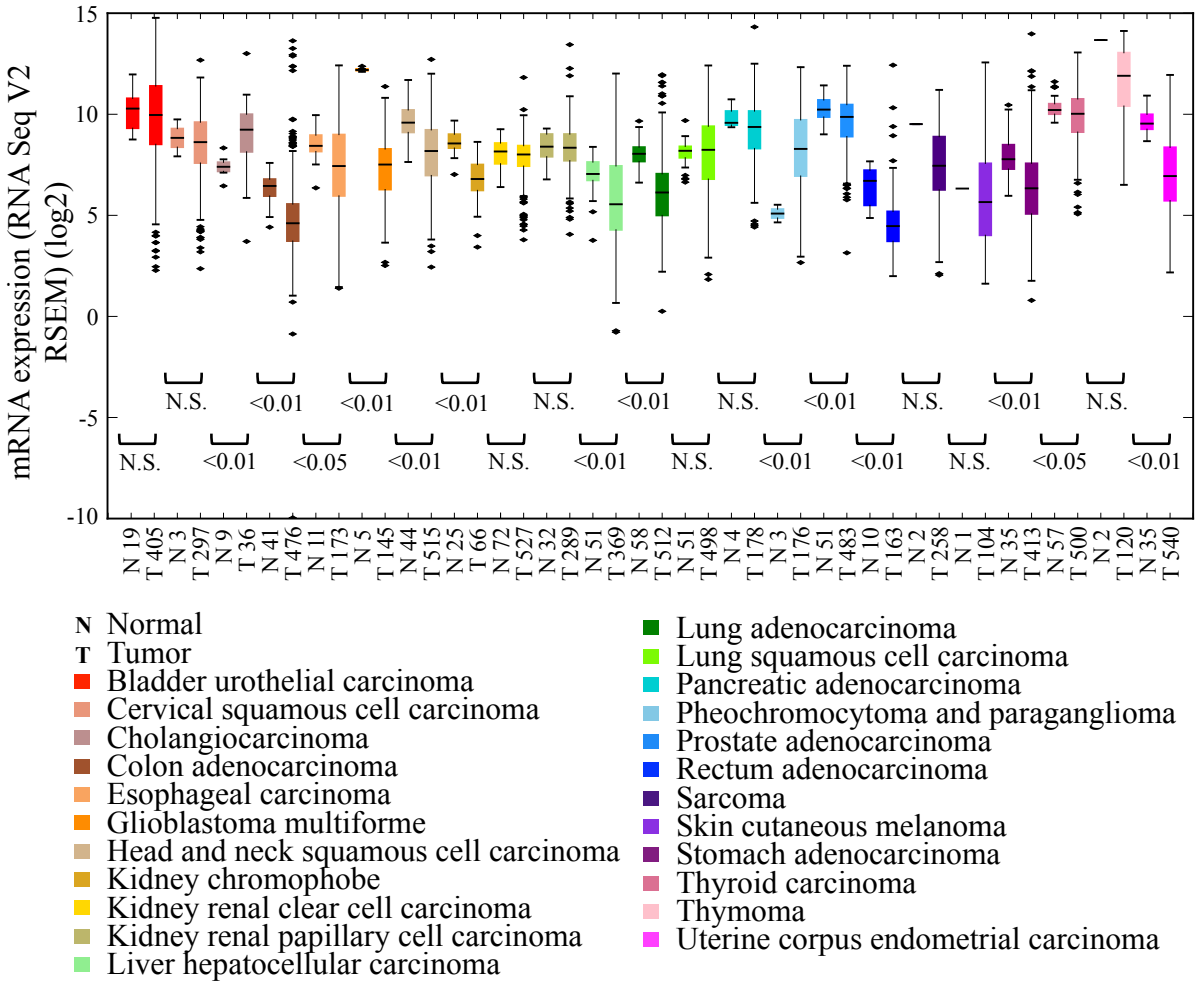

Figure 4.1 EPHB6 expression is downregulated in many malignancies

A box-and-whisker plot showing EPHB6 expression data for different cancer types and matching normal tissue controls provided by The Cancer Genome Atlas (TCGA). The data provided by TCGA showed mRNA expression levels, which had been analyzed using RNA Seq V2 and was normalized using the RSEM normalization according to TCGA standards. The number of samples analyzed is shown on the x-axis. Statistical significance was computed using the Mann-Whitney U test. A full description of box-and-whisker plot interpretation is included in the Materials and Methods.

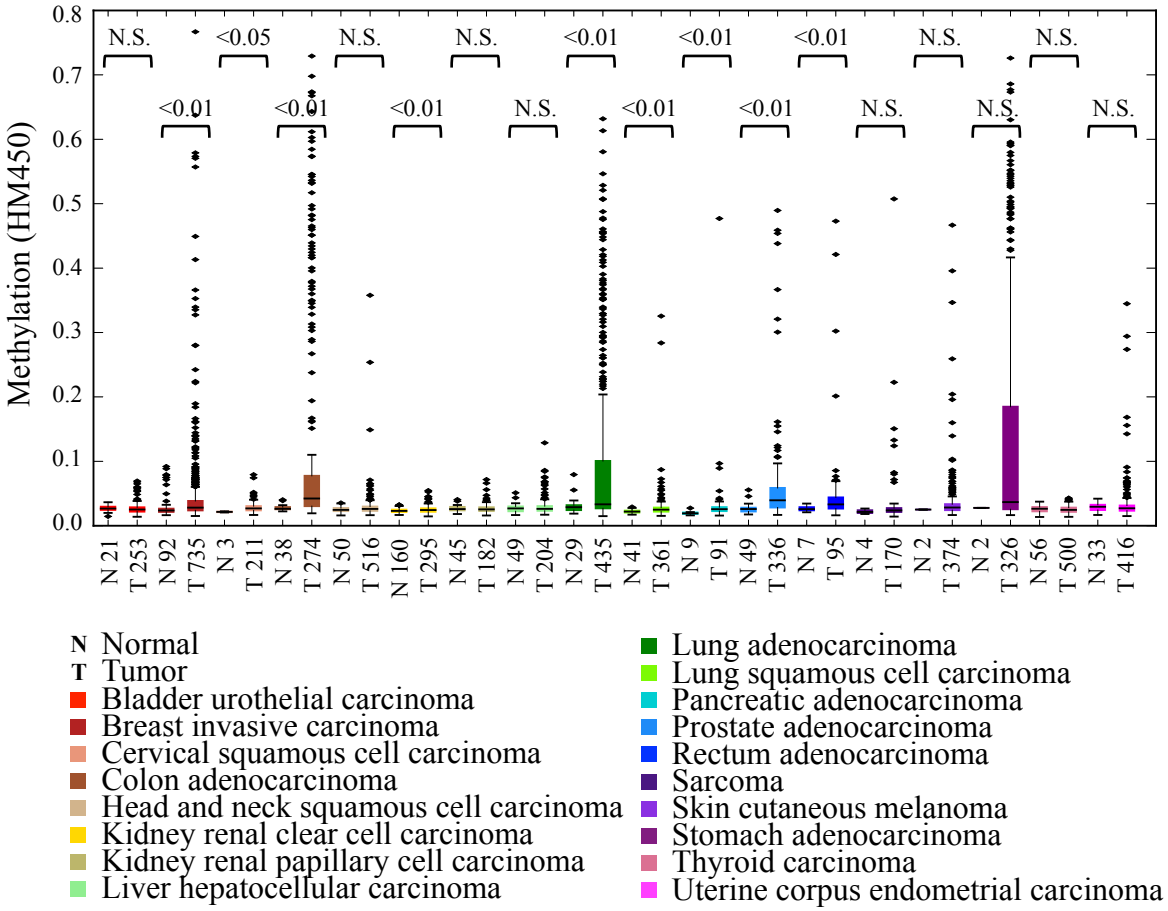

Figure 4.2 The *ephb6* promoter is methylated in multiple malignancies

A box-and-whisker plot showing *ephb6* methylation data for different cancer types and matching normal tissue controls provided by The Cancer Genome Atlas (TCGA). For each cancer type, one *ephB6* methylation site was selected that most negatively correlated with EPHB6 expression. This methylation site was then compared between normal and tumor tissues. The number of samples analyzed is shown on the x-axis. A full description of box-and-whisker plot interpretation is included in the Materials and Methods.

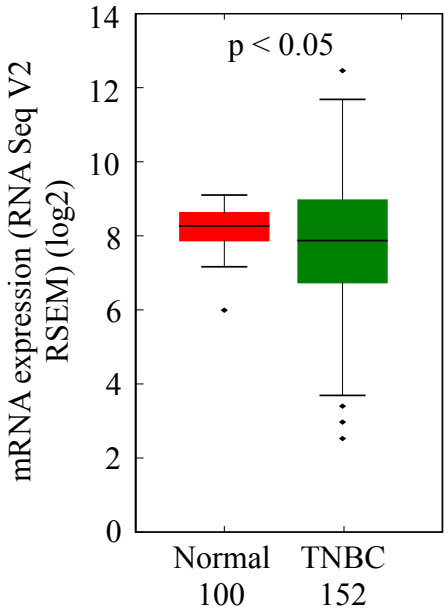

Figure 4.3 EPHB6 expression in normal and TNBC samples

A box-and-whisker plot showing EPHB6 expression data for triple negative breast cancer (TNBC) and matching normal tissue controls provided by The Cancer Genome Atlas (TCGA). The data provided by TCGA showed mRNA expression, which had been analyzed using RNA Seq V2 and was normalized using the RSEM normalization according to TCGA standards. The number of samples analyzed is shown on the x-axis. Statistical significance was computed using the Mann-Whitney U test. A full description of box-and-whisker plot interpretation is included in the Materials and Methods.

4.2 Pooled Screen Results

Because there is a strong need for a targeted therapy in TNBC, the EPHB6 SL screens were conducted in well-characterized TNBC cells, MDA-MB-231, which are often used in breast cancer-related research (Wang *et al*., 2014; Zhang *et al*., 2013). MDA-MB-231 represented an excellent model for the investigation, as the EPHB6 promoter is methylated and EPHB6 receptor expression is missing in these cells (Fox and Kandpal, 2004; Fox and Kandpal, 2006). For use in pooled screening, as well as for the following experiments, it was necessary to have isogenic cell lines that differed only in presence or absence of EPHB6 expression. Therefore, because MDA-MB-231 cells do not express EPHB6, it was necessary to generate a cell line with restored EPHB6 expression, which was achieved by transfecting MDA-MB-231 cells with the pcDNA3 expression vector encoding wild-type EPHB6 (MDA-B6), or Myc

tagged EPHB6 (MDA-B6-M). In addition, MDA-MB-231 cells were transfected with the empty pcDNA3 vector for use as a control (MDA-pc3) (Figure 4.4). These cells were described in previous work by the Freywald lab (Truitt *et al*., 2010). In addition, appropriate expression of the EPHB6 receptor on the surface of MDA-B6 and MDA-B6-M cells was confirmed by flow cytometry (Figure 4.5).

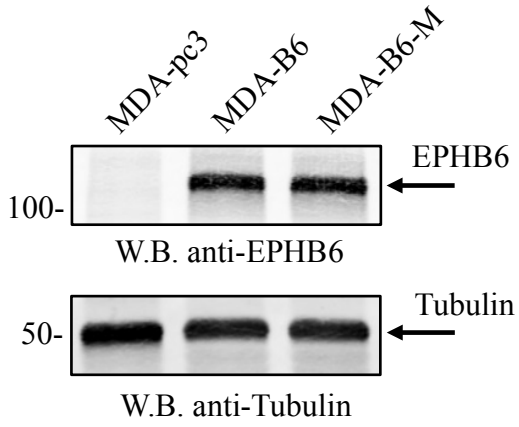

Figure 4.4 EPHB6 expression in MDA-MB-231 cells lines

EPHB6 expression is shown in EPHB6-deficient triple negative MDA-MB-231 breast cancer cells stably transfected with the pcDNA3 expression vector encoding EPHB6 (MDA-B6), myc-tagged EPHB6 (MDA-B6-M), or mock-transfected with empty pcDNA3 (MDA-pc3). Expression of EPHB6 was examined by Western blotting with anti-EPHB6 antibody. Western blotting with anti-tubulin was used as a loading control.

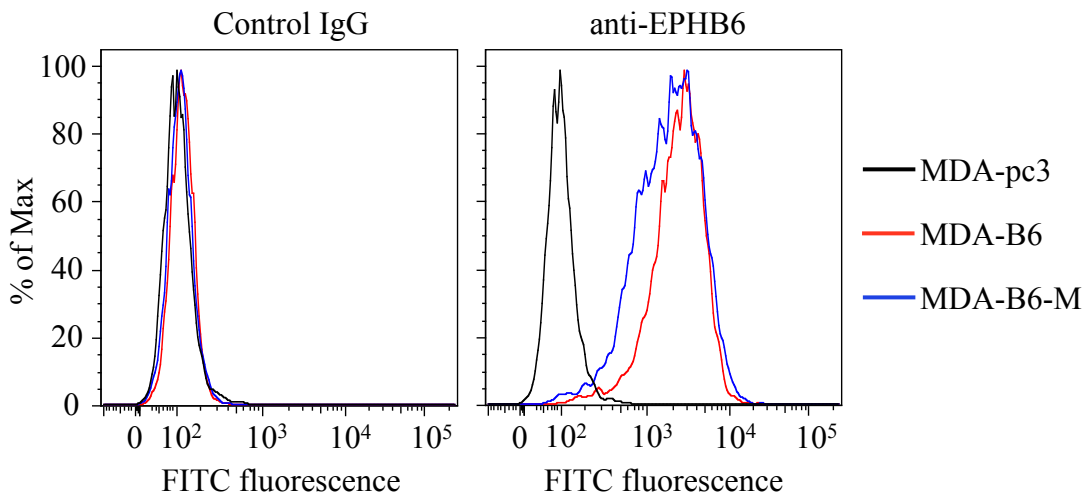

Figure 4.5 EPHB6 expression on MDA-MB-231 cell surfaces

To observe expression of EPHB6 on cell surfaces, MDA-pc3, MDA-B6, and MDA-B6-M cells were stained with anti-EPHB6 and a FITC-conjugated secondary antibody, and analyzed by flow cytometry and the FlowJo software. Matching non-specific IgG was used as a control (Control IgG).

The first experimental step was to carry out a large-scale pooled screen to assess synthetic lethal interactions with EPHB6 in MDA-MB-231 cells. A lentiviral library containing 90,000 (90K) unique viral hairpins representing 18,000 human genes was used to analyze thousands of di-genic interactions across three genetic backgrounds (MDA-B6, MDA-B6-M, and MDA-pc3) in duplicates. The cells were infected with the 90K library, selected with puromycin, and then allowed to grow for 17 days. Genomic DNA samples were taken from each replicate when cells were passaged upon reaching ~80 % confluency. These genomic DNA samples were then used to generate microarray probes, whereby gene knockdowns that caused lethality were identified by the loss of associated microarray barcodes (Figure 1.6). The abundance of each *sh*RNA was quantified through amplification of the hairpin sequences from the genomic DNA as a single mixture using vector-backbone directed universal primers. More specifically, *sh*RNAs that dropped out in MDA-pc3, but not in MDA-B6 and MDA-B6-M cell populations were expected to target genes that are SL with deficiency of EPHB6. Three time points (T0, T10, and T17) from the pooled screen were assessed by microarray analysis, in order to provide a beginning, middle, and end time point for each replicate.

After the microarrays were scanned, it was necessary to assess the correlation between the replicates from each cell line and time point. It was expected that there would be at least some difference between the replicates, not least of all due to the differential SL effects in the MDA-pc3 populations relative to the EPHB6-expressing cell lines. However, genetic interactions are not common (Boone *et al*., 2007), meaning that a high degree of similarity between the various replicates would be anticipated. A Pearson analysis measures the linear correlation between two sets of data, and was performed between each of the replicates from the pooled screen, from each cell line and time point. The data was represented as a correlation clustergram, wherein the density plots of the three screens (MDA-B6, MDA-B6-M, and MDA-pc3) showed a great deal of similarity among the replicates (Figure 4.6). This ensured high reproducibility, thereby permitting further analysis of the data.

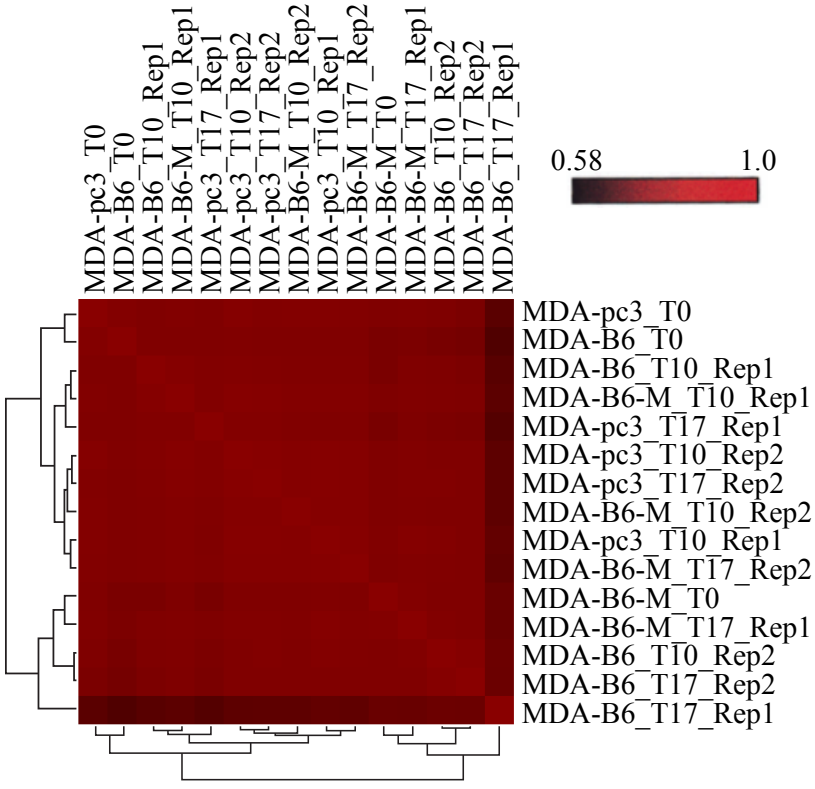

Figure 4.6 Clustergram showing Pearson correlation for EPHB6 screens

Pearson analysis showing linear correlation between replicates of the EPHB6 synthetic lethal pooled screen. Each cell line and time point is clustered using hierarchical clustering with complete linkage. The time points are T0, T10, or T17, representing days after the start of the experiment. The replicates of each cell line are represented as Rep1 or Rep2.

Because genetic interactions are rare (Boone *et al*., 2007), it was important that the different replicates all displayed a relatively high correlation, which was even observable at the different time points. This confirmed that a few highly sensitive SL interactions were detected in the screens, in both the MDA-B6 and MDA-B6-M cell lines. Once a fitness score was determined for all genes from the MDA-B6, MDA-B6-M, and MDA-pc3 screens, these values were compared to known sets of essential and non-essential genes. A recent framework was developed for evaluating the quality of genome-scale lethality screens through the assembly of reference sets of both essential and non-essential genes, while providing a Bayesian classifier of gene essentiality (Hart *et al*., 2014). Such an analysis utilizes both precision and recall, where precision indicates how accurate a screen is in determining essential genes, while recall indicates how many of the total known essential genes were identified by the screen. Precision and recall are then combined for a value known as the F-measure, meaning that F-measure correlates directly with the screen performance. Using this measuring stick, it was found that all three screens recorded excellent performance scores, with F-measures of >0.7 (Figure 4.7).

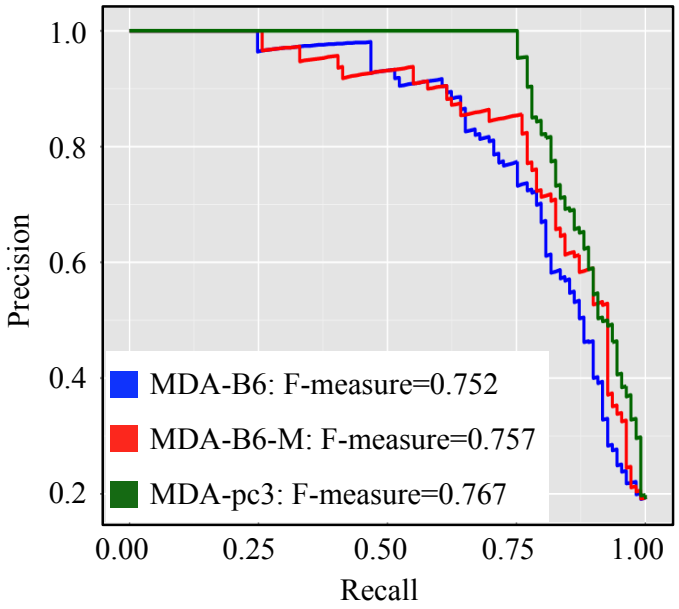

Figure 4.7 Precision recall curve showing performance of EPHB6 screens

Precision (accuracy compared to known essential genes) recall (amount of known essential genes identified by the screen) curve measuring the core essential and non-essential genes identified by the EPHB6 pooled screen against a known set of essential genes. F-measures combine precision and recall, with an F-measure of > 0.7 indicating a high performance.

The trend of the hairpins that dropped out specifically in EPHB6-deficient cells at different time points was computed as the Difference of Cumulative Change (DCC) score to identify top hits. Essentially, the DCC score represents the comparison between the EPHB6-expressing and the EPHB6-deficient cells, with a lower score denoting a lower relative fitness in the EPHB6-deficient cells for a given gene. In calculation of the DCC score, the use of the top two hairpin scores per gene increased the confidence of the SL hits and allowed avoidance of possible off-target effects. Both myc-tagged (MDA-B6-M) and untagged (MDA-B6) versions of EPHB6 in EPHB6-positive cells were used for comparison against EPHB6-deficient MDA-pc3. Therefore, the DCC scores from both screens (MDA-B6-M vs. MDA-pc3 and MDA-B6 vs. MDA-pc3) were compared, and the overlap was used to identify 113 statistically significant overlapping hits ($P < 0.05$) (Figure 4.8) (Table 4.1). This approach identified a number of potential therapeutic candidates that predominantly functioned in cell signaling pathways (Figure 4.9), including molecules such as DDR2, SRC, ROCK, and MET.

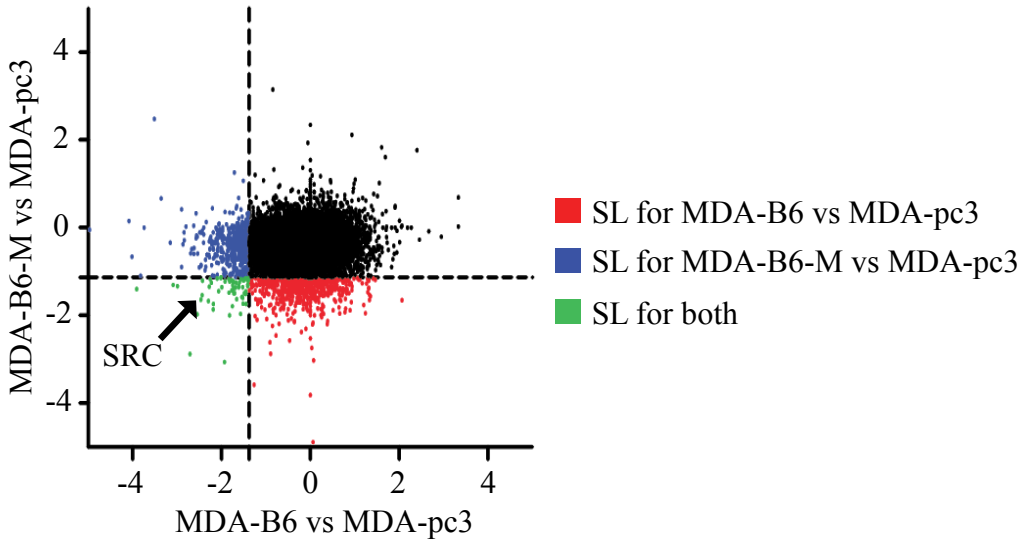

Figure 4.8 Overlapping significant hits from both EPHB6-positive screens

Scatter plot showing the difference of cumulative change (DCC) score for every gene when MDA-pc3 is compared to both MDA-B6 and MDA-B6-M. A low DCC score for a given gene means that when that gene is inactivated, there is a loss of fitness in the EPHB6-deficient cells, but not in the EPHB6-expressing cells. Alternatively, a high DCC score means the fitness of EPHB6-deficent cells is high relative to that of EPHB6-expressing cells when the given gene is inactivated.

Table 4.1 Significant EPHB6 synthetic lethal hits

Gene ID	Gene Symbol	Gene ID	Gene Symbol	Gene ID	Gene Symbol
22848	AAK1	51575	ESF1	5188	PET112L
84680	ACCS	54932	EXD3	9867	PJA2
2182	ACSL4	84668	FAM126A	5315	PKM2
348158	ACSM2B	220965	FAM13C	5334	PLCL1
202	AIM1	2091	FBL	10631	POSTN
23780	APOL2	2210	FCGR1B	5636	PRPSAP2
55156	ARMC1	2260	FGFR1	167681	PRSS35
405	ARNT	2574	GAGE2C	51195	RAPGEFL1
570	BAAT	2632	GBE1	9584	RBM39
28984	C13orf15	81025	GJA9	5979	RET
56260	C8orf44	65056	GPBP1	9475	ROCK2
56934	CA10	3001	GZMA	6235	RPS29
1233	CCR4	3601	IL15RA	122042	RXFP2
925	CD8A	54756	IL17RD	55176	SEC61A2
997	CDC34	3656	IRAK2	5268	SERPINB5
28316	CDH20	23281	KIAA0774	219855	SLC37A2
1044	CDX1	57542	KLHDC5	254428	SLC41A1
64781	CERK	342574	KRT27	6533	SLC6A6
254263	CNIH2	84456	L3MBTL3	162394	SLFN5
1355	COX15	64175	LEPRE1	4184	SMCP
1348	COX7AP2	4294	MAP3K10	23049	SMG1
151835	CPNE9	23101	MCF2L2	57154	SMURF1
1441	CSF3R	1954	MEGF8	8303	SNN
168002	DACT2	4233	MET	11166	SOX21
4921	DDR2	79083	MLPH	6659	SOX4
8694	DGAT1	93380	MMGT1	6709	SPTAN1
55567	DNAH3	51373	MRPS17	6714	SRC
4189	DNAJB9	51649	MRPS23	30968	STOML2
1776	DNASE1L3	4693	NDP	374618	TEX9
1801	DPH1	4722	NDUFS3	55706	TMEM48
1781	DYNC1I2	4763	NF1	7132	TNFRSF1A
8798	DYRK4	28511	NKIRAS2	7166	TPH1
1909	EDNRA	93034	NT5C1B	22974	TPX2
30846	EHD2	10204	NUTF2	80128	TRIM46
84285	EIF1AD	57489	ODF2L	25989	ULK3
2020	EN2	56288	PARD3	8975	USP13
2036	EPB41L1	64081	PBLD	23174	ZCCHC14
29924	EPN1	27043	PELP1		

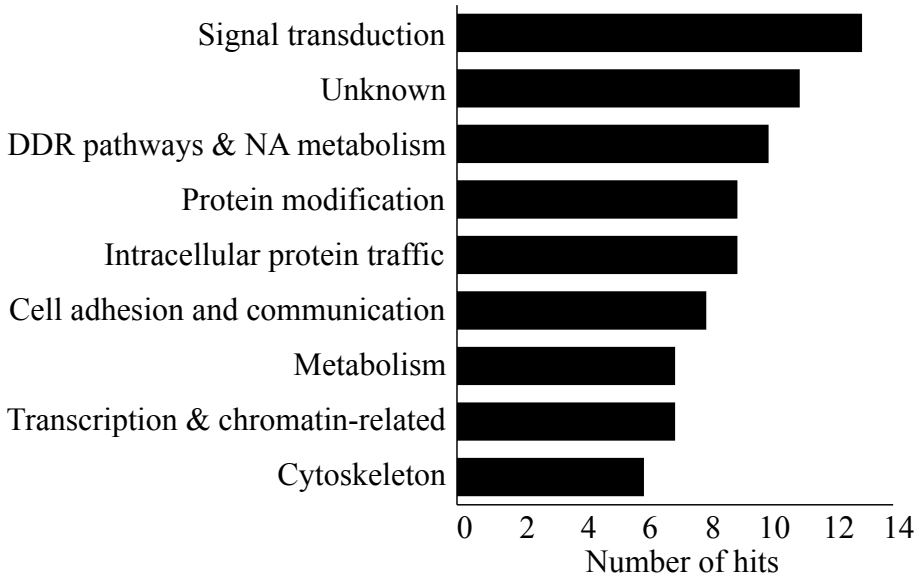

Figure 4.9 Known Gene Ontology terms for EPHB6 significant hits

Analysis showing Gene Ontology Consortium (geneontology.org) terms associated with each significant hit in the EPHB6 synthetic lethal screen. Genes are assigned specific Gene Ontology terms based on a combination of the molecular function, cellular component, and biological process associated with that gene.

In addition to analysis using Gene Ontology terms, further analysis was carried out for of the 113 significant hits using the Compartments Subcellular Localization Database (CSLD) (compartments.jensenlab.org). The CSLD provides information on the most probable cellular locations of expressed gene products based on past research. Consistent with the receptor functions of EPHB6, and its inherent cell membrane affiliation, cellular analysis with CSLD revealed that several of the functional products of significant gene hits also spatially associated with the cell surface (Figure 4.10). This was interesting to note, as genetic interactions are rare (Boone *et al*., 2007), and so it would be expected, though not necessarily required, that at least some of the negative genetic interactions with EPHB6 would also be found associated with the same cellular region. In fact, more than 30 % of the 113 significant hits had a high likelihood of expression either at the cellular membrane, or in the extracellular space.

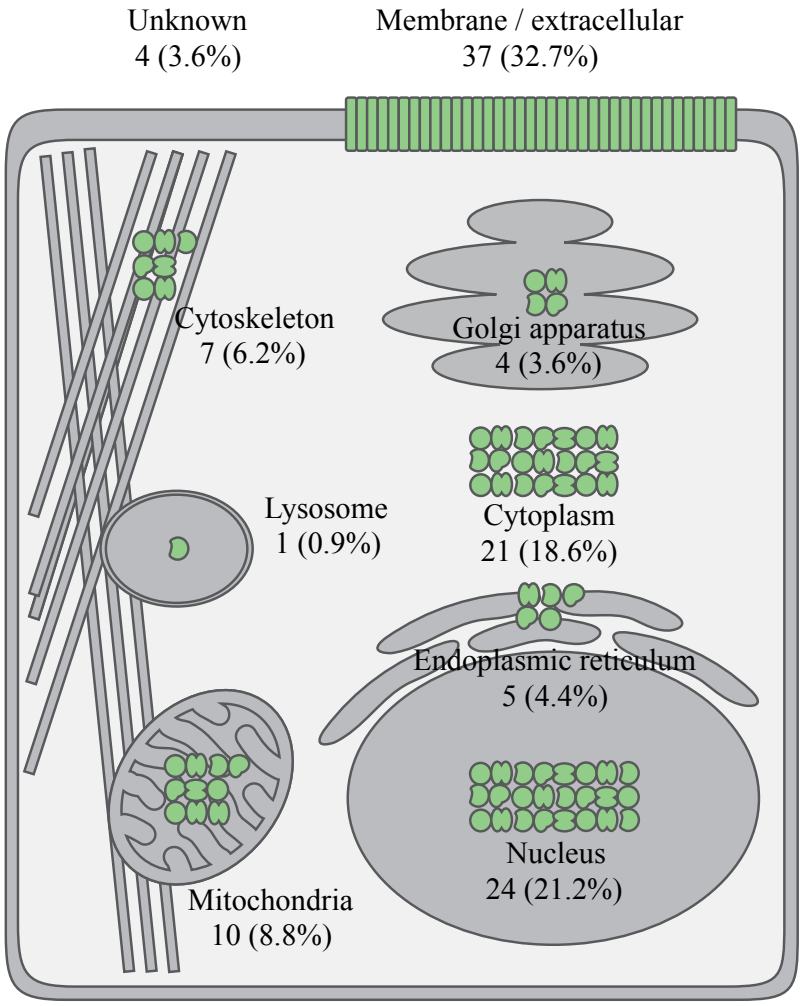

Figure 4.10 Expected cellular locations of significant hits

Expected cellular distribution of each significant hit from the EPHB6 synthetic lethal screen according to information from the Compartments Subcellular Localization Database (compartments.jensenlab.org). The database identifies protein cellular distribution based on literature, high-throughput screens, automatic text mining, and sequence-based predictions.

4.3 Identification and Validation of SRC as a Therapeutic Target

The next step was to prioritize a potential target for further validation from the EPHB6 SL screen. To systematically identify potential candidates for further investigation, a novel approach was utilized, whereby SL data was coupled with gene expression profiling. It seemed rational that increased expression of a SL gene in EPHB6-deficient cells would most likely represent an essential compensatory mechanism. In order to identify such essential molecules, the correlation between EPHB6 expression and that of each SL hit was compiled and analyzed.

This analysis was carried out across 25 different tumor types and specifically searched for a negative correlation between expression of EPHB6 and a SL gene. Remarkably, it was found that the non-receptor tyrosine kinase, SRC, was clustered with a set of genes that mostly correlated negatively with EPHB6 expression (Figure 4.11). Consistent with this finding, TCGA data, analyzed in the Freywald lab by Frederick Vizeacoumar, showed that SRC is overexpressed in multiple malignancies (Figure 4.12).

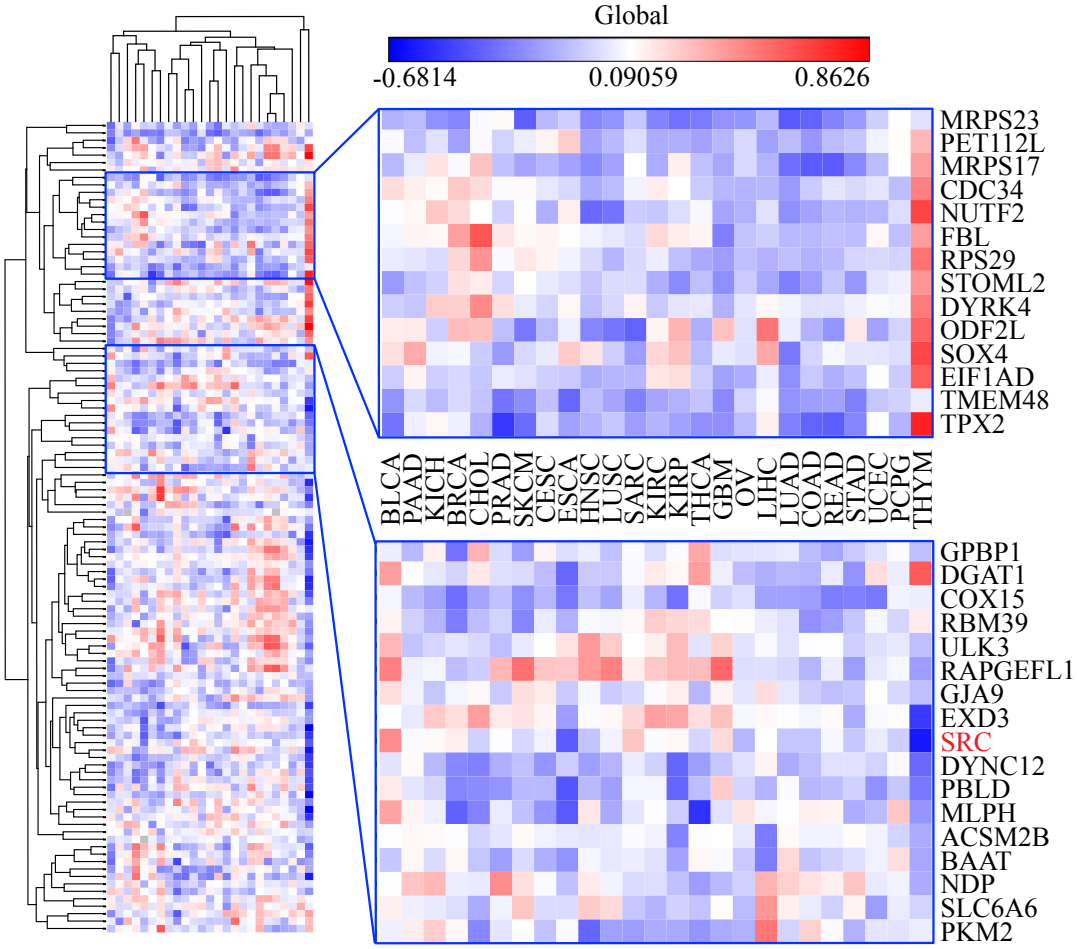

Figure 4.11 SRC clusters with genes negatively correlated with EPHB6 expression

Correlation clustergram showing the expression of significant synthetic lethal hits (vertical) from the EPHB6 screen, relative to EPHB6 expression in various cancer types (horizontal). Negative expression correlations are blue and positive correlations are red. Expression data was provided by The Cancer Genome Atlas (TCGA). The data provided by TCGA showed mRNA expression levels, which had been analyzed using RNA Seq V2 and was normalized using the RSEM normalization.

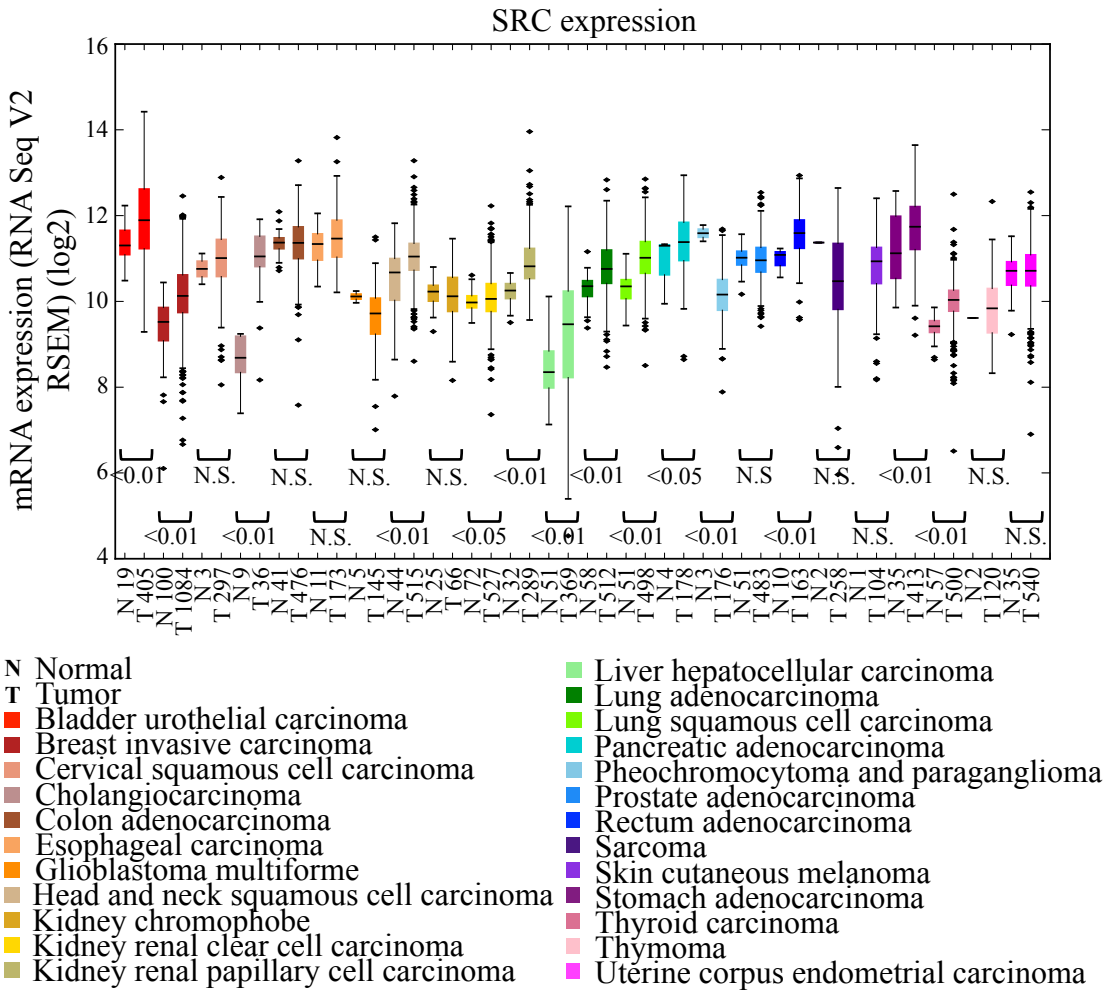

Figure 4.12 SRC is overexpressed in many malignancies

A box-and-whisker plot showing SRC expression data for different cancer types and matching normal tissue controls provided by The Cancer Genome Atlas (TCGA). The data provided by TCGA showed mRNA expression levels, which had been analyzed using RNA Seq V2 and was normalized using the RSEM normalization according to TCGA standards. The number of samples analyzed is shown on the x-axis. Statistical significance was computed using the Mann-Whitney U test. A full description of box-and-whisker plot interpretation is included in the Materials and Methods.

Not only is SRC often overexpressed in multiple malignancies, but it is also highly connected to many of the other hits obtained from the screen. A functional network analysis of all of the 113 hits was carried out using the STRING 10 database (http://string-db.org), which quantitatively integrates genomic and previously established interactions. This analysis

positioned SRC as a hub with high connectivity to the rest of the hits (Figure 4.13).

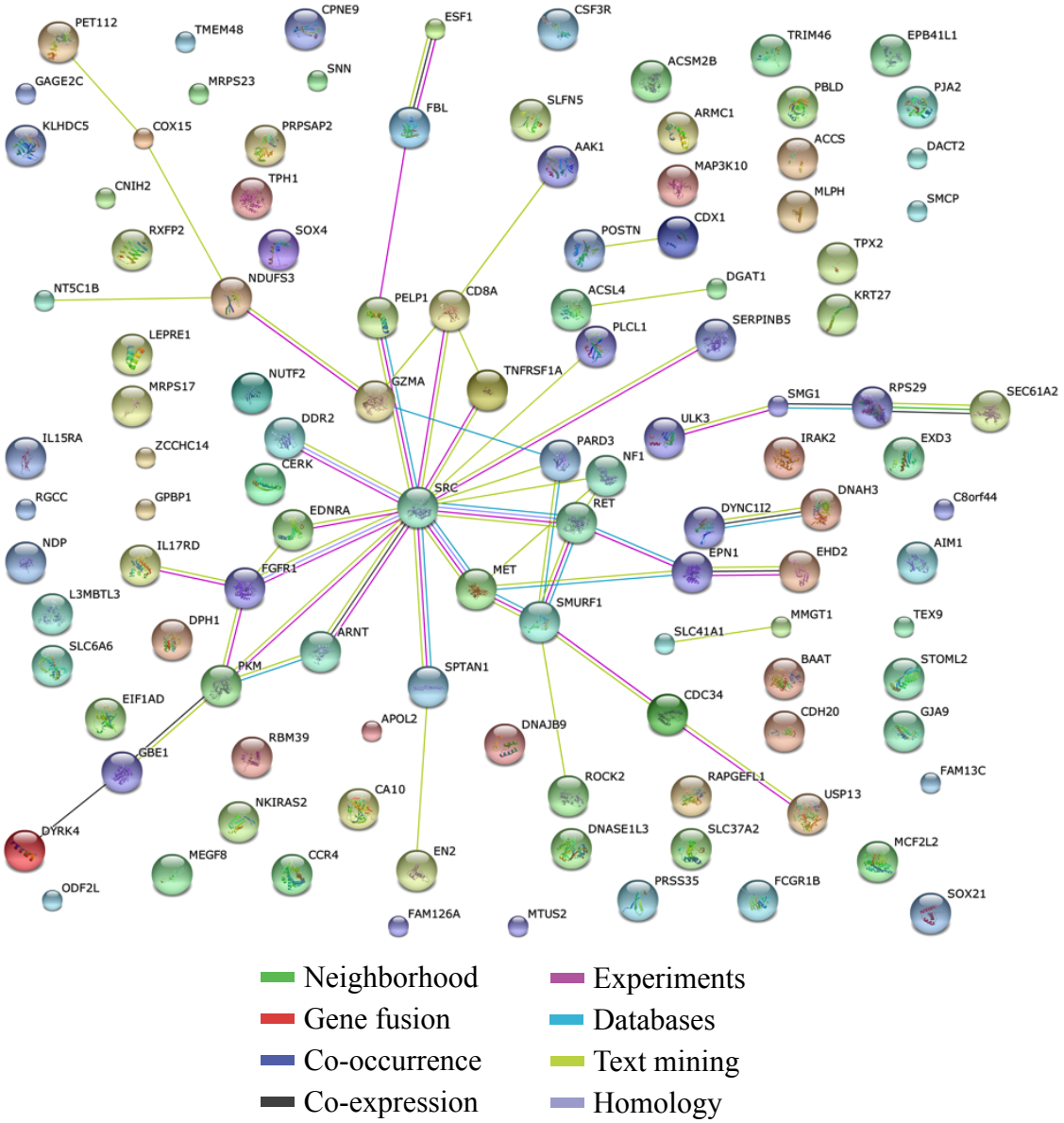

Figure 4.13 STRING 10 analysis of EPHB6 synthetic lethal hits

Network generated from the STRING 10 database (http://string-db.org) based on known interactions of the 113 significant hits from the EPHB6 synthetic lethal screen. The interactions include both direct (physical) and indirect (functional) associations. Each interaction stems from computational predictions, from knowledge transfer between organisms, and from interactions aggregated from other databases.

SRC was identified as a significant SL hit associated with EPHB6 deficiency (Table 4.1). It was also shown to be negatively correlated with EPHB6 expression (Figure 4.11), suggesting that it plays some compensatory role, which was validated by the observation that SRC is overexpressed in a number of different malignancies (Figure 4.12). Lastly, SRC is shown to have a high connectivity to many of the other 113 SL hits from the EPHB6 screen. Overall, these observations identified SRC as a molecule of choice for targeting EPHB6-deficient breast cancer cells. Therefore, to validate the SL properties of SRC in EPHB6-deficient cells, an individual hairpin that efficiently silenced SRC expression was used in the MDA-B6 and MDA-pc3 cell lines (Figure 4.14A). In agreement with the SL screen, it was found that silencing of SRC with this hairpin caused a preferential suppression of EPHB6-deficient MDA-pc3 cells (Figure 4.14B).

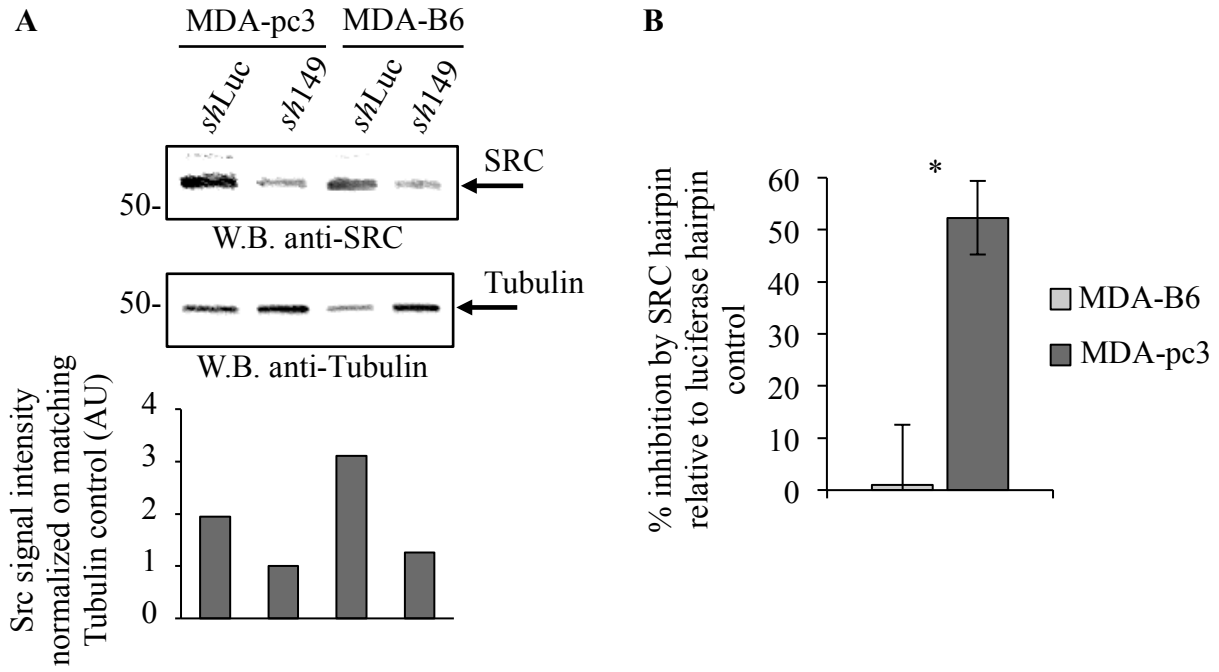

Figure 4.14 Validation of synthetic lethality with a SRC-targeting hairpin

A) SRC expression after MDA-pc3 and MDA-B6 cells were transduced with SRC-targeting *sh*RNA (*sh*149), or non-silencing shLuciferase (*sh*Luc). SRC expression was analyzed by Western blotting with anti-SRC. Western blotting with anti-tubulin was used as a loading control. B) MDA-pc3 and MDA-B6 cells were transduced with SRC-targeting *sh*RNA and cultured for 96 hr after puromycin selection. Cells were stained with resazurin and fluorescence was measured using a SpectraMax M5 microplate reader to determine cell suppression. The experiment was performed at least three times. *, $P < 0.05$.

To completely exclude the involvement of potential off-target effects of *sh*RNA molecules, a further validation of the SL relationship between EPHB6 and SRC was carried out using the CRISPR/Cas9-based system (Figure 4.15). CRISPR/Cas9 utilizes single guide RNAs (sgRNA), which direct Cas9 to the gene of interest for cleavage. Because Cas9 only cuts the individual gene of interest, this allows for effective knockout, with little off-target effect. To this end, MDA-B6 and MDA-pc3 cells were transduced with a construct containing an sgRNA targeting *src*. The stably transduced cells were then transfected with Cas9, thereby initiating knockout of *src*, and were imaged over a period of six days (Figure 4.16). Consistent with the earlier observations based on SRC-silencing *sh*RNAs, knockout of *src* with the CRISPR/Cas9 approach mostly affected EPHB6-defficient MDA-pc3 cells and produced only a limited effect on MDA-B6, thus further confirming the SL interaction between EPHB6 and SRC (Figure 4.17A). The preferential negative effect on MDA-pc3 cell survival, compared to MDA-B6 cells, was additionally confirmed through determination that both MDA-B6 and MDA-pc3 were both transfected with Cas9 with a similar efficiency (Figure 4.17B). Efficiency of cleavage of *src* by Cas9 was confirmed using the GeneArt Genomic Cleavage Detection kit (Figure 4.18).

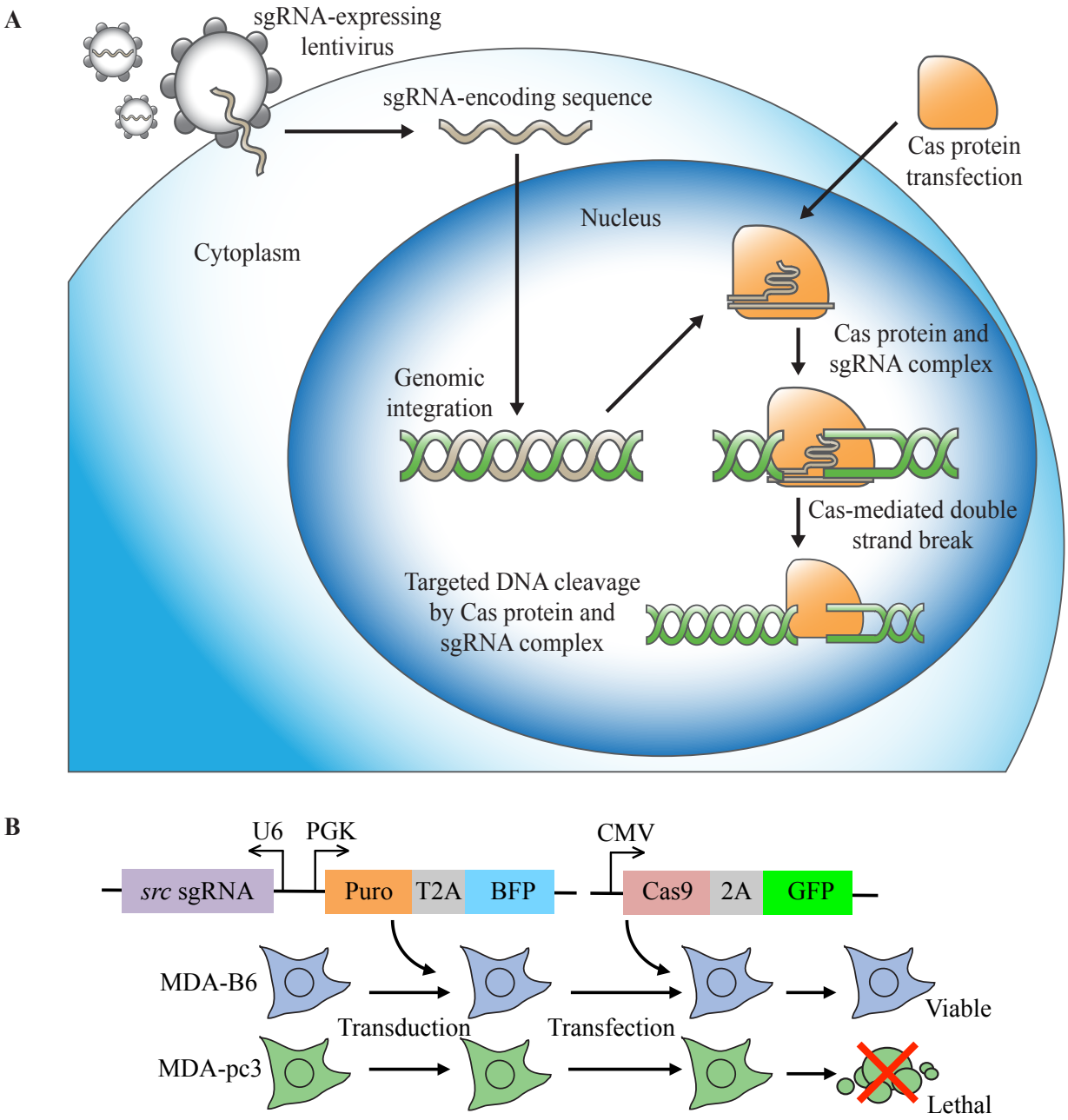

Figure 4.15 Outline of the CRISPR/Cas9 method used for cleavage of *src*

A) A sgRNA-encoding plasmid is inserted into the cell via a lentiviral vector and is directed to the genome where it is integrated. The encoded sgRNA then forms a complex with a cellular apoptosis susceptibility (Cas) protein. In this scenario, Cas is inserted into the cell via transient transfection. Once the complex is formed, the sgRNA directs Cas to the target gene where Cas mediates a double strand break and knockdown of the gene at the genomic level. B) Schematic representation of the CRISPR/Cas9 strategy to validate the SL interaction. Cells of interest are stably transduced with a construct encoding *src*-targeting sgRNA and blue fluorescent protein (BFP), followed by the selection in the presence of 2 µg/mL of puromycin. The selected cells are transiently transfected with a construct encoding Cas9-2A-GFP.

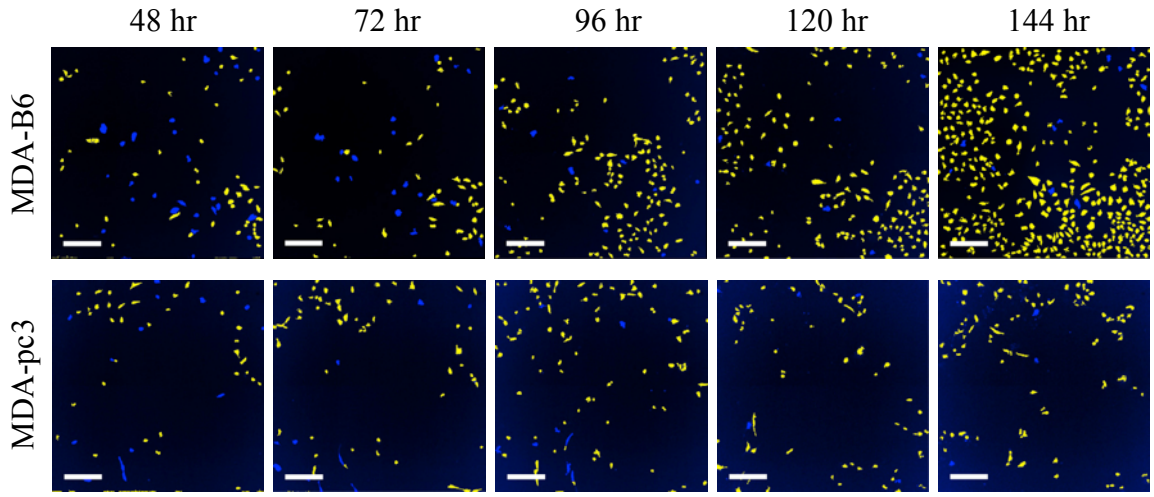

Figure 4.16 Images of MDA-B6 and MDA-pc3 cells following Cas9 transfection

MDA-pc3 and MDA-B6 cells were stably transduced with a *src*-targeting sgRNA construct that also encoded the blue fluorescent protein (BFP) and selected in the presence of 2 μg/ml of puromycin. The selected cells were transiently transfected with Cas9-GFP in 96-well plates. Green and blue fluorescence was quantified using the ImageXpress Micro XLS widefield automated fluorescence microscope and the MetaXpress version 6 software. The figure shows representative images of MDA-pc3 and MDA-B6 cells at consistent locations over the period of six days following Cas9 transfection. Yellow-highlighted cells represent those expressing BFP, while blue-highlighted cells represent those co-expressing BFP and GFP, according to the MetaXpress standard software settings. Scale bar, 250 μM.

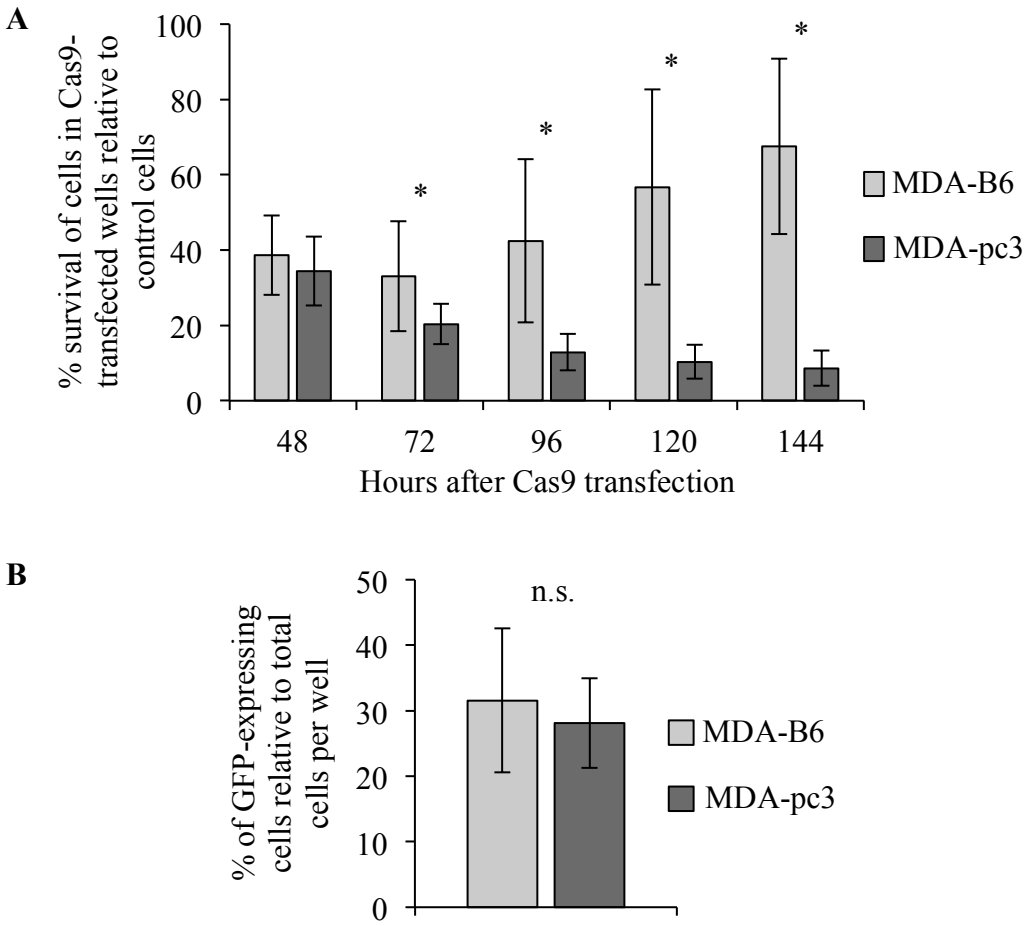

Figure 4.17 Effect of *src* knockout by CRISPR/Cas9 and validation of transfection

A) Following Cas9 transfection, surviving transfected cells were quantified at the indicated time points with the ImageXpress Micro XLS microscope and the MetaXpress software. The graph represents survival of transfected cells as a percentage relative to numbers of matching cells expressing sgRNA/BFP only. The graph represents two independent experiments. At least ten wells were analyzed per condition in each experiment. *, $P < 0.05$, Student's t-test. B) MDA-pc3 and MDA-B6 cells were stably transduced with the *src*-targeting sgRNA construct that also encoded the blue fluorescent protein (BFP) and selected in the presence of 2 μg/ml of puromycin. The selected cells were transiently transfected with Cas9-GFP in 96-well plates and consistent transfection efficiency was confirmed by quantifying cells with green and blue fluorescence using the ImageXpress Micro XLS widefield automated fluorescence microscope and the MetaXpress version 6 software. The graph represents the percentage of cells co-expressing Cas9-GFP and BFP relative to total cell numbers per well 48 hr after transfection. The graph represents two independent experiments. At least ten wells were analyzed per condition in each experiment. n.s., statistically not significant.

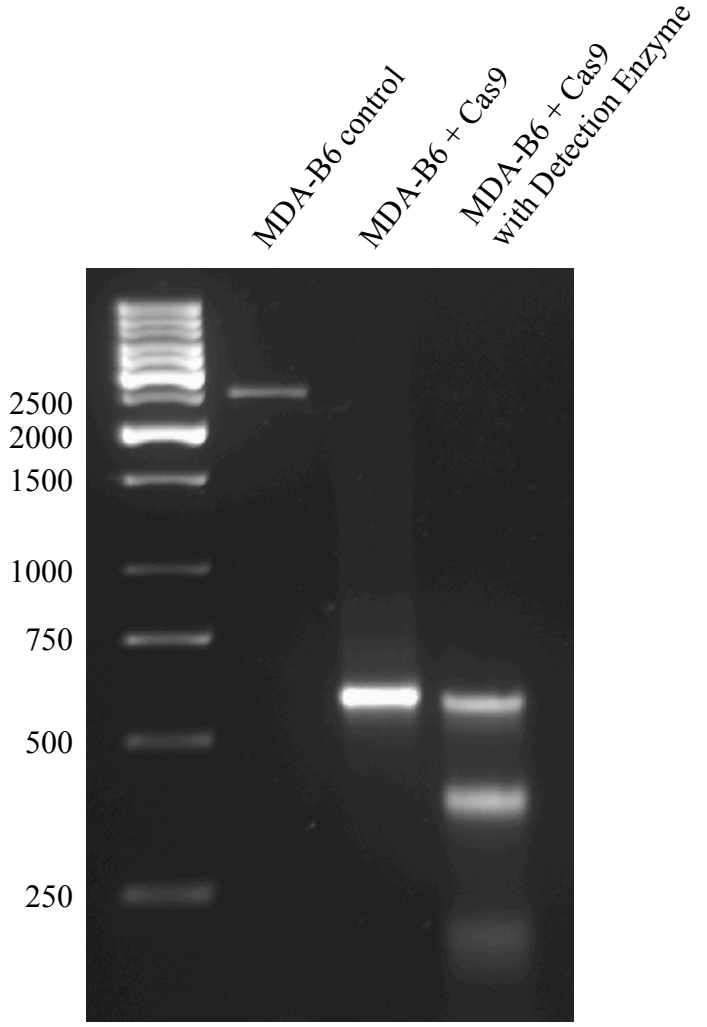

Figure 4.18 Confirmation of *src* cleavage by CRISPR/Cas9

MDA-B6 cells were transduced with lentiviral particles containing two *src*-targeting sgRNAs, followed by transfection with Cas9. Regions of DNA containing the *src* gene were PCR-amplified from the MDA-B6 cells that had been transfected with Cas9, as well as from MDA-B6 cells that had not been transfected with Cas9 (control). A smaller band in the Cas9 lane indicates that the gene of interest was cleaved by Cas9 at both sgRNA sites (the fragments then recombined without the cleaved portion). Cas9-cleaved samples were further cut by a Detection Enzyme (GeneArt Genomic cleavage detection kit) that cuts DNA sequences at insertion/deletion sites, resulting in even smaller bands if successful. In the left-most column, a ladder indicates band sizes.

4.4 Drug Sensitivity Assays in MDA-MB-231 Cells

SRC plays an important role in breast cancer progression and several SRC inhibitors are already being tested in breast cancer clinical trials (Hosford and Miller, 2014). In order to model the SL interaction that was observed between SRC and EPHB6 by chemical genetics, various concentrations of the SRC inhibitor, SU6656, were used to treat MDA-pc3 and MDA-B6 cells. Consistent with the inhibitory effect of the SRC-targeting *sh*RNA (Figure 4.14B), application of SU6656 showed a preferential suppression of the EPHB6-deficient MDA-pc3 cells when compared to MDA-B6 (Figure 4.19).

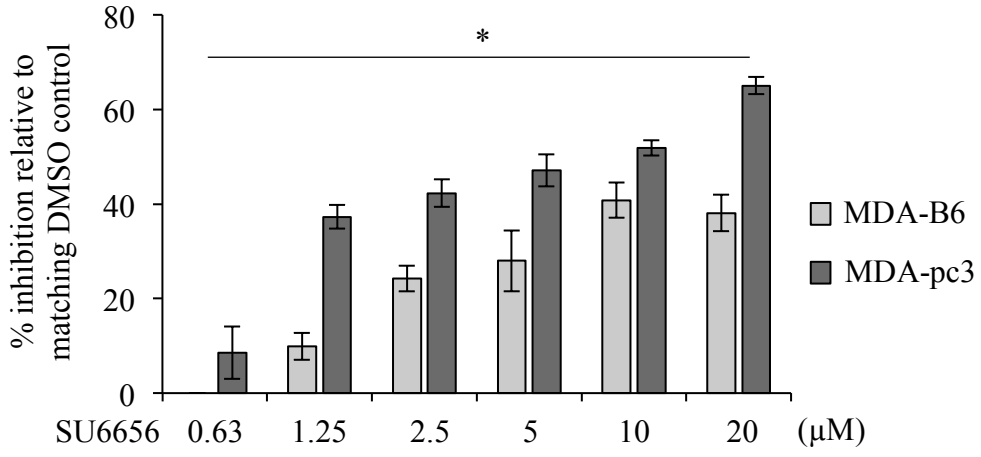

Figure 4.19 Treatment of MDA-B6 and MDA-pc3 with SU6656

MDA-pc3 and MDA-B6 cells were cultured in 96-well plates with indicated concentrations of SU6656 or a matching volume of DMSO for 72 hr. Cells were stained with resazurin and fluorescence was measured using a SpectraMax M5 plate reader to determine cell suppression. Five wells were analyzed per condition. The graph shows percentage of inhibition relative to DMSO control. *, $P < 0.05$, Student's t-test.

Another SRC inhibitor, KX2-391, has been tested in phase II clinical trials for prostate cancer treatment, where it showed a relatively modest effect (Antonarakis *et al*., 2013). KX2-391 is also currently being tested for breast cancer treatment (NCT01764087) and the finding that there is a SL relationship between EPHB6 and SRC indicated that KX2-391 treatment might work more efficiently if applied specifically to EPHB6-deficient TNBC cells. To assess

this possibility, MDA-pc3 and MDA-B6 cells were incubated with increasing concentrations of KX2-391 or a matching solvent control. In similarity to SU6656 action, KX2-391 caused a significantly stronger suppression of the EPHB6-deficent MDA-pc3 cells compared to MDA-B6 (Figure 4.20), suggesting that KX2-391 treatment may indeed potentially benefit from a more personalized approach, where it would be applied exclusively to EPHB6-deficient tumors.

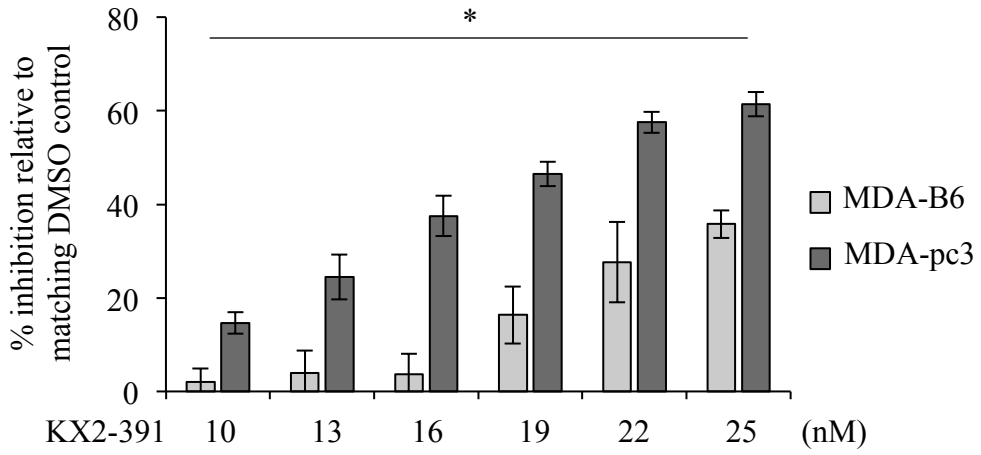

Figure 4.20 Treatment of MDA-B6 and MDA-pc3 with KX2-391

MDA-pc3 and MDA-B6 cells were cultured in 96-well plates with indicated concentrations of KX2-391 for 72 hr. Cells were stained with resazurin and fluorescence was measured using a SpectraMax M5 plate reader to determine cell suppression. Five wells were analyzed per condition. The graph shows percentage of inhibition relative to DMSO control. *, $P < 0.05$, Student's t-test.

In the initial drug sensitivity assay, it was shown that KX2-391 caused a stronger suppression of EPHB6-deficient cells. Therefore, it was desirable to carry out a further drug sensitivity assay, wherein MDA-B6 and MDA-pc3 were co-cultured and exposed to the drug. This was important, as it allowed for exclusion of any influence of potential differences in tissue culture conditions on experimental outcomes for separate treatment of MDA-B6 and MDA-pc3. In order to successfully co-culture the different cell lines, MDA-B6 and MDA-pc3 were both stably transduced with a lentiviral vector expressing green or red fluorescent

proteins. This resulted in four cell lines: MDA-B6-RFP, MDA-B6-GFP, MDA-pc3-RFP, and MDA-pc3-GFP (Figure 4.21).

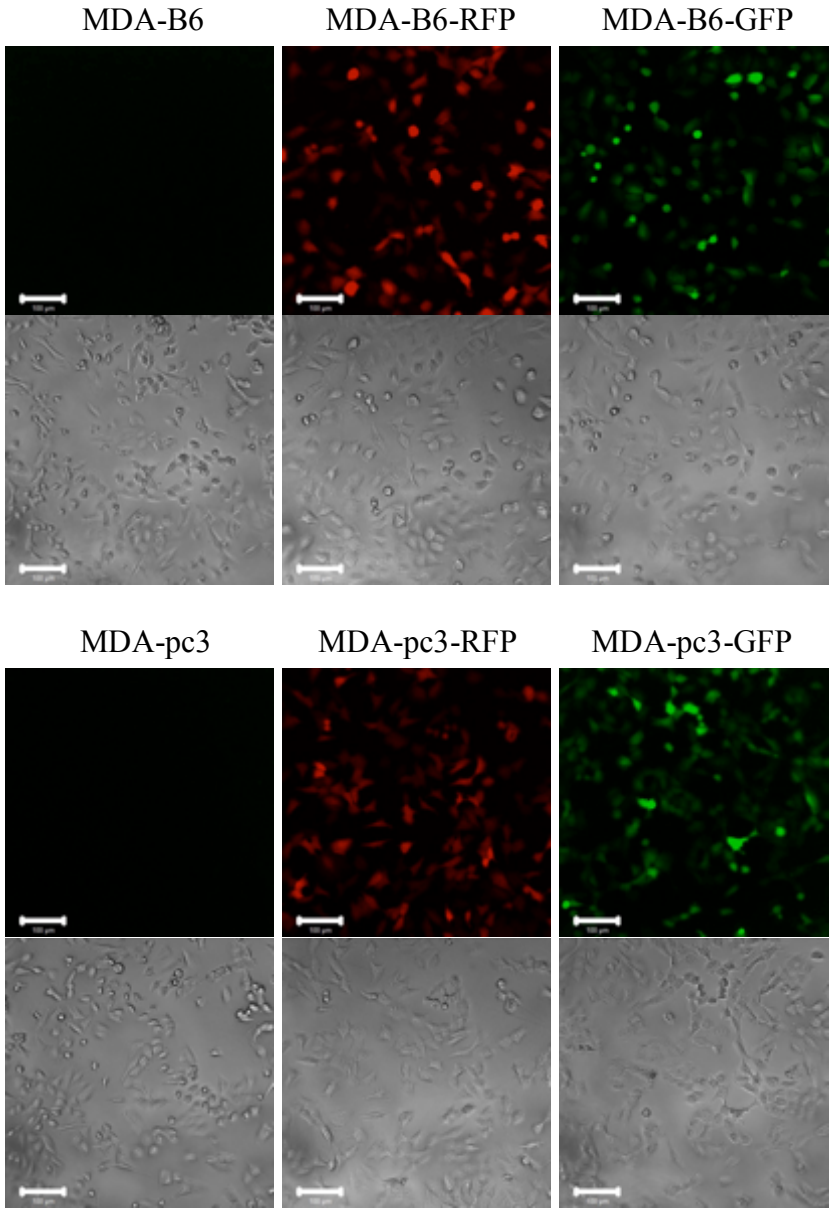

Figure 4.21 MDA-B6 and MDA-pc3 fluorescent cell lines

MDA-B6 and MDA-pc3 cells were transduced with lentivirus encoding either pLD-GFP-Puro or pLD-RFP-Puro in medium containing 8 µg/mL polybrene. After 24 hr, cells were selected with 2 µg/mL puromycin for 48 hr. Scale bar, 100 µM.

For co-culturing EPHB6-expressing and EPHB6-deficient cell lines, mixtures of either MDA-B6-GFP and MDA-pc3-RFP, or MDA-B6-RFP and MDA-pc3-GFP were prepared. These cells were mixed, co-seeded in equal numbers, and treated with KX2-391 or a solvent control. After 72 hr, the cells were collected and analyzed by flow cytometry in order to look for the prevalence of one color over the other. This approach showed clearly that the EPHB6-deficient cells, being either MDA-pc3-RFP or MDA-pc3-GFP, were more strongly inhibited than the corresponding EPHB6-expressing cell line (Figure 4.22 and 4.23). This shows that even in situations where EPHB6-expressing and EPHB6-deficient cells are growing in close proximity, there will still be a noticeable SL effect induced by KX2-391. This is important, as EPHB6-deficient tumors in patients will inevitably be found among normal tissues with normal EPHB6 expression. Therefore, it is critical that the chemical inhibitors being employed have a stronger effect on the tumor itself, without equally inhibiting the surrounding tissues.

4.5 Cell Death Assays in MDA-MB-231 Cells

Treatment with SRC inhibitors resulted in a preferential inhibition of EPHB6-deficient MDA-MB-231 cells. This result was not surprising, as SRC was found to exhibit a SL interaction with EPHB6. This meant that the relative inhibition of EPHB6-deficient cells was likely due to an increased killing from the SL interaction. In order to test this, cells were treated with KX2-391 and then stained with PI. PI is used to stain DNA, as it binds by intercalating between the DNA bases. However, PI is also membrane impermeant, and therefore, it is generally unable to enter healthy cells. Because of this, increased cell killing results in a higher amount of PI staining, as dying cells' membranes start to break down. Accordingly, it was found that KX2-391-treated EPHB6-deficient cells displayed a higher amount of PI staining relative to solvent-treated control cells, when compared to EPHB6-expressing cells (Figure 4.24). This finding indicated that inhibition of SRC caused increased lethality when EPHB6 expression was removed from cells.

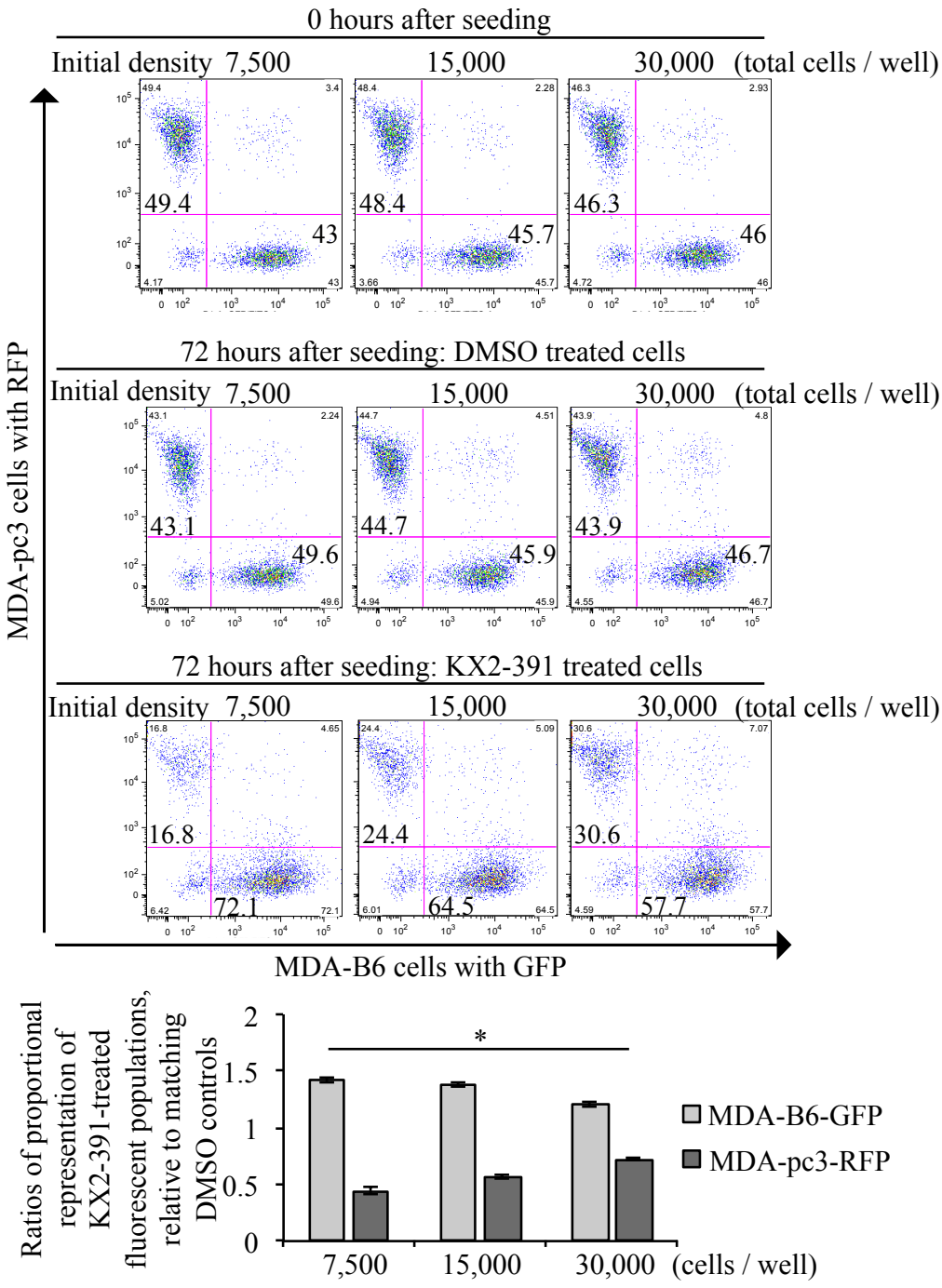

Figure 4.22 Treatment of mixed MDA-B6-GFP and MDA-pc3-RFP with KX2-391

Fluorescently-labeled MDA-B6-GFP and MDA-pc3-RFP cells were combined in equal numbers at indicated cell densities in 24-well plates and cultured with 25 nM KX2-391 for 72 hr. Cells were collected and analyzed by flow cytometry and the FlowJo software, and fluorescence was compared between DMSO controls and KX2-391-treated cells. The graph shows ratios of proportional representation of KX2-391-treated population relative to DMSO control and represents analysis of triplicates. *, $P < 0.05$, Student's t-test.

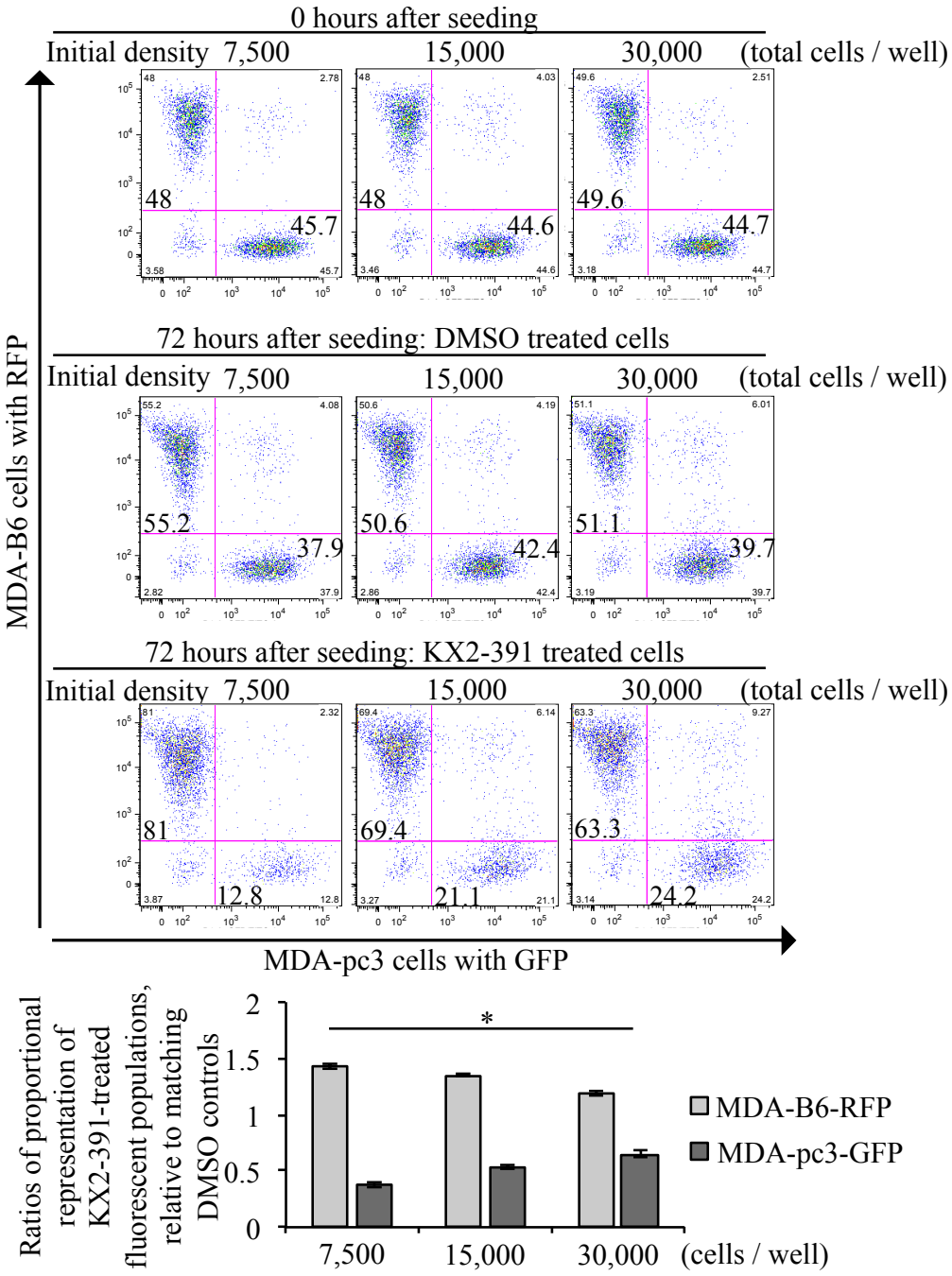

Figure 4.23 Treatment of mixed MDA-B6-RFP and MDA-pc3-GFP with KX2-391

Fluorescently-labeled MDA-B6-RFP and MDA-pc3-GFP cells were combined in equal numbers at indicated cell densities in 24-well plates and cultured with 25 nM KX2-391 for 72 hr. Cells were collected and analyzed by flow cytometry and the FlowJo software and fluorescence was compared between DMSO controls and KX2-391-treated cells. The graph shows ratios of proportional representation of KX2-391-treated population relative to DMSO control and represents analysis of triplicates. *, $P < 0.05$, Student's t-test.

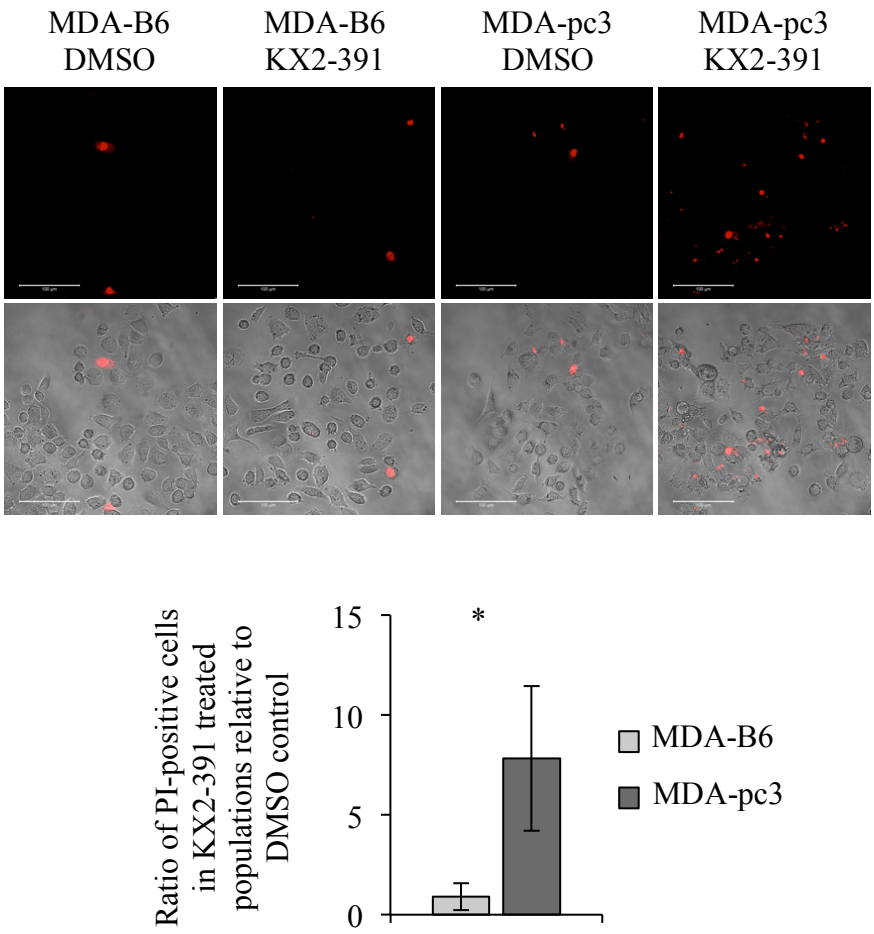

Figure 4.24 Propidium iodide staining of KX2-391-treated MDA-B6 and MDA-pc3 cells

MDA-B6 and MDA-pc3 cells were cultured in glass-bottom plates in the presence of 25 nM KX2-391 for 72 hr. Cells were stained for 12 min with 2.7 µg/mL propidium iodide (PI) in phenol red-free medium. Cells were imaged using confocal microscopy at 200 x magnification and the number of PI-stained cells were counted and compared between DMSO control and KX2-391-treated plates. Scale bar, 100 µm. *, $P < 0.05$, Student's t-test.

In addition to PI staining, cells were also put through staining with 7-AAD after treatment with KX2-391. 7-AAD, which also binds to DNA, is also membrane impermeant and is, therefore, often used as an indicator of late-apoptosis. As in the case of PI, it was found that MDA-MB-231 cells missing EPHB6-expression exhibited increased 7-AAD staining following treatment with the SRC inhibitor KX2-391 (Figure 4.25). This provided further validation that

the inhibitory effect caused by KX2-391 was due to increased killing, resulting from the SL relationship between SRC and EPHB6.

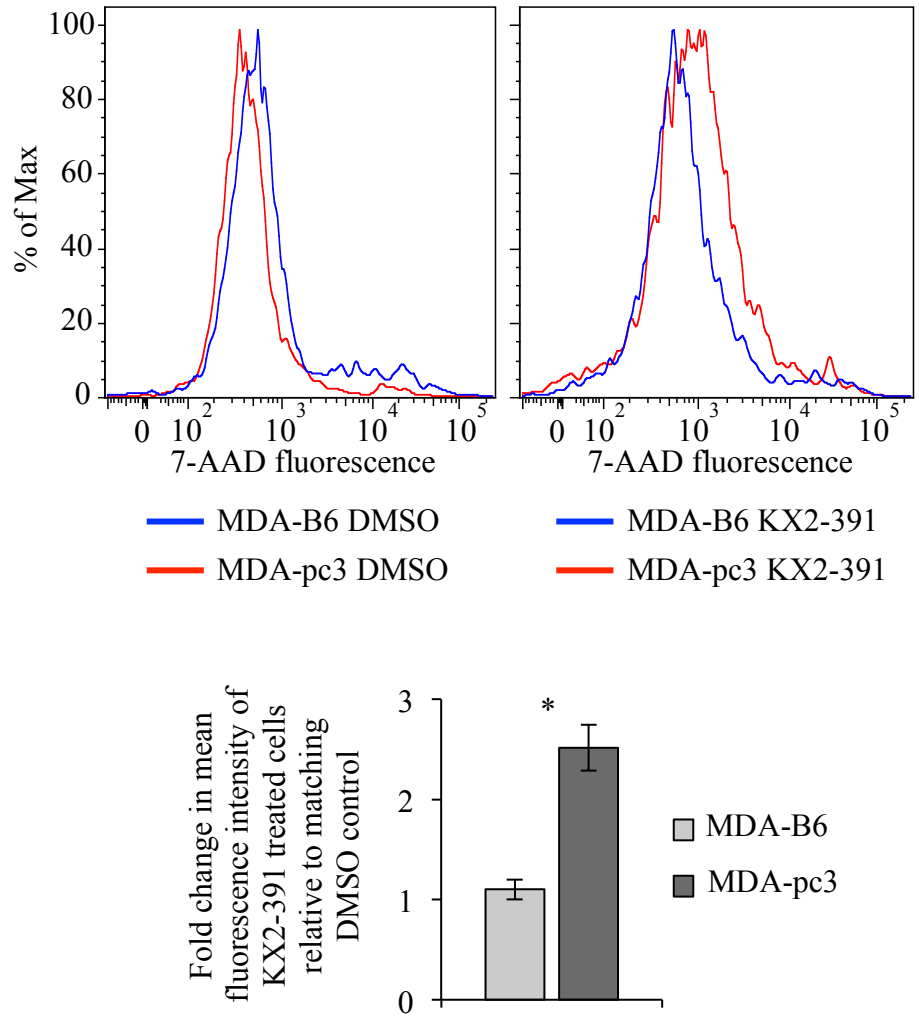

Figure 4.25 7-AAD staining of KX2-391-treated MDA-B6 and MDA-pc3 cells

MDA-B6 and MDA-pc3 cells were cultured in 6-well plates in the presence of 25 nM KX2-391 for 72 hr. Cells were collected and stained with 7-AAD for fifteen minutes while covered at room temperature. Cells were analyzed by flow cytometry and the FlowJo software, and mean immunofluorescence was compared between DMSO controls and KX2-391-treated cells. The graph shows fold change relative to DMSO control and represents analysis of triplicates. *, $P < 0.05$, Student's t-test.

4.6 Drug Sensitivity Assays in BT-20 Cells

Importantly, the SL interaction observed between EPHB6 and SRC was not restricted to MDA-MB-231 cells alone, but were also observed in the BT-20 TNBC cell line. Unlike MDA-MB-231 cells, which have lost EPHB6 expression during cancer progression, BT-20 cells inherently retain expression of EPHB6. Parental BT-20 cells were transduced with an *sh*RNA targeting EPHB6 (BT20-B6-s*h*RNA), or else with a non-silencing *sh*RNA (BT20-NS) (Figure 4.26). This provided the opportunity to compare the SL interaction between EPHB6 and SRC in both a cell line utilizing EPHB6-restoration, as well as a cell line utilizing EPHB6 silencing.

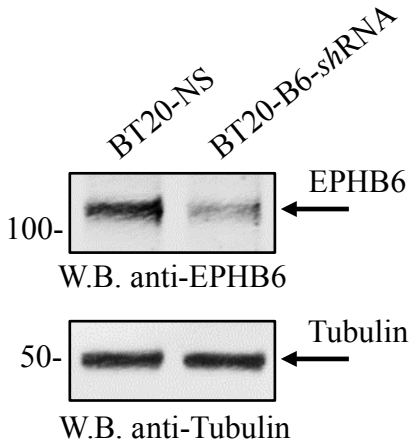

Figure 4.26 EPHB6 expression in BT-20 cell lines

Triple negative breast cancer cells, BT-20, were transduced with an EPHB6-targeting *sh*RNA (BT20-B6-*sh*RNA), or non-silencing *sh*RNA (BT20-NS). EPHB6 expression was analyzed by Western blotting with anti-EPHB6 and quantified by densitometry. Western blotting with anti-tubulin was used as a loading control.

It was important to ensure that the SL interaction between EPHB6 and SRC could be exploited in other TNBC cells. Therefore, the first step was to test the SU6656 SRC inhibitor on the BT-20 cell lines in order to assess percentage of inhibition. BT20-NS and BT20-B6-*sh*RNA cells were treated with increasing concentrations of the SU6656 SRC inhibitor and the resulting inhibition of cell viability was compared to corresponding solvent controls. Consistent with the results in MDA-MB-231 cells, application of SU6656 caused preferential suppression of the EPHB6-silenced BT20-B6-*sh*RNA cells (Figure 4.27).

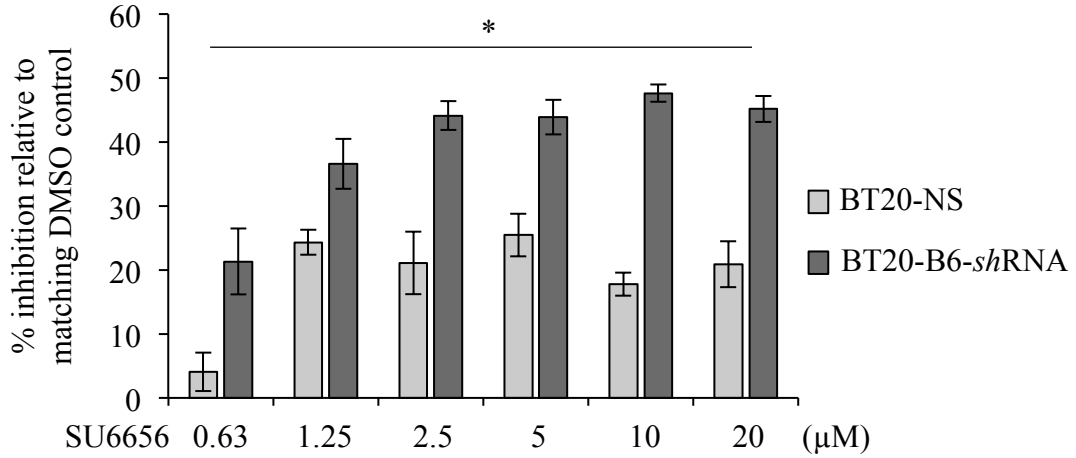

Figure 4.27 Treatment of BT20-NS and BT20-B6-*sh*RNA with SU6656

BT-20 cells were cultured in 96-well plates with indicated concentrations of SU6656 or matching volumes of DMSO for 96 hr. Cells were stained with resazurin and fluorescence was measured using a SpectraMax M5 plate reader to determine cell suppression. Five wells were analyzed per condition. The graph shows percentage of inhibition relative to matching DMSO controls. *, $P < 0.05$, Student's t-test.

Because the SRC inhibitor, KX2-391, has been used in phase II prostate cancer trials with modest effect (Antonarakis *et al*., 2013), and due to the fact that its use on MDA-MB-231 cells showed a preferential inhibition of EPHB6-deficient cells, it was important to be able to emulate the inhibitory effects with BT-20 cells. This would lend further support toward the use of KX2-391 for patients with TNBC tumors exhibiting a loss of EPHB6 expression. Therefore, BT20-NS and BT29-B6-*sh*RNA cells were treated with KX2-391 or matching solvent control and then analyzed to determine percentage inhibition of cell viability. In a similar fashion to treatment with SU6656, and as was observed in the case of MDA-MB-231 cell viability assays, KX2-391 caused a significantly stronger suppression of EPHB6-deficient BT-20 cells (Figure 4.28).

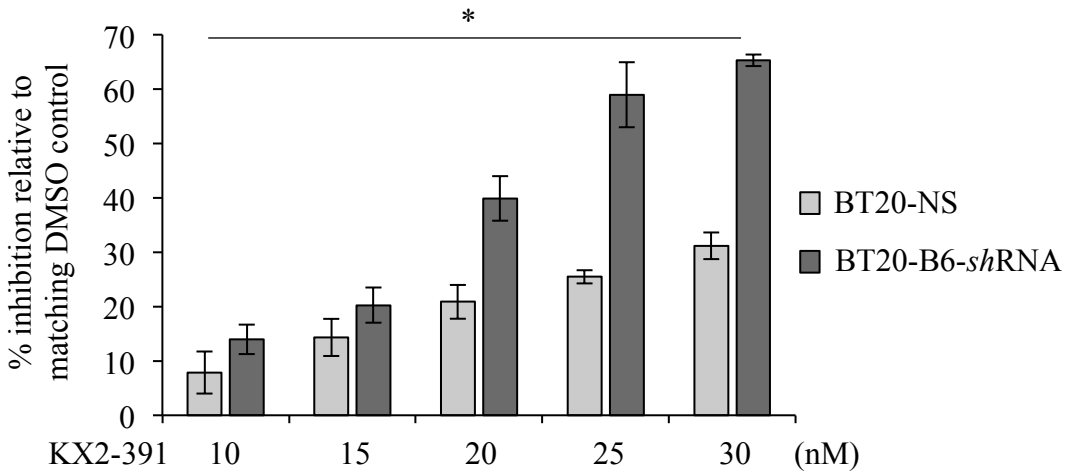

Figure 4.28 Treatment of BT20-NS and BT20-B6-*sh*RNA with KX2-391

BT-20 cells were cultured in 96-well plates with indicated concentrations of KX2-391 or matching volumes of DMSO for 96 hr. Cells were stained with resazurin and fluorescence was measured using a SpectraMax M5 plate reader to determine cell suppression. Five wells were analyzed per condition. The graph shows percentage inhibition relative to DMSO control. *, $P < 0.05$, Student's t-test.

4.7 Cell Death Assays in BT-20 Cells

As in the case of MDA-MB-231 cells, EPHB6-deficient BT-20 cells also underwent increased inhibition following treatment with SRC-inhibitors. Therefore, it was suspected that the BT-20 cells were also undergoing an increased killing due to the SL interaction between SRC and EPHB6. To test this, BT-20 cells were also exposed to the PI and 7-AAD compounds following treatment with KX2-391. As anticipated, EPHB6-deficient BT-20 cells displayed a significant increase of staining with PI (Figure 4.29), as well as with 7-AAD (Figure 4.30) following SRC-inhibitor treatment. This indicated an increase of cell killing, which could be attributed to SL.

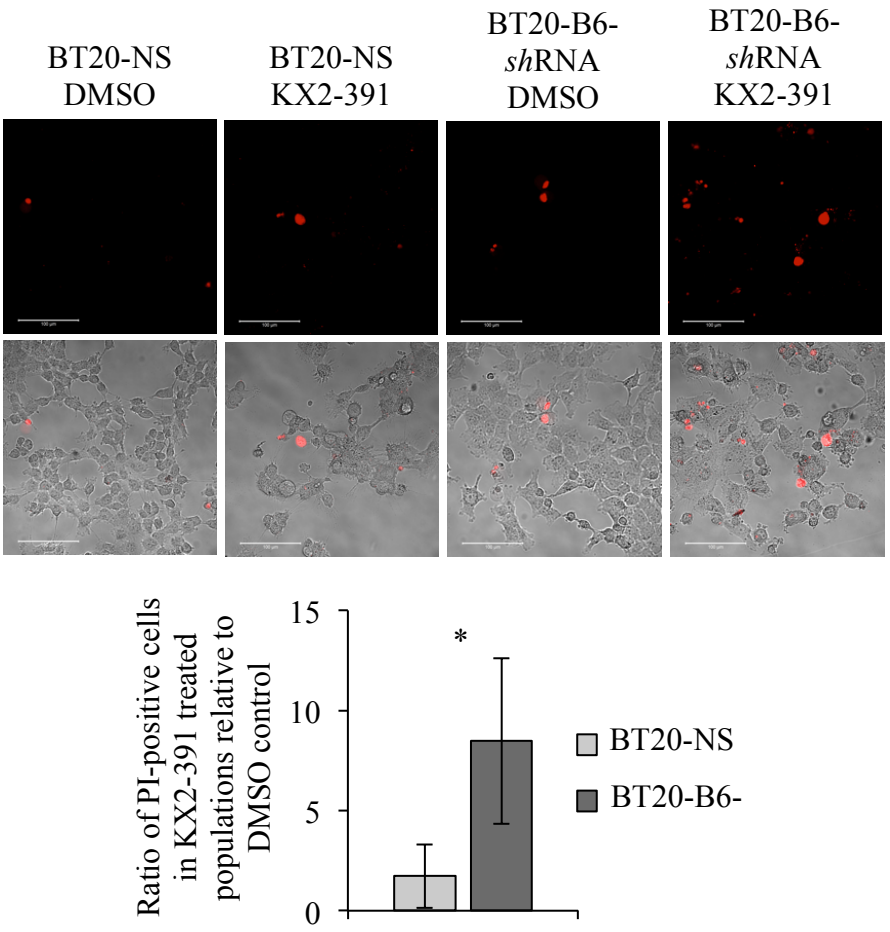

Figure 4.29 Propidium iodide staining of KX2-391-treated BT-20 cells

BT20-B6-*sh*RNA and BT20-NS were cultured in glass-bottom plates in the presence of 35 nM KX2-391 or DMSO for 96 hr. Cells were stained with 2.7 µg/mL propidium iodide (PI) in phenol red-free medium and imaged using confocal microscopy. PI-positive cells were counted in at least 10 randomly captured fields. Counts of PI-positive cells were normalized on the total cell numbers in matching frames. The graph shows the ratio of PI-positive cells in KX2-391-treated populations relative to matching DMSO controls. Scale bar, 100 µm. *, $P < 0.05$, Student's t-test.

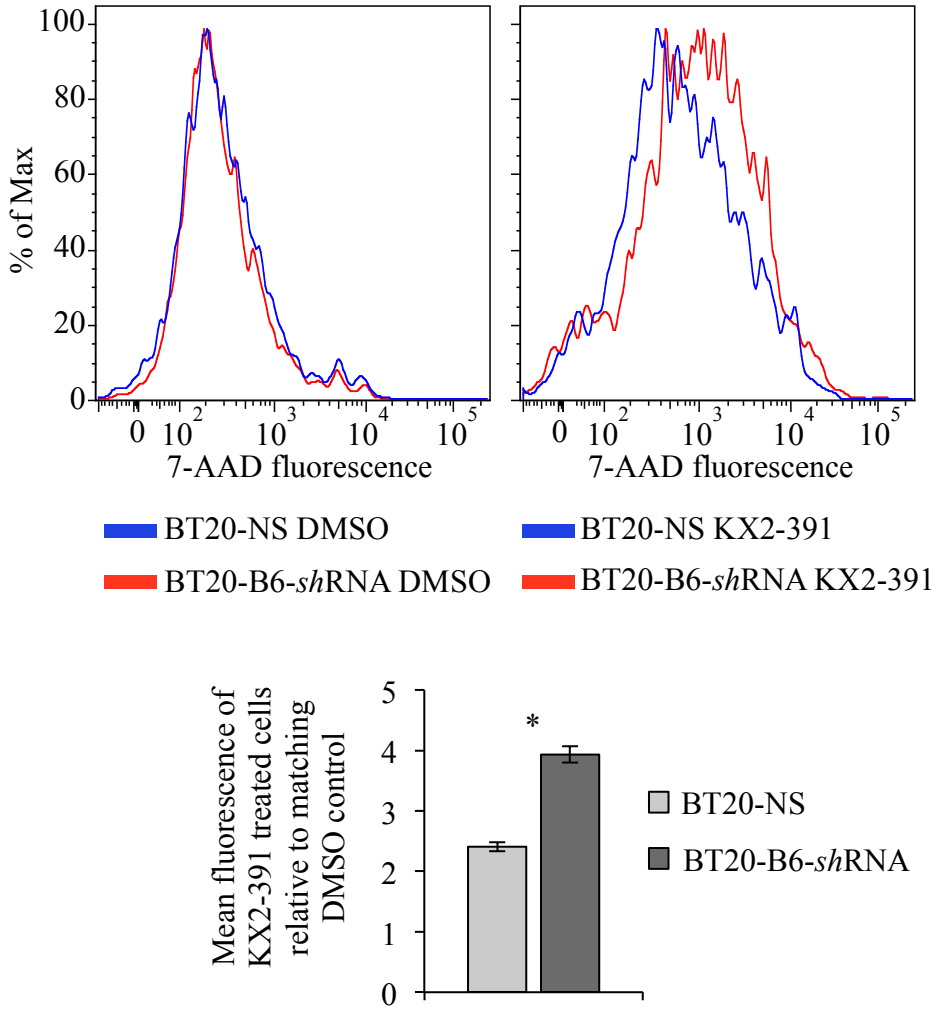

Figure 4.30 7-AAD staining of KX2-391-treated BT-20 cells

BT20-NS and BT20-B6-*sh*RNA cells were cultured in 6-well plates in the presence of 25 nM KX2-391 for 96 hr. Cells were collected and stained with 7-AAD for fifteen minutes covered at room temperature. Cells were analyzed by flow cytometry and the FlowJo software, and mean immunofluorescence was compared between DMSO controls and KX2-391-treated cells. The graph shows fold change relative to DMSO control and represents analysis of triplicates. *, $P < 0.05$, Student's t-test.

4.8 Tumor Xenograft Studies

4.8.1 Mouse Models

The use of SRC inhibitors to generate a SL effect in EPHB6-deficient cells proved to be effective in monolayer cell culture. Lethality was observed whether the EPHB6-expressing and EPHB6-deficient cell lines were cultured separately, or co-seeded together. The preferential inhibition of EPHB6-deficient TNBC cells continued when tested with the BT20-B6-*sh*RNA cell line, showing a similar trend to that seen with MDA-pc3. Taking this into account, it was determined that the SL interaction between EPHB6 and SRC might be used to target TNBC tumors. In order to test this, TNBC tumors were produced in experimental animals by injecting MDA-B6 and MDA-pc3 cells into mammary fat pad regions of immunodeficient female NOD.Cg-*Prkdc*^{scid} *Il2rg*^{tm1Wjl}/SzJ (NOD-SCID) mice. These mice do not express the *prkdc* gene or the *il2rg* gene and are deficient in mature lymphocytes, without detectable serum Ig. Treatment of the animals with KX2-391 was initiated when tumors reached a detectable size and was then carried out until the mice had to be sacrificed in accordance with the guidelines established by the Animal Research Ethics Board. Upon measurement of tumors, it was shown that treatment with KX2-391, indeed, more efficiently suppressed the growth of EPHB6-deficient MDA-pc3 TNBC tumors in comparison with EPHB6-expressing MDA-B6 (Figure 4.31). This was important because if EPHB6-deficient tumors are to be targeted with SRC inhibitors in patients, there should be significantly less detrimental effect to the surrounding, normal tissues.

4.8.2 Immunohistochemistry

Treatment of monolayer cells with KX2-391 showed a preferential suppression of EPHB6-deficient cells, and the same was found to be true in the case of EPHB6-deficient tumors. It has been shown that some SRC inhibitors directly affect the process of angiogenesis (Schenone *et al*., 2007). Therefore, it was important to determine whether the inhibition of EPHB6-deficient tumors was due to a direct SL effect, or whether it was due to a preferential suppression of blood vessel formation. Therefore, tumor sections from the xenograft models were stained with an antibody targeting CD34, which is a blood vessel marker. Upon staining, it was found that there was not a statistically significant difference in the neovascularization of either EPHB6-deficient or EPHB6-expressing tumors after treatment with KX2-391. This

indicated that inhibitory effect on EPHB6-deficient tumors was not related to angiogenesis, but was instead due to the SL relationship between SRC and EPHB6 (Figure 4.32).

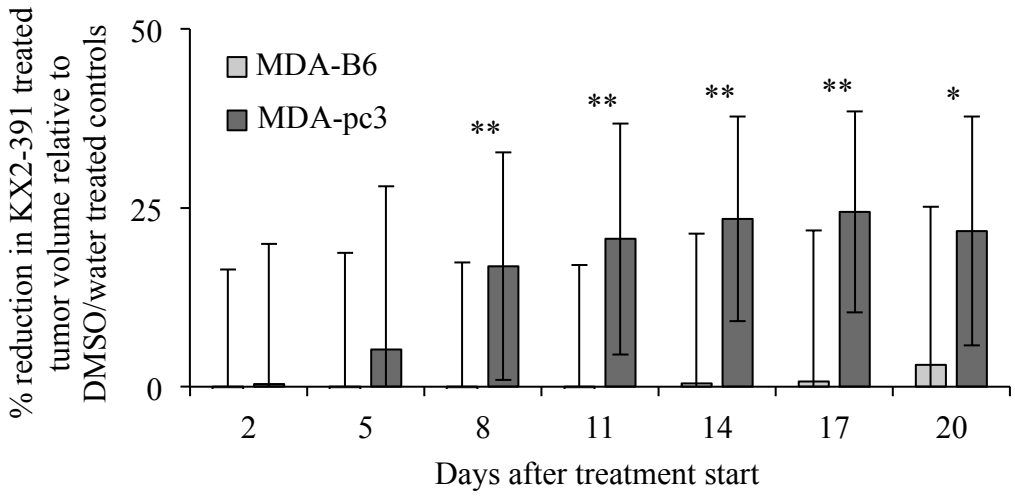

Figure 4.31 Treatment of MDA-B6 and MDA-pc3 xenograft tumors with KX2-391

MDA-pc3 and MDA-B6 cells were injected into the mammary fat pad region of 4-6 weeks old NOD-SCID mice (1 x 10^6 cells per mouse). Mice with detectable tumors were treated twice per day with 5 mg/kg KX2-391 in DMSO/water solvent or solvent alone by oral feeding (at least 6 animals per experimental condition). Tumor size was measured every 3 days and tumor volume was calculated with the equation: $A/2*B^2$, where A was long and B was short diameter of the tumor. The reduction in tumor growth in KX2-391-treated mice is presented as a percentage relative to matching solvent controls. The graph summarizes two independent experiments. Day 0 indicates the beginning of treatment with KX2-391 or matching solvent control. The experiments were terminated upon tumor ulceration according to the guidelines established by the Animal Research Ethics Board, University of Saskatchewan. *, $P < 0.05$; **, $P < 0.01$, Student's t-test.

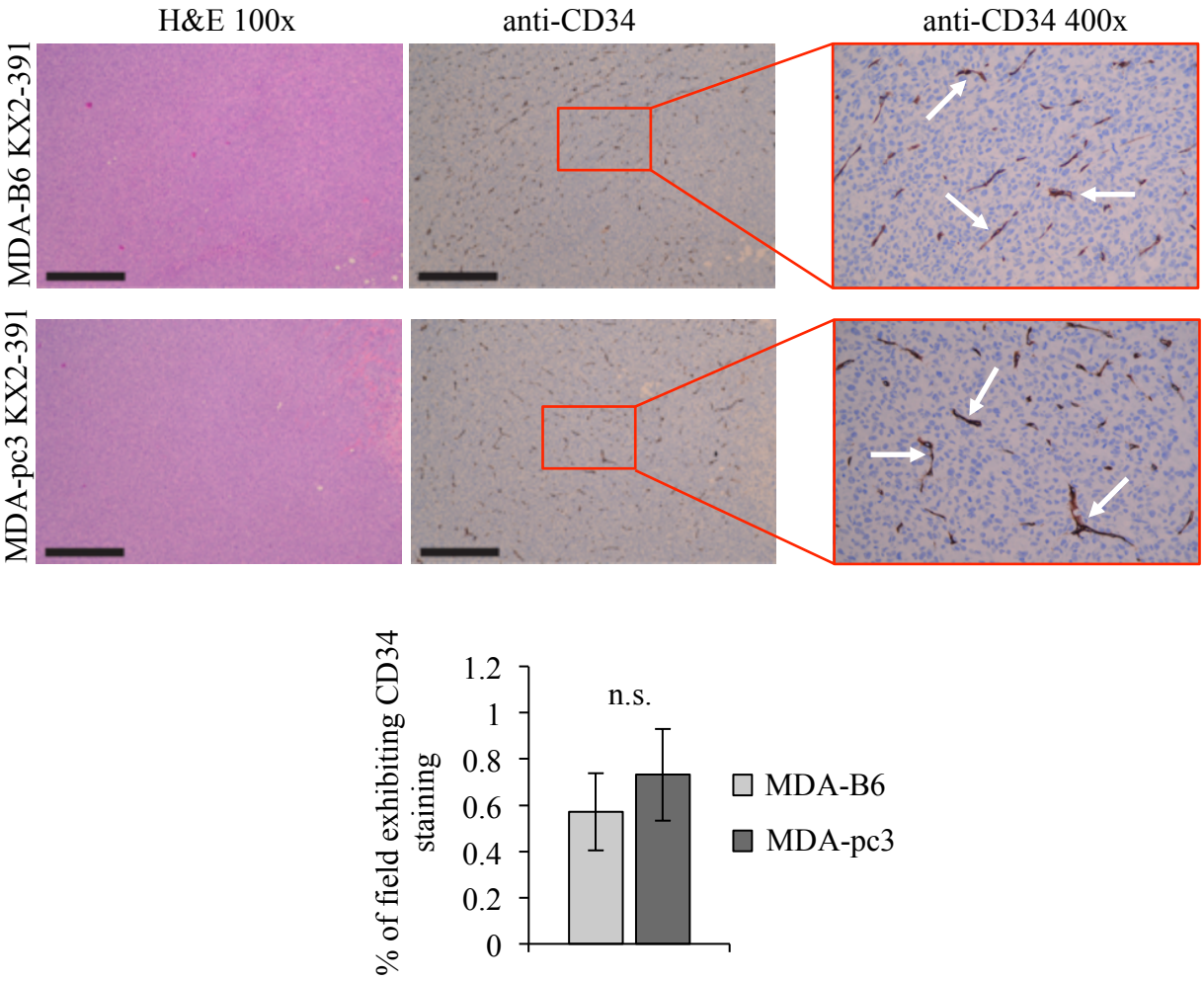

Figure 4.32 Immunohistochemical staining of MDA-B6 and MDA-pc3 tumor sections

MDA-B6 and MDA-pc3 tumors from mouse models were collected at day 42 after injection, fixed in 10% neutral-buffered formalin, and paraffin embedded. Tumor sections were processed for immunohistochemical staining with anti-CD34 or stained with haematoxylin and eosin (H&E). Four representative fields (at 3, 6, 9, and 12 o'clock) per each stained tumor section (one for each extracted tumor) were imaged at 100 x magnification and the blood vessel density per each field was analyzed with the Image-Pro Premier software. The graph represents percentage of anti-CD34-positive area relative to the overall field of view. Images of representative areas highlighted by red rectangles are shown at 400 x magnification. Arrows indicate representative examples of anti-CD34-stained blood vessels. At least 6 stained sections per each experimental condition representing independent tumors were used for the analysis. Scale bar, 500 μM. n.s., statistically not significant.

5.0 Discussion

5.1 Analyzing Significant Synthetic Lethal Hits for EPHB6

The study of SL interactions has opened a new avenue for developing targeted therapies and personalized medicine. For example, at least three clinical trials have been initiated using EGFR and BRAF inhibitors within three years after the SL relation between EGFR and BRAF was identified (Prahallad *et al*., 2012) (NCT01791309; NCT01750918; NCT01719380). Such rapid progress into clinical trials is triggered by selective focusing on well-studied targets with FDA approved inhibitors. In many cases, approved inhibitors exist for various gene products, but only produce a modest effect when used in clinical trials. However, with the advent of SL screening, and the discovery that inhibition of SL partners can cause killing in cells that are otherwise difficult to treat, many inhibitors may now stand forth in a new light. It should be noted, though, that even though many inhibitors may be found to be useful in the case of SL-based therapy, some may still show a more pronounced effect than others. This is one of the reasons why it is important that large-scale SL screens produce at least several significant SL hits.

SL screening of EPHB6 in MDA-MB-231 TNBC cells did not disappoint, as the screen produced 113 statistically significant hits. Being significant, each one of these SL hits could have been considered as a possible therapeutic target for preferentially killing the cancer cells. However, research time and funding both have limitations, and with such an abundance of potential targets, it was important to validate an effective therapeutic target in a timely fashion. There is, of course, no standard method for drawing one hit out of a pool of 113, as small as that number might seem compared to the total of 18,000 genes that are being targeted by *sh*RNAs in our pooled library. Therefore, determination of an appropriate target had to rest on several factors. This included finding out which genes already had FDA-approved inhibitors, as an approved inhibitor could find its way into clinics much faster if it was shown to exhibit the desired SL effect. In addition to this, analysis was carried out to determine which genes showed an inverse expression pattern to that of EPHB6, as this would likely indicate an essential compensatory mechanism when EPHB6 is lost. These analyses revealed SRC as an ideal candidate for targeted therapy, and were further corroborated by study of the STRING 10 database, which showed that SRC is a hub and highly connected to many of the other hits.

Based on a number of qualifiers, SRC inhibitors were then used in initial monolayer treatments to determine the effect of the SL interaction predicted by the screen. Though experiments with SRC were successful, and the desired SL interaction was observed both in cell culture and in animal models, this does not discount the potential displayed by the other gene hits. Some SL hits also had FDA-approved inhibitors in place, and others also displayed an inverse expression pattern with EPHB6. However, this illustrates the importance of a logical approach to determining the best target for treatments, and such steps should be taken following any such large-scale SL screen. One important reason for this is that patients require treatments as soon as possible, and so validation of effective targets must be carried out in a timely fashion. Of course, the qualifiers to determine which therapeutic target that should be used depend greatly on the gene that is being screened. Researchers would be prudent to study the hits produced by any given screen for some time in order to ensure that the appropriate steps are taken. Additionally, future researchers would be prudent to invest time into further investigation of the remainder of the SL hits in order to determine the therapeutic advantages of each.

5.2 The Role of SRC in Breast Cancer Progression

It is very intriguing that SRC came up as a hit in the EPHB6 synthetic lethal screen, as it has been known for some time that SRC plays an active role in the initiation and progression of a number of different cancer types. For example, in the case of colon cancer, it has been shown that SRC accelerates metastasis, as well as providing a level of resistance to therapeutic drugs (Chen *et al*., 2014). In head and neck squamous cell carcinoma and non-small cell lung carcinoma, SRC has been observed promoting survival of cancer cells by acting alongside STAT3, another known culprit in cancer progression (Byers *et al*., 2008; Sen *et al*., 2009). But more importantly for this discussion, it has been found that SRC promotes the progression of breast cancer, with SRC activity reaching up to 20 times higher than that in normal tissues (Irby and Yeatman, 2000). This is not surprising, as under normal circumstances, SRC is involved in the regulation of a number of pathways that ultimately moderate cell survival, proliferation, migration, and angiogenesis (Wheeler *et al*., 2009). SRC is a tyrosine kinase that functions by adding phosphate groups to tyrosine residues in downstream targets, thereby activating or inactivating them. However, while tyrosine kinases can be found in many of the steps in

different cellular pathways, SRC holds a prestigious position at the head of a number of key, potentially oncogenic pathways, including the STAT3, RAS, and PI3K pathways (Wheeler *et al*, 2009). Therefore, it is no surprise that altered SRC expression levels are involved in so many different cancers. For this reason, a number of SRC inhibitors are already passing through the different phases of clinical trials. However, as the next section will discuss, the results of inhibitors until now have been modest (Antonarakis *et al*., 2013). It may be that targeting SRC alone is not a full solution, which brings the discussion to synthetic lethality and interaction between SRC and EPHB6.

5.3 EPHB6 Interaction with SRC

The genome-wide SL screens discussed in this study revealed a novel genetic interaction between the SRC kinase and EPHB6 in TNBC cells (Paul *et al*., 2016). Moreover, network assessment directly indicated that SRC is a central player with a high connectivity. An expression analysis also showed that SRC clusters with the genes that negatively correlate with EPHB6 expression in various tumor types. This indirectly suggested that SRC overexpression might act as an essential compensatory mechanism for the loss of EPHB6 in cancer cells, indicating that the SL interaction observed between EPHB6 and SRC may represent a promising therapeutic target. Such a SL interaction was observed in initial experiments using both *sh*RNAs and the CRISPR/Cas9 system to target SRC in EPHB6-defiecient cells, thereby indicating that chemical inhibitors should be the next step. The SRC kinase inhibitor, KX2-391, was already being tested in clinical trials, but had not yet been used in the context of EPHB6 expression. Therefore, KX2-391 was used to treat both monolayer TNBC cells, and subsequently, TNBC tumors in mouse models of human malignancy. In each case, the use of KX2-391 was shown to produce the same SL effect toward EPHB6-deficient cells that was observed in the initial screen. Therefore, this investigation provides a new rationale for the selective use of the KX2-391 SRC inhibitor in patients that have lost expression of the EPHB6 receptor in their tumors.

The relevance of the findings presented here are further supported by recent unfortunate observations, revealing that although SRC is frequently overexpressed in cancer, in some clinical trials randomly applied SRC inhibition produced limited positive effects on cancer patients (Antonarakis, et al., 2013). The report of the SL relationship between EPHB6 and SRC

may help to overcome this problem, and improve the efficiency of SRC inhibiting approaches in cancer therapy. This is accomplished by showing that treatment with SRC inhibitors should be personalized, and mostly applied to patients with reduced or missing EPHB6 expression. In this context, it was important that our analysis confirmed that small molecule SRC inhibitors could efficiently target the SL interaction between SRC and EPHB6. Accordingly, our work revealed that EPHB6-deficient TNBC cells were, indeed, much more sensitive to these compounds, and were strongly inhibited relative to cells with normal EPHB6 expression. The experimental data in this study suggests that EPHB6 does not protect SRC from inhibition and we suspect that EPHB6 most likely acts by partially compensating for the loss of the biological functions of the SRC kinase. This apparent compensation also helps to explain the ability of EPHB6 to protect cancer cells from *sh*RNA-induced silencing of SRC or *src* knockout observed in initial experiments. This model fits a classical definition of a SL interaction (Dixon *et al*., 2009) and provides a rationale for the limited effectiveness of SRC-inhibiting therapy currently observed in some cancer patients (Antonarakis *et al*., 2013).

5.4 Building Synthetic Lethal Networks

The research carried out in this study revealed SRC as a SL partner of EPHB6, along with an additional 112 significant hits. This is useful information, as SRC inhibitors have been shown to preferentially kill EPHB6-deficient cells, which means that the screening methodology has produced a potential therapeutic strategy. However, there are many other mutations implicated in cancer progression, meaning that the work carried out in this study, though valuable on its own, is only part of the larger picture. It has been shown that other such screens have also produced a wide array of potential targets (Vizeacoumar *et al*., 2013). This previous work also revealed that screening of SL interactions for different proteins such as PTEN, KRAS, and others has shown that there are often a number of hits that are in common. This means that these crossover hits, when targeted therapeutically, could prove to be beneficial for multiple cancer-related mutations. Therefore, as SL screens are carried out for more and more individual mutations, it is likely that an increasing number of crossover hits will be found (Figure 5.1).

Although each individual screen, such as the EPHB6 screen, is valuable on its own, much more similar work would need to be carried out on many different genes mutated in cancer.

Such findings would help to build a much larger network of NGIs for different cancer mutations, as well as the many therapeutic targets that are in common between different genes families. Of course, this would require large collaborative efforts within the cancer research community, as screening for one gene alone, as well as the subsequent examination and validation of SL therapeutic targets is a substantial amount of work. However, armed with such knowledge, medical professionals would be able to use the genetic profile of individual tumors to increasingly greater success. As it now stands, the scientific community has already learned a great deal about the various mutations that are involved in cancer, as well as the many ways to provide appropriate therapies. However, with the construction of a comprehensive interaction map of cancer-causing genes, and their SL partners, the ability to develop patient-specific, and even tumor-specific therapies will become increasingly viable. In time, it may even be possible that such SL interaction maps will generate therapies for many of the cancers for which painful and uncomfortable strategies such as chemotherapy, radiation therapy, and surgery are the only options. In fact, with more personalized therapies, less patients may have to be exposed to such broad-spectrum strategies altogether. All told, a collaborative construction of a SL interaction map for cancer genetics would be a boon for both doctors and patients, and would provide a strong platform for further cancer research.

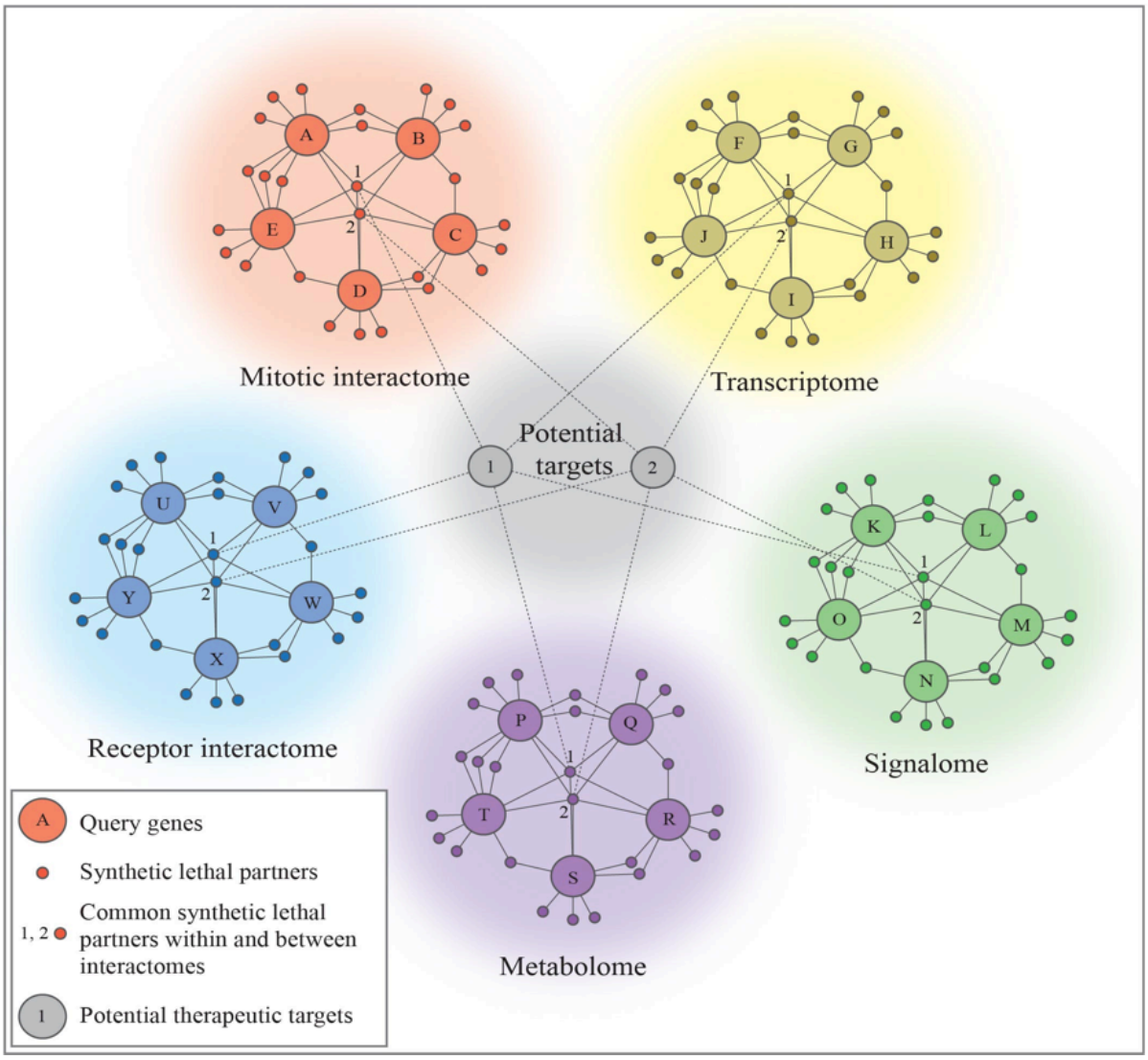

Figure 5.1 Building synthetic lethal networks

As genetic interactions are confirmed between various genes in a given biological process, sub-interaction networks begin to emerge. Such interactomes, or E-MAPs (epistatic mini array profiles), are networks of query genes (nodes represented with alphabets) that relate to particular cellular systems, such as metabolism, signaling, transcription, translation, or others. Within each E-MAP, potential gene targets (synthetic lethal partners – depicted as tiny nodes) are determined to be synthetic lethal partners. As more of these E-MAPs are generated, common synthetic lethal partners from each can be found (nodes represented in numericals), thereby pointing to therapeutic targets for cancer treatment on a whole-cell level.

6.0 Conclusions and Future Work

6.1 Conclusions

In the past, SRC inhibitors have been used to treat different cancer types, albeit, with varying degrees of success. The findings reported here indicate that a more selective application of SRC inhibitors may be necessary, as opposed to the broad application that has been utilized thus far. These observations indicate that EPHB6 may be efficiently used as a biomarker for selecting exclusively EPHB6-deficient TNBC tumors for the treatment with SRC inhibitors. This means that, due to the SL relationship between SRC and EPHB6, SRC inhibitors may only be beneficial when tumors display a decrease of EPHB6 expression. Such a discovery might even begin to explain why treatment with SRC inhibitors has only had modest effects; as such treatments have not previously been used in the context of EPHB6 expression. Such a personalized approach is likely to increase the chance of success when utilizing SRC inhibitors for TNBC treatment. Additionally, this model may also potentially be applicable to multiple other tumor types, where EPHB6 expression is reduced according to previously published observations and according to the findings reported here.

There are other reasons why EPHB6 is important as a biomarker for SRC inhibitor treatment. An equally important outcome of this research is that it would also benefit patients with EPHB6-positive TNBC by preventing their involvement in ineffective treatment protocols. SRC inhibitors have been used in the past with varying degrees of success, which means that some patients have been involved in such treatment strategies without necessarily seeing the desired outcome. In the case of cancer treatment, time may often be a limiting factor, and the ability to apply effective treatments is of paramount importance. Therefore, with the knowledge that EPHB6 is a biomarker for SRC inhibitor treatment, patients with high EPHB6 expression in their tumors would be able to avoid using a potentially ineffective treatment strategy, while being directed to more appropriate therapeutic options. This would help to prioritize the time that is available to patients battling cancer, and would additionally prevent any possible adverse reactions to drugs that may not be beneficial in their case anyway. Furthermore, appropriate use of SRC inhibitors based on EPHB6 expression would decrease unnecessary application of drugs by the health care systems involved, thereby saving resources for other endeavors.

In addition to the findings pertaining to EPHB6 and its importance in regard to prioritization of SRC inhibition strategies, there are other important findings revealed in this research. This investigation utilized a genome-wide SL screen in order to finding targetable weaknesses in an otherwise deadly cancer type. Screening was followed by a successful validation of its results, both in cell culture and in an animal model of human malignancy. This shows the value of large-scale SL screening, as one such screen can produce both immediate therapeutic options (as in the case of SRC inhibitors), as well as many other possible targets for future research. In addition, even though TNBC is normally untargetable due to the inherent loss of ER, PR, and lack of HER2 overexpression, the research presented here has shown that methodologies such as large-scale SL screening are able to produce alternative therapeutic targets. This is valuable as it presents other options to patients, rather than simply being forced to resort to more broad or invasive strategies. Therefore, this provides a strong support for the use of such a methodology in finding new therapeutic targets and developing personalized treatment approaches.

6.2 Future Work

The research presented here naturally lends itself to several avenues of future work. First, the pooled screen identified a total of 113 genes that were shown to be SL with EPHB6 in TNBC cells. This means that even though SRC was found to be strong candidate for SL killing, future studies may benefit from following up on a number of the other hits that were found. This would be straightforward to do as many of the hits already have chemical inhibitors in place. In addition, it might even be shown that multiple SL hits may be targeted together for effective killing of EPHB6-deficient TNBC cells. However, this need not be confined to TNBC alone, as the SL relationship between EPHB6 and SRC may extend to other cancer types as well. Therefore, SRC inhibitors should be used on other types of cancer exhibiting known EPHB6 loss, starting with tissue culture conditions, and moving to animal models if results prove favorable. This might broaden the range of uses for SRC inhibitors, while simultaneously providing new treatment options for patients with other cancers besides TNBC. Of course, in order to ensure the efficacy of this treatment strategy for actual patients, a further evaluation of EPHB6 function in freshly obtained tumor samples would be necessary. Lastly, in addition to the screening of EPHB6, other large-scale screens should carried out,

particularly in the case of genes that are lost during cancer progression, as these deficiencies are otherwise difficult to treat due to the lack of function products to target. This screening could continue to utilize *sh*RNA libraries, or other methods such as CRISPR/Cas9 analysis could be brought to bear. This would require a large scale CRISPR library, with sgRNAs targeting all of the genes that are covered by the current *sh*RNA library used in this research. However, the results may exhibit great precision, as the CRISPR/Cas9 system results in knockout at the genomic level.

7.0 References

1. Akada, M., Harada, K., Negishi, M., and Katoh, H. (2014). EphB6 promotes anoikis by modulating EphA2 signaling. Cell Signal. *26*, 2879-2884.

2. Antonarakis, E.S., Heath, E.I., Posadas, E.M., Yu, E.Y., Harrison, M.R., Bruce, J.Y., Cho, S.Y., Wilding, G.E., Fetterly, G.J., Hangauer, D.G., Kwan, M.F., Dyster, L.M., and Carducci, M.A. (2013). A phase 2 study of KX2-391, an oral inhibitor of Src kinase and tubulin polymerization, in men with bone-metastatic castration-resistant prostate cancer. Cancer Chemoth. Pharm. *71*, 883-892.

3. Bajrami, I., Frankum, J.R., Konde, A., Miller, R.E., Rehman, F.L., Brough, R., Campbell, J., Sims, D., Rafiq, R., Hooper, S., Chen, L., Kozarewa, I., Assiotis, I., Fenwick, K., Natrajan, R., Lord, C.J., and Ashworth, A. (2014). Genome-wide profiling of genetic synthetic lethality identifies CDK12 as a novel determinant of PARP1/2 inhibitor sensitivity. Cancer Res. *74*, 287-297.

4. Bassik, M.C., Kampmann, M., Lebbink, R.J., Wang, S., Hein, M.Y., Poser, I., Weibezahn, J., Horlbeck, M.A., Chen, S., Mann, M., Hyman, A.A., Leproust, E.M., McManus, M.T., and Weissman, J.S. (2013). A systematic mammalian genetic interaction map reveals pathways underlying ricin susceptibility. Cell. *152*, 909-922.

5. Boone, C., Bussey, H., and Andrews, B.J. (2007). Exploring genetic interactions and networks with yeast. Nat. Rev. Genet. *8*, 437-449.

6. Boyle, P. (2012). Triple-negative breast cancer: epidemiological considerations and recommendations. Ann. Oncol. *23*, 7-12.

7. Brenton, J.D., Carey, L.A., Ahmed, A.A., and Caldas, C. (2005). Molecular classification and molecular forecasting of breast cancer: ready for clinical application? J. Clin. Oncol. *23*, 7350-7360.

8. Byers, L.A., Sen, B., Saigal, B., Diao, L., Wang, J., Nanjundan, M., Cascone, T., Mills, G.B., Heymach, J.V., and Johnson, F.M. (2009). Reciprocal regulation of c-Src and STAT3 in non-small cell lung cancer. Clin. Cancer Res. *15*, 6852-6861.

9. Chen, J., Elfiky, A., Han, M., Chen, C., and Saif, M.W. (2014). The role of Src in colon cancer and its therapeutic implications. Clin. Colorectal Cancer. *13*, 5-13.

10. Choung, C.M., Bhat, R., Widelitz, R.B., and Bissell, M.J. (2014). SnapShot: Branching Morphogenesis. Cell. *158*, 1199-1209

11. Chumley, M.J., Catchpole, T., Silvany, R.E., Kernie, S.G., and Henkemeyer, M. (2007). EphB receptors regulate stem/progenitor cell proliferation, migration, and polarity during hippocampal neurogenesis. J. Neuro Sci. *27*, 13481-13490.

12. Collins, S.R., Miller, K.M., Maas, N.L., Roguev, A., Fillingham, J., Chu, C.S., Schuldiner, M., Gebbia, M., Recht, J., Shales, M., Ding, H., Xu, H., Han, J., Ingvarsdottir, K., Cheng, B., Andrews, B., Boone, C., Berger, S.L., Hieter, P., Zhang, Z., Brown, G.W.,

Ingles, C.J., Emili, A., Allis, C.D., Toczyski, D.P., Weissman, J.S., Greenblatt, J.F., and Krogan, N.J. (2007). Functional dissection of protein complexes involved in yeast chromosome biology using a genetic interaction map. Nature. *446*, 806-810.

13. Dai, X., Li, T., Bai, Z., Yang, Y., Liu, X., Zhan, J., and Shi, B. (2015). Breast cancer intrinsic subtype classification, clinical use and future trends. Am. J. Cancer Res. *5*, 2929-2943.

14. Dixon, S.J., Costanzo, M., Baryshnikova, A., Andrews, B., and Boone, C. (2009). Sytematic mapping of genetic interaction networks. Annu. Rev. Genet. *43*, 601-625.

15. Ferlay, J., Soerjomataram, I., Dikshit, R., Eser, S., Mathers, C., Rebelo, M., Parkin, D.M., Foreman, D., and Bray, F. (2015). Cancer incidence and mortality worldwide: sources, methods and major patterns in GLOBOCAN 2012. Int. J. Cancer. *136*, 359-389.

16. Fox, B.P., and Kandpal, R.P. (2004). Invasiveness of breast carcinoma cells and transcript profile: Eph receptors and ephrin ligands as molecular markers of potential diagnostic and prognostic application. Biochem. Bioph. Res. Co. *318*, 882-892.

17. Fox, B.P., and Kandpal, R.P. (2006). Transcriptional silencing of EphB6 receptor tyrosine kinase in invasive breast carcinoma cells and detection of methylated promoter by methylation specific PCR. Biochem. Bioph. Res. Co. *340*, 268-276.

18. Fox, B.P., and Kandpal, R.P. (2009). EphB6 receptor significantly alters invasiveness and other phenotypic characteristics of human breast carcinoma cells. Oncogene. *28*, 1706-1713.

19. Freywald, A., Sharfe, N., and Roifman, C.M. (2002). The kinase-null EphB6 receptor undergoes transphosphorylation in a complex with EphB1. J. Biol. Chem. *277*, 3823-3828.

20. Gu, Y., Li, F., Qian, N., Chen, X., Wang, H., and Wang, J. (2016). Expression of EphB6 in ovarian serous carcinoma is associated with grade, TNM stage and survival. J. Clin. Pathol. *69*, 448-453.

21. Gurley, K.E., and Kemp, C.J. (2001). Synthetic lethality between mutation in Atm and DNA-PK(cs) during murine embryogenesis. Curr. Biol. *11*, 191-194.

22. Gurniak, C.B., and Berg, L.J. (1996). A new member of the Eph family of receptors that lacks protein tyrosine kinase activity. Oncogene. *13*, 777-786.

23. Hafner, C., Bataille, F., Meyer, S., Becker, B., Roesch, A., Landthaler, M., and Vogt, T. (2003). Loss of EphB6 expression in metastatic melanoma. Int. J. Oncol. *23*, 1553-1559.

24. Hart, T., Brown, K.R., Sircoulomb, F., Rottapel, R., and Moffat, J. (2014). Measuring error rates in genomic perturbation screens: gold standards for human functional genomics. Mol. Syst. Biol. *10*, 733.

25. Hartwell, L.H., Szankasi, P., Roberts, C.J., Murray, A.W., and Friend, S.H. (1997). Integrating genetic approaches into the discovery of anticancer drugs. Science. *278*, 1064-1068.

26. Himanen, J.P., Saha, N., and Nikolov, D.B. (2007). Cell-cell signaling via Eph receptors and ephrins. Curr. Opin. Cell Biol. *19*, 534-542.

27. Holmberg, J., Genander, M., Halford, M.M., Anneren, C., Sondell, M., Chumley, M.J., Silvany, R.E., Henkemeyer, M., and Frisen, J. (2006). EphB receptors coordinate migration and proliferation in the intestinal stem cell niche. Cell. *125*, 1151-1163.

28. Hosford, S.R., and Miller, T.W. (2014). Clinical potential of novel therapeutic targets in breast cancer: CDK4/6, Src, JAK/STAT, PARP, HDAC, and PI3K/AKT/mTOR pathways. Pharmgenomics Pers. Med. *7*, 203-215.

29. Irby, R.B., and Yeatman, T.J. (2000). Role of Src expression and activation in human cancer. Oncogene. *19*, 5636-5642.

30. Kumar, S.R., Singh, J., Xia, G., Krasnoperov, V., Hassanieh, L., Ley, E.J., Scehnet, J., Kumar, N.G., Hawes, D., Press, M.F., Weaver, F.A., and Gill, P.S. (2006). Receptor tyrosine kinase EphB4 is a survival factor in breast cancer. Am. J. Pathol. *169*, 279-293.

31. Liberali, P., Snijder, B., and Pelkmans, L. (2014). A hierarchical map of regulatory genetics in membrane trafficking. Cell. *157*, 1473-1487.

32. Liersch-Lohn, B., Slavova, N., Buhr, H.J., and Bennani-Baiti, I.M. (2016). Differential protein expression and oncogenic gene network link tyrosine kinase ephrin B4 receptor to aggressive gastric and gastroesophageal junction cancers. Int. J. Cancer. *138*, 1220-1231.

33. Lugli, A., Spichtin, H., Maurer, R., Mirlacher, M., Kiefer, J., Huusko, P., Azorsa, D., Terracciano, L., Sauter, G., Kallioniemi, O.P., Mousses, S., and Tornillo, L. (2005). EphB2 expression across 138 human tumor types in a tissue microarray: high levels of expression in gastrointestinal cancers. Clin. Cancer Res. *11*, 6450-6458.

34. Matsuoka, H., Iwata, N., Ito, M., Shimoyama, M., Nagata, A., Chihara, K., Takai, S., and Matsui, T. (1997). Expression of a kinase-defective Eph-like receptor in the normal human brain. Biochem. Bioph. Res. Co. *235*, 487-492.

35. Matsuoka, H., Obama, H., Kelly, M.L., Matsui, T., and Nakamoto, M. (2005). Biphasic functions of the kinase-defective EphB6 receptor in cell adhesion and migration. J. Biol. Chem. *280*, 29355-29363.

36. Mayer, I.A., Abramson, V.G., Lehmann, B.D., and Pietenpol, J.A. (2014). New strategies for triple-negative breast cancer – deciphering the heterogeneity. Clin. Cancer Res. *20*, 782-790.

37. Mertens-Walker, I., Fernandini, B.C., Maharai, M.S., Rockstroh, A., Nelson, C.C, Herington, A.C., and Stephenson, S.A. (2015). The tumor-promoting receptor tyrosine kinase, EphB4, regulates expression of integrin-ß8 in prostate cancer cells. B.M.C. Cancer. *22*, 164-173.

38. Mohamed, E.R., Noguchi, M., Hamed, A.R., Eldahshoury, M.Z., Hammady, A.R., Salem, E.E., and Itoh, K. (2015). Reduced expression of erythropoietin-producing hepatocyte B6 receptor tyrosine kinase in prostate cancer. Oncol. Lett. *9*, 1672-1676.

39. Muller-Tidow, C., Diederichs, S., Bulk, E., Pohle, T., Steffen, B., Schwable, J., Plewka, S., Thomas, M., Metzger, R., Schneider, P.M., Brandts, C.H., Berdel, W.E., and Serve, H. (2005). Identification of metastasis-associated receptor tyrosine kinases in non-small cell lung cancer. Cancer Res. *65*, 1778-1782.

40. Munthe, E., Rian, E., Holien, T., Rasmussen, A., Levy, F.O., and Aasheim, H. (2000). Ephrin-B2 is a candidate ligand for the Eph receptor, EphB6. Febs. Letters. *466*, 169-174.

41. Murai, K.K., and Pasquale, E.B. (2003). 'Eph'ective signaling: forward, reverse and crosstalk. J. Cell Sci. *116*, 2823-2832.

42. Pan, X., Yuan, D.S., Ooi, S.L., Wang, X., Sookhai-Mahadeo, S., Meluh, P., and Boeke, J.D. (2007). dSLAM analysis of genom-wide genetic interactions in *Saccharomyces cerevisiae*. Methods. *41*, 206-221.

43. Pasquale, E.B. (2005). Eph receptor signalling casts a wide net on cell behaviour. Nat. Rev. Mol. Cell Biol. *6*, 462-475.

44. Pasquale, E.B. (2008). Eph-ephrin bidirectional signaling in physiology and disease. Cell. *133*, 38-52.

45. Pasquale, E.B. (2010). Eph receptors and ephrins in cancer: bidirectional signalling and beyond. Nat. Rev. Cancer. *10*, 165-180.

46. Paul, J.M., Templeton, S.D., Baharani, A., Freywald, A., and Vizeacoumar, F.J. (2014). Building high-resolution synthetic lethal networks: a 'Google map' of the cancer cell. Trends Mol. Med. *20*, 704-715.

47. Paul, J.M., Toosi, B., Vizeacoumar, F.S., Bhanumathy, K.K., Li, Y., Gerger, C., El Zawily, A., Freywald, T., Anderson, D.H., Mousseau, D., Kanthan, R., Zhang, Z., Vizeacoumar, F.J., and Freywald, A. (2016). Targeting synthetic lethality between the SRC kinase and the EPHB6 receptor may benefit cancer treatment. Oncotarget. *7*, 50027-50042.

48. Perou, C.M., Sørlie, T., Eisen, M.B., van de Rijn, M., Jeffrey, S.S., Rees, C.A., Pollack, J.R., Ross, D.T., Johnsen, H., Akslen, L.A., Fluge, O., Pergamenschikov, A., Williams, C., Zhu, S.X., Lønning, P.E., Børresen-Dale, A.L., Brown, P.O., and Botstein, D. (2000). Molecular portraits of human breast tumours. Nature. *406*, 747-752.

49. Poliakov, A., Cotrina, M., and Wilkinson, D.G. (2004). Diverse roles of eph receptors and ephrins in the regulation of cell migration and tissue assembly. Dev. Cell. *7*, 465-480.

50. Prahallad, A., Sun, C., Huang, S., Di Nicolantonio, F., Salazar, R., Zecchin, D., Beijersbergen, R.L., Bardelli, A., and Bernards, R. (2012). Unresponsiveness of colon cancer to BRAF(V600E) inhibition through feedback activation of EGFR. Nature. *483*, 100-103.

51. Roguev, A., Talbot, D., Negri, G.L., Shales, M., Cagney, G., Bandyopadhyay, S., Panning, B., and Krogan, N.J. (2013). Quantitative genetic-interaction mapping in mammalian cells. Nat. Methods. *10*, 432-437.

52. Sajesh, B.V., Bailey, M., Lichtensztejn, Z., Hieter, P., and McManus, K.J. (2013). Synthetic lethal targeting of superoxide dismutase 1 selectively kills RAD54B-deficient colorectal cancer cells. Genetics. *195*, 757-767.

53. Schenone, S., Manetti, F., and Botta, M. (2007). SRC inhibitors and angiogenesis. Curr. Pharm. Design. *13*, 2118-2128.

54. Sen, B., Saigal, B., Parikh, N., Gallick, G., and Johnson, F.M. (2009). Sustained Src inhibition results in signal transducer and activator of transcription 3 (STAT3) activation and cancer cell survival via altered Janus-activated kinase-STAT3 binding. Cancer Res. *69*, 1958-1965.

55. Sørlie, T., Perou, C.M., Tibshirani, R., Aas, T., Geisler, S., Johnsen, H., Hastie, T., Eisen, M.B., van de Rijn, M., Jeffrey, S.S., Thorsen, T., Quist, H., Matese, J.C., Brown, P.O., Botstein, D., Lønning, P.E., and Børresen-Dale, A.L. (2001). Gene expression patterns of breast carcinomas distinguish tumor subclasses with clinical implications. Proc. Natl. Acad. Sci. U.S.A. *98*, 10869-10874.

56. Stokowski, A., Shi, S., Sun, T., Bartold, P.M., Koblar, S.A., and Gronthos, S. (2007). EphB/ephrin-B interaction mediates adult stem cell attachment, spreading, and migration: implications for dental tissue repair. Stem Cells. *25*, 156-164.

57. Swaminathan, G., and Tsygankov, A.Y. (2006). The Cbl family proteins: ring leaders in regulation of cell signaling. J. Cell. Physiol. *209*, 21-43.

58. Tang, X.X., Evans, A.E., Zhao, H., Cnaan, A., London, W., Cohn, S.L., Brodeur, G.M., and Ikegaki, N. (1999). High-level expression of EPHB6, EFNB2, and EFNB3 is associated with low tumor stage and high TrkA expression in human neuroblastomas. Clin. Cancer Res. *5*, 1491-1496.

59. Tang, X.X., Zhao, H., Robinson, M.E., Cnaan, A., London, W., Cohn, S.L., Cheung, N.K., Brodeur, G.M., Evans, A.E., and Ikegaki, N. (2000). Prognostic significance of EPHB6, EFNB2, and EFNB3 expressions in neuroblastoma. Med. Pediatr. Oncol. *35*, 656-658.

60. Tischler, J., Lehner, B., and Fraser, A.G. (2008). Evolutionary plasticity of genetic interaction networks. Nat. Genet. *40*, 390-391.

61. Truitt, L., Freywald, T., DeCoteau, J., Sharfe, N., and Freywald, A. (2010). The EphB6 receptor cooperates with c-Cbl to regulate the behavior of breast cancer cells. Cancer Res. *70*, 1141-1153.

62. Truitt, L., and Freywald, A. (2011). Dancing with the dead: Eph receptors and their kinase-null partners. Biochem. Cell Biol. *89*, 675-686.

63. Vallejos, C.S., Gómez, H.L., Cruz, W.R., Pinto, J.A., Dyer, R.R., Velarde, R., Suazo, J.F., Neciosup, S.P., León, M., de la Cruz, M.A., and Vigil, C.E. (2010). Breast cancer classification according to immunohistochemistry markers: subtypes and association with clinicopathologic variables in a peruvian hospital database. Clin. Breast Cancer. *10*, 294-300.

64. Vizeacoumar, F.J., Arnold, R., Vizeacoumar, F.S., Chandrashekhar, M., Buzina, A., Young, J.T., Kwan, J.H., Sayad, A., Mero, P., Lawo, S., Tanaka, H., Brown, K.R., Baryshnikova, A., Mak, A.B., Fedyshyn, Y., Wang, Y., Brito, G.C., Kasimer, D., Makhnevych, T., Ketela, T., Datti, A., Babu, M., Emili, A., Pelletier, L., Wrana, J., Wainberg, Z., Kim, P.M., Rottapel, R., O'Brien, C.A., Andrews, B., Boone, C., and Moffat, J. (2013). A negative genetic interaction map in isogenic cancer cell lines reveals cancer cell vulnerabilities. Mol. Syst. Biol. *9*, 696-712.

65. Vogelstein, B., Papadopoulos, N., Velculescu, V.E., Zhou, S., Diaz, L.A. Jr., and Kinzler, K.W. (2013). Cancer genome landscapes. Science. *339*, 1546-1558.

66. Wang, L., Zhao, Z., Meyer, M.B., Saha, S., Yu, M., Guo, A., Wisinski, K.B., Huang, W., Cai, W., Pike, J.W., Yuan, M., Ahlquist, P., and Xu, W. (2014). CARM1 methylates chromatin remodeling factor BAF155 to enhance tumor progression and metastasis. Cancer Cell. *25*, 21-36.

67. Wheeler, D.L., Iida, M., and Dunn, E.F. (2009). The role of Src in solid tumors. Oncologist. *14*, 667-678.

68. Wood, L.D., Parsons, D.W., Jones, S., Lin, J., Sjöblom, T., Leary, R.J., Shen, D., Boca, S.M., Barber, T., Ptak, J., Silliman, N., Szabo, S., Dezso, Z., Ustyanksky, V., Nikolskaya, T., Nikolsky, Y., Karchin, R., Wilson, P.A., Kaminker, J.S., Zhang, Z., Croshaw, R., Willis, J., Dawson, D., Shipitsin, M., Willson, J.K., Sukumar, S., Polyak, K., Park, B.H., Pethiyagoda, C.L., Pant, P.V., Ballinger, D.G., Sparks, A.B., Hartigan, J., Smith, D.R., Suh, E., Papadopoulos, N., Buckhaults, P., Markowitz, S.D., Parmigiani, G., Kinzler, K.W., Velculescu, V.E., and Vogelstein, B. (2007). The genomic landscapes of human breast and colorectal cancers. Science. *318*, 1108-1113.

69. Yersal, O., and Barutca, S. (2014). Biological subtypes of breast cancer: Prognostic and therapeutic implications. World J. Clin. Oncol. *5*, 412-424.

70. Zhang, K., Corsa, C.A., Ponik, S.M., Prior, J.L., Piwnica-Worms, D., Eliceiri, K.W., Keely, P.J., and Longmore, G.D. (2013). The collagen receptor discoidin domain receptor 2 stabilizes SNAIL1 to facilitate breast cancer metastasis. Nat. Cell Biol. *15*, 677-687.